MULTI-DEVICE ANTENNAS

by

Pablo FERNANDEZ MARQUES
Elisa HUYGHUES DESPOINTES

MASTER THESIS
for the degree of
MASTER IN MOBILE COMMUNICATIONS

Department of Electronic Systems
Aalborg University

June 2012

Long Master Thesis Information:

TITLE:
Multi-Device Antennas

PROJECT PERIOD:
September 2011- May 2012

PROJECT GROUP:
1011

MEMBERS:

Pablo Fernández Marqués

Elisa Huyghues Despointes

SUPERVISORS:

Gert Frølund Pedersen
Mauro Pelosi
Samantha Caporal Del Barrio

Number of pages in report: 73

Number of pages in appendix: 20

Total number of pages: 107

Number of copies printed: 6

ABSTRACT:

Nowadays it exists an ever-increasing pressure to **reduce the form factor** of the antenna while increasing or keeping **acceptable efficiency, bandwidth and antenna isolation**. Every time the size of the ground plane is modified, antenna engineers implement a **new design**.

However this fact provokes additional costs to the antenna design. Thus, **portability** of a fix antenna for different ground plane sizes might be worth. Moreover, isolation between antenna in **MIMO systems** is a big issue, specially for **small devices** operating at low frequencies. Then, the industry seek for innovative designs that can improve the performance of the classic top-bottom MIMO configuration.

Lateral designs are presented as a promising candidate. For these reasons, a **comparison of two antenna designs over different ground plane formats** is analyzed, leading to the conclusion that the portability of a lateral design provides very **good performance** if proper **decoupling techniques** are implemented.

By signing this document, each member of the group confirms that all participated in the project work and thereby all members are collectively liable for the content of the report.

Preface

This Master Thesis has been written by Pablo Fernández Marqués and Elisa Huyghues Despointes, group number 1011, from September 2011 to May 2012. The outcome of this thesis is to acquire a degree in Mobile Communications.

This thesis has been written in LaTeX and consists of the following chapters: Introduction, Antenna theory background, Antenna design background, Simulations, Discussion and future work and Conclusions. For all the report, additional technical details can be found in different appendices. The appendix is composed of two chapters, A: Theory and B: Simulations. Inside each chapter there are several numerated sections.

All tables and graphs presented in this report were generated using several MATLAB scripts. The different calculations and simulations were supported by a FDTD MATLAB code deployed through a remote server, Fyrkat, to accelerate considerably the computation time.

Most of the literature references follow IEEE recommendations, and the rest are extracts from theoretical books or articles. Quotations and literature are referenced using a number in brackets referring to the position in the bibliography presented at the end of this thesis before the appendices. Equations, figures and tables are presented as follow:

Text quotation [Reference Number]
Equation (Chapter number/letter. Equation number)
Figure (Chapter number/letter. Figure number)
Table (Chapter number/letter. Table number)

Contents

List of Figures

List of Tables

Acronyms

ABC: Absorbing Boundary Conditions

AMPS: Advanced Mobile Phone System

AR: Axial Ratio

BTS: Base Transceiver Station

CDMA: Code Division Multiple Access

CTIA: Cellular Telecommunications Industry Association

EDGE: Enhanced Data for Global Evolution

Ev-DO: Evolution-Data Optimized

DC: Direct Current

DCS: Digital Communication System

DVB-H: Digital Video Broadcasting- Handheld

ESA: Electrically Small Antenna

EUC: European Union Council

FCC: Federal Communication Commission

FDD: Frequency Division Duplexing

FDMA: Frequency Division Multiple Access

FDTD: Finite-Difference Time Domain

FET: Field Effect Transistor

GP: Ground plane

GPRS: General Packet Radio System

GPS: Global Positioning System

GSM: Global System for Mobile

HPBW: Half Power Beam-Width

HSPA: High Speed Packet Access

IFA: Inverted-F Antenna

ILA: Inverted-L Antenna

IMT-A: International Mobile Telecommunications Advance

IP: Internet Protocol

ITU: International Telecommunications Union

LAN: Local Area Network

LTE: Long Term Evolution

MEG: Mean Effective Gain

MEMS: Micro Electro-Mechanical Systems

MIMO: Multiple-Input Multiple-Output

MLA: Meandered Line Antenna

MLDA: Meandered-Line Dipole Antenna

MME: Mobility Management Entity

MU-MIMO: Multi-User Multiple-Input Multiple-Output

NLOS: Non Line of Sight

NMT: Nordic Mobile Telephone

OFDMA: Orthogonal Frequency Division Multiple Access

PEC: Perfect Electric Conductor

PCB: Printed Circuit Board

PCS: Personal Communications Service

PIFA: Planar Inverted-F Antenna

PML: Perfectly Matched Layers

PSTN: Pubic Switched Telephone Network

RF: Radio Frequency

RNC: Radio Network Controller

S-GW: Serving GateWay

SAR: Specific Absorption Rate

SC-FDMA: Single Carrier Frequency Division Multiple Access

SLA: Straight Line Antenna

SLDA : Straight-Line Dipole Antenna

SMS: Short Message Service

SU-MIMO: Single-User Multiple-Input Multiple-Output

TACS: Total Access Communications System

TDD: Time Division Duplexing

TDMA: Time Division Multiple Access

TIS: Total Isotropic Sensitivity

TRP: Total Radiated Power

UE: User Equipment

UMTS: Universal Mobile Telecommunications System

VHF : Very High Frequency

VoIP: Voice over Internet Protocol

VSWR: Voltage Standing Wave Ratio

WCDMA: Wideband Code Division Multiple Access

WiMAX: Worldwide Interoperability for Microwave Access

1G: First Generation

2D: 2-Dimensions

2G: Second Generation

2.5G: Second and a half Generation

3D: 3-Dimensions

3G: Third Generation

3GPP: Third Generation Partnership Project

4G: Fourth Generation

Problem Definition

Nowadays, the rising demand for wireless communications has been speeding-up conception of antennas that operate in multi frequency bands for different handset terminals. The antenna is implemented on a Printed Circuit Board (PCB) and when only the size of the PCB increases, the requirements of the phone or the antenna parameters are evolving. Every time the PCB size is modified, engineers design a new antenna model. However, designing a new antenna model every time the PCB changes is not efficient if it is possible to design a model which keeps acceptable antenna properties for any PCB formats, or at least for the most common ones as the Candybar, the Smartphone and the Tablet. This is the reason why the convenience of using portability of a unique model is analyzed. Moreover, since according to the market requirements, phones should be always as small and thin as possible, a big challenge arises when small devices have to operate at low frequencies in MIMO systems. Since the antennas are very close to each other, the isolation level between them is very poor, leading to a deterioration of the antenna performance. This is the reason why decoupling techniques will be implemented and analyzed. Additionally, low band services require longer antennas and this fact may be an important issue for small PCB formats. Indeed, the larger is the area occupied by the antennas over the PCB, the less is the space available to place other components. Hence, industry seeks for compact models and some of them will be tested in this thesis. Another last important drawback arises from the fact that usually the bandwidths in the low bands are not wide enough to cover an entire Long Term Evolution (LTE) band. Then, since tunability of the antenna operation frequency is required for many of the low band services, tuning techniques will be also investigated in this thesis. Therefore, the goal is to design a Multiple Inputs Multiple Outputs (MIMO) antenna system operating in multiband that is spatially efficient, highly decoupled and tunable for any kind of mobile device format, focusing the analysis on the most common ones: Candybar, Smartphone and Tablet.

Introduction

Forth Generation (4G) Overview

Nowadays, worldwide communication technology utilization is ubiquitous and essential for society fast development. Over the past twenty-five years, wireless networks technology has evolved from basic analog to high-speed digital. Indeed, the first two mobile generations were able to transmit voice but for low speed data whereas the third generation has revolutionized the world of telecommunications with the appearance of images and hypertext. The user needs and demands are constantly increasing and that is the reason why researchers have begun to investigate the 4G technologies even before the third generation has been widely implemented. With the 4G, users would be able to transmit and receive voice and speech but also video at a high-speed rate and low latency thanks to packet switch network technology. [1]

First Generation (1G)

The first generation of Global System for Mobile (GSM) communications consisted on sending analog waveforms signal essentially for voice but also for a limited amount of data with a data bandwidth of 1.9Kbps (Kilo bit per second) and a peak at 14.4Kbps. Since more than three technologies such as Advanced Mobile Phone System (AMPS), Nordic Mobile Telephone (NMT) and Total Access Communication System (TACS) were used and more than eight different cellular systems were created in Europe, this first generation of communication was not very efficient. 1G used a multiple-access method called Frequency Division Multiple Access (FDMA) in order to allocate a frequency or a channel for every users.

Second Generation (2G)

The second generation of mobile communications used a digital cellular network in order to send digital bits. Compare to 1G, 2G works over narrowband and a circuit data technology. On a data point of view, this generation was not very efficient and the peak stayed at 14.4Kbps but it introduced a new service called Short Message Service (SMS). The spectral efficiency improved from the analog to the digital GSM and, as consequence, the network could handle more users and more simultaneous conversations. Time Division Multiple Access (TDMA) is one of the channel access method used in 2G and allows several users to share the same frequency channel with the principle of time slots. Code Division Multiple Access (CDMA) is the other channel access method and used spread-spectrum technology in order to allow several users to share the same bandwidth.

Second and a half Generation (2.5G)

Instead of circuit data, the second and a half generation deployed in addition a packet data technique so the users can obtained a range of 20-40Kbps of throughput with a peak at 171Kbps. The

technique used in this generation is the General Packet Radio System (GPRS) and the channel access methods implemented are TDMA and CDMA.

Third Generation (3G)

The third generation was a real step forward for mobile communications. 3G used a digital cellular with packet data only but this time they deployed broadband instead of narrowband. With a throughput between 500-700Kbps and a peak at 3.1Mbps (Mega bit per second), 3G was a real improvement in term of efficiency. Regarding to the operator, different technologies were implemented such as CDMA2000, Universal Mobile Telecommunications System (UMTS) and an evolution of GPRS called Enhanced Data for Global Evolution (EDGE). The users could achieve a throughput of 144Kbps while moving at a rapid rate and 384Kbps while not moving so fast. If the users are stationary, 2 Mbps of throughput could be reach. Like the 2G, this generation used TDMA and CDMA as channel access methods. [2]

Third and a Half Generation: 3.5G

This generation is called 3.5G because it is faster than 2Mbps and can range from 3.6 to 7.2Mbps. The users can expect a throughput of 1 to 3Mbps with a peak at 14.4Mbps. To achieve such a data rate, the technology use is High Speed Packet Access (HSPA).
Nowadays, the users always want more throughput and higher data speed so researchers decided to use a new telecommunication technology but there is still no formal definition of 4G accepted.

Forth Generation (4G)

4G is the forth generation of cellular wireless standards even though the first designs began in 2000. This new generation will also be with digital, broadband and packet based but this time the services will be completely Internet Protocol (IP)-oriented with Voice over IP (VoIP) and a very high data throughput superior to 100Mbps which can reach a peak of 300Mbps. The forth generation is a new revolution for real time application such as games or video conferences. The maximum and typical throughput while moving is 3-5Mbps due to the technologies such as Worldwide Interoperability for Microwave Access (WiMAX) and LTE, the evolution of UMTS. The performance of 4G will be shown on WiFi networks also with a throughput of more than 100Mbps and the WiFi cellular technology who can supports handoff and high motion speeds. The success of 4G going forward could be based on one key word, *integration*, with the ability to handoff between different technologies and different devices. [3]

Difference from 3G to 4G: Network topology

The main difference between 3G and 4G appears on the network topology. On the Evolution-Data Optimized (Ev-DO) networks, the control and user planes transmit from the Base Transceiver Station (BTS) are centralized on the Radio Network Controller (RNC) whereas on the LTE network, the control plane data is sending from the eNode B to the Serving Gateway (S-GW) and the user plane data is controlling by the Mobility Management Entity (MME). This different topology creates new benefits such as lower latencies and better performance in the system and also a higher throughput.

LTE and LTE Advanced

LTE was standardized in 2008 under Release 8 and developed by the Third Generation Partnership Project (3GPP). It allows all the operators to complement their 3G networks by using a wider

spectrum. LTE simplifies the migration to 4G networks characterized by a faster data speed, an IP based radio access technology and also a high speed packet access system. LTE is an evolution of the EDGE and HSPA technologies. The services of LTE will be really performant in real time applications such as games or video conferences with a low latency and a high peak of data rate. The channel bandwidths 1.4, 3, 5, 10, 15 and 20MHz are very useful for mobile broadband and good multimedia services. In order to prevent from multi-path, frequencies selective fading and inter-cell interferences, LTE used in downlink a single processing technique called Orthogonal Frequency Division Multiple Access (OFDMA) whereas in uplink it involved Single Carrier-Frequency Division Multiple Access (SC-FDMA). The two coding schemes Time Division Duplexing (TDD) and Frequency Division Duplexing (FDD) and a Multi-User MIMO (MU-MIMO) are also supported by LTE in uplink and downlink. With all of these techniques used, the peak data rate can exceed 100Mbps in downlink and 50Mbps in uplink. [4]
Even though the design of algorithm and the techniques implemented in LTE are more complex, they offer better performance for the users. Compare to HSPA Release 6, the gain of the cell spectrum efficiency is multiplied by two or three in the uplink and three or four in the downlink of LTE networks. According to the International Telecommunication Union (ITU), LTE advanced or Release 10 is a concept for International Mobile Telecommunications Advanced (IMT-A) and also an enhancement of the 3GPP LTE standard finalized in 2011. The first requirement was to obtain a peak data rate superior to 1Gbps but the features of the LTE Advanced are to increase network capacity, improve user performance at the cell edge, use efficiently the low power nodes and provides user fairness. These peaks data rate of 1Gbps in downlink and 500Mbps in uplink are achieved thanks to a channel bandwidth extension from 20MHz to 100MHz. With the carrier integration techniques, LTE Release 8 and LTE Advanced Release 10 are compatible and can be combined. Indeed in LTE Advanced, the bandwidth is increasing to 100MHz by receiving and transmitting data on many component carriers compare to LTE. The Figure 1 below explain through a table the different LTE categories. [4]

Item	Sub-category	LTE target	LTE-Advanced (4G) target	IMT-Advanced (4G) requirement
Peak spectral efficiency (b/s/Hz)	Downlink	16.3 (4x4 MIMO)	30 (up to 8x8 MIMO)	15 (4x4 MIMO)
	Uplink	4.32 (64QAM SISO)	15 (up to 4x4 MIMO)	6.75 (2x4 MIMO)
Downlink cell spectral efficiency b/s/Hz/user Microcellular 3 km/h, 500 m ISD	(2x2 MIMO)	1.69	2.4	
	(4x2 MIMO)	1.87	2.6	2.6
	(4x4 MIMO)	2.67	3.7	
Downlink cell-edge user spectral efficiency (b/s/Hz/user) (5 percentile, 10 users), 500m ISD	(2x2 MIMO)	0.05	0.07	
	(4x2 MIMO)	0.06	0.09	0.075
	(4x4 MIMO)	0.08	0.12	

Figure 1: Comparative table, [5]

Multiple-input multiple-output

MIMO is a technique based on multiple smart antennas to improve wireless communications performances and applications efficiency. It increases data throughput by using multiple transmit

antennas requiring more transmission power but not more bandwidth. MIMO is used in different standards such as 3GPP LTE, WiMAX, HSPA+ and 4G systems to provide high-speed mobile data and services but also to improve link quality, bit rate, overall capacity of the system presented in [6]. Between the BTS and the mobile phone, there are a lot of path loss due to Non Line Of Sight (NLOS) but this indirect signal path provides good signal diversity, which is an advantage. Indeed, effectiveness of MIMO applications is enhanced thanks to these multiple paths created by buildings, cars, airplanes, people and other objects. The principle of MIMO is based on OFDM technology, which transmits symbols in parallel using a narrow bandwidth and a longer period of transmission time for each symbol. MIMO radio channel in Figure 2 is composed of three different modes, which are Single-User MIMO (SU-MIMO), multi-user MIMO and cooperative MIMO. MU-MIMO defines two users sending data to the nodeB by using two transmit antennas in each device. Both antennas are transmitting different data while using the same frequency thanks to very advance digital signal processing technologies. SU-MIMO represents the transmission of data between the base station (nodeB) and the User Equipment (UE). The BTS is transmitting different data streams on the same frequency but on two different transmitter antennas while the two receiver antennas implemented in the mobile phone recombine the signal into a single stream. [6]
By using OFDM techniques the recovering process of the signal is much easier and the receiver antennas can differentiate the data streams, which improve the efficiency of spectrum use. If the device is equipped with multiple antennas, the overall effectiveness of the system can double or triple. By using more antennas in both ends the diversity order and spectral efficiency increases significantly. Indeed, depending on the number of receive antennas, the capacity expressed in bps/Hz increases linearly and the formula to calculate the capacity in MIMO systems is defined in [7].

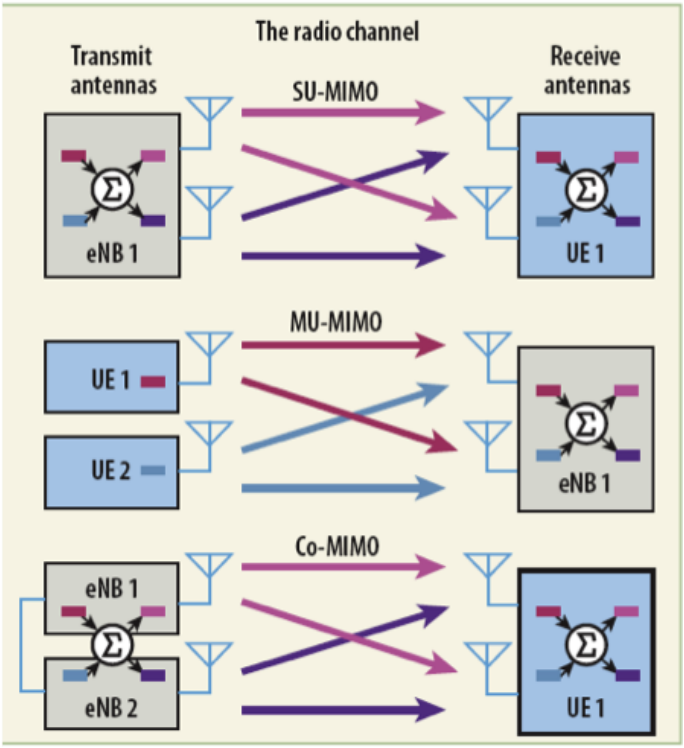

Figure 2: MIMO channel, [8]

Finite-Difference Time-Domain (FDTD) Software

The software used for launching our simulations was developed by Ondrej Franek and Mauro Pelosi from Aalborg University. The script is written in FORTRAN and it runs over MATLAB. It has an easy user interface which allows the user to design any kind of electronic device by using ideal sources, wires, rectangles, bricks and lumped components. Once the design is done, the software outcomes the main parameters used in electromagnetism to characterize an antenna like resonant frequencies, bandwidth, input impedance, reflection coefficient, antenna efficiency, currents, and E-H fields. The code is based in the FDTD method which applies the Maxwell's equations in deterministic scenarios. For every simulation, a tridimensional cell has to be defined in order to set the area where the different parameters are calculated. It also provides the option of choosing whether the near fields are desired to be computed or not. This is very relevant, for example, when the user wants to obtain the current running through the wires. Since FDTD simulations can be long, they are done by using very powerful servers available at Aalborg University in order to gain computational time. In our case, we have been registered in a Supercomputer called Fyrkat, where our simulations are launched and our results are stored. In order to access to Fyrkat, we have to connect to the remote server Xming and access to Fyrkat by typing "fyrkat.grid.aau.dk" in the PuTTy software which allows the user to connect to a remote directory, where the simulations run.

Chapter 1

Antenna theory background

1.1 Antenna parameters

An antenna can be defined as an electrical component which acts as the coupling between a guided electrical signal and an unguided medium, usually is the connecting device between free space and a transmission line. Thereby the antenna transforms electrical signals into electromagnetic waves or radio waves [6].

In this section we will show some of the parameters which characterize the different antennas. The typical parameters of antennas are radiation pattern, gain, polarization, antenna efficiency, bandwidth, directivity and impedance.

1.1.1 Radiation pattern

The radiation pattern is a mathematical function, sometimes represented as a 2-Dimensions (2D) or 3-Dimensions (3D) plot, of the radiation properties in space coordinates. These properties include radiation intensity, power flux density, field strength, directivity, phase or polarization. In the radiation pattern we can observe the major, minor and back lobes as well as the direction of the main lobe. The different patterns get names like omnidirectional, directional or isotropic. But in general they can be very different depending on the shape and the length of the antenna, see Figure 1.1.

Typically the radiation patterns are represented in logarithmic scale due to the fact that the values are more accentuated and it is easier to observe the difference among lobes. A very good design of any antenna implies that the side lobes have to be lower than -30 dB, [9]. There are three different kinds of antenna patterns: directional, omni-directional and isotropic, but in real life only exists the two first ones, the last one is just a reference model used in order to compare the performance of the real antennas.

- Directional pattern: when two principal planes E and H are directive. It means that the radiated intensity is higher in some directions than in others.
- Omni-directional pattern: when one of the principal planes is directive and the other one is non-directional. A pattern is non-directive when it radiates with the same intensity in all directions.
- Isotropic: when the two principal planes are non-directive.

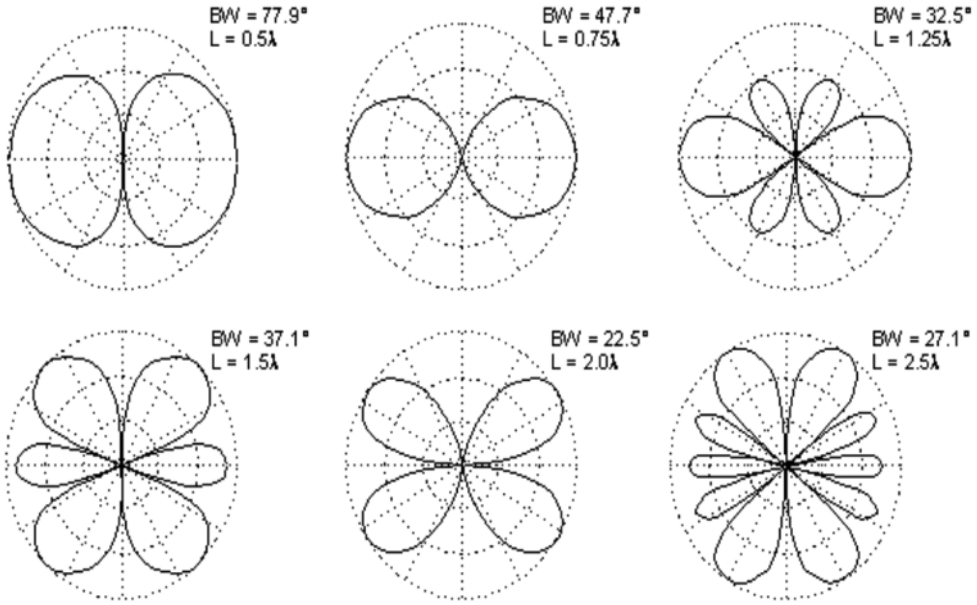

Figure 1.1: Different radiation patterns, [9]

The behavior of the antenna radiation properties changes depending on the observation point. Thus, three spatial regions can be defined: reactive near-field, radiating near-field (Fresnel) and far-field (Fraunhofer) regions as shown in Figure 1.2. Typically, the radiation pattern is given for the far-field region, where most of the fields are radiating ones

The reactive near-field region is the closest region to the antenna surrounding and it is defined as the portion of the near field region wherein the reactive fields predominate. In most of the antennas the boundary of the regions is taken at distances $R < 0.62\sqrt{D^3/\lambda}$, where λ is the wavelength and D is the largest dimension of the antenna. The radiating near-field region is defined as the near-field region between the reactive near-field and the far-field wherein the radiation fields predominate and wherein the angular field distribution is depending upon the distance from the antenna. The inner boundary is taken for distances $R \geq 0.62\sqrt{D^3/\lambda}$ and the outer boundary is taken for distances $R < 2D^2/\lambda$. Note that if the maximum dimension of the antenna is not large compared to the wavelength, this field region may not exist. The far-field region is defined as the region where the angular field distribution is essentially independent of the distance from the antenna.The distances where this field region exists are greater than $2D^2/\lambda$, whenever they are much greater than both the maximum dimension of the antenna and the wavelength [9].

With respect to the appearance of the pattern in these regions, in the reactive-near field the pattern is spread and nearly uniform, in the radiating near-field the pattern begins to smooth and form lobes, while in the far-field the pattern is well formed, usually with few minor lobes and one, or more major lobes. [9]

1.1.2 Voltage Standing Wave Ratio (VSWR)

The voltage standing wave ratio is the ratio between the maximum and minimum value of the voltage in a transmission line. The VSWR is usually expressed as function of the reflection

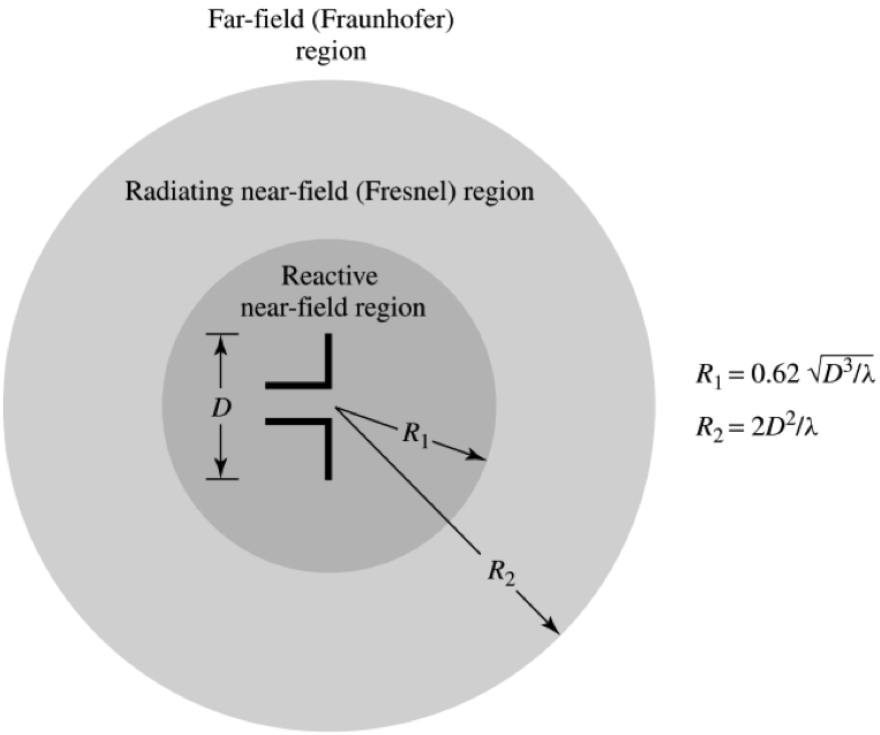

Figure 1.2: Field regions in the antenna

coefficient S_{11} as it is given by equation 1.1. The mathematical development of the expression is detailed in Appendix A.1.

$$VSWR = \frac{1+|S_{11}|}{1-|S_{11}|} \tag{1.1}$$

1.1.3 Directivity

The directivity on an antenna defines the ratio of the radiation intensity in a specified direction to the radiation intensity averaged over all the directions [9]. Mathematically it can be expressed as shown in equation 1.2.

$$D(\theta,\phi) = \frac{U(\theta,\phi)}{U_0} = \frac{4\pi U(\theta,\phi)}{P_{rad}} \tag{1.2}$$

where,

- $U(\theta,\phi)$ is the radiation intensity in a certain direction given by the polar and azimuth angles,θ and ϕ respectively
- U_0 is the average radiation intensity
- P_{rad} is the total radiated power by the antenna

In other terms, the directivity can be expressed as the ratio of the radiation intensity in a specified direction to the radiation intensity of an isotropic antenna with the same radiated power than the antenna under study. When the direction is not specified, usually the directivity is expressed as the

ratio shown above in the direction of maximum radiation. By developing the general expression [10], it can be expressed as shown in equation 1.3

$$D_0 = \frac{4\pi}{\Omega_A} \tag{1.3}$$

where Ω_A is the beam solid angle.

In directive patterns the beam solid angle can be approximated as the product of the beam-widths in the two principal planes of the pattern.

1.1.4 Gain

Closely related to the directivity, the gain is the ratio of the radiation intensity in a specific direction to the radiation intensity corresponding to an isotropic antenna with the same accepted power. The expression of the gain is specified in equation 1.4.

$$G(\theta,\phi) = \frac{4\pi U(\theta,\phi)}{P_{in}} \tag{1.4}$$

where P_{in} is the total input power, is function of both conduction-dielectric efficiency e_{cd} and the radiated power P_{rad}, as it is described by equation 1.5

$$P_{in} = e_{cd} P_{rad} \tag{1.5}$$

Then, the maximum value of the gain is proportional to the maximum value of the directivity,weighted by the conduction-dielectric efficiency, as it is expressed in equation 1.6

$$G_0 = e_{cd} D_0 \tag{1.6}$$

Moreover, the absolute gain G_{abs} is defined. It also takes into account the reflection efficiency e_0 which determines the losses when the antenna is connected to a transmission line. This absolute gain can be expressed as shown in equation 1.7

$$G_{abs}(\theta,\phi) = e_0 D(\theta,\phi) \tag{1.7}$$

Therefore the maximum value of the absolute gain is expressed as follows

$$G_{0,abs} = e_0 D_0 \tag{1.8}$$

1.1.5 Impedance

In electromagnetism, there are four different definitions of impedance depending upon the medium where this one is calculated. These impedances are: the characteristic impedance, the input impedance, the intrinsic impedance and the wave impedance. The characteristic and the input impedances are referred to a bounded medium like a transmission line. However, the intrinsic and the wave impedances are referred to an unbounded medium. In the following, the two more relevant ones regarding antenna issues are presented: the characteristic impedance and the intrinsic impedance.

Characteristic impedance

In a transmission line, the characteristic impedance Z_o is considered as the ratio between the voltage V(z) and the current I(z) when there is not reflected wave.

Intrinsic impedance

The intrinsic impedance of the medium is a characteristic of itself. It is the impedance of the medium that the wave propagates in. This parameter is the ratio of the magnitude of the E-field to the magnitude of the H-field for a plane wave in a generic medium [11].

$$\eta = \frac{|E|}{|H|} \tag{1.9}$$

By applying Maxwell equations, the expression of the intrinsic impedance for a loss medium with conductivity σ, with permittivity ε and permeability μ is given by equation 1.10 [9].

$$\eta = \sqrt{\frac{j\omega\mu}{\sigma + j\omega\varepsilon}} \tag{1.10}$$

It can be observed that in this case, the intrinsic impedance is a complex number, which means that the loss medium induces a phase shift between the electric and the magnetic field. Hence, in the particular case of lossless medium (zero conductivity), the intrinsic impedance expression is simplified as equation 1.11 shows

$$\eta = \sqrt{\frac{\mu}{\varepsilon}} = \sqrt{\frac{\mu_r \mu_0}{\varepsilon_r \varepsilon_0}} \tag{1.11}$$

where μ is the relative permeability of the medium, $\mu = 4\pi\ 10^{-}7$ [H/m] is the permeability in free space, ε_r is the relative permittivity of the medium and $\varepsilon_o = 8.85\ 10^{-12}$ [F/m] is the permittivity in free space. Hence, the intrinsic impedance in free space η_0, where both relative permeability and permittivity are equal to 1, is given by equation1.12 and the general expression for any medium can be expressed as shown in equation 1.13.

$$\eta_0 = \sqrt{\frac{\mu_0}{\varepsilon_0}} = 120\pi[\Omega] \tag{1.12}$$

$$\eta = \sqrt{\frac{\mu_r}{\varepsilon_r}}\eta_0 \tag{1.13}$$

1.1.6 Polarization

The polarization of the antenna is the same as the one of the wave that it transmits. It can be linear, circular or elliptical polarization depending on the phase shift and the Axial Ratio (AR) of the two electric field components perpendicular to the direction of travel.

1.1.7 Resonance frequency

Near resonance, a microwave resonator can be implemented by either a series or parallel RLC circuit. As it was shown in [11], for both cases the resonant frequency f_0 is given by

$$f_0 = \frac{1}{2\pi LC} \tag{1.14}$$

1.1.8 Bandwidth

The bandwidth is the range of frequencies at which the antenna can transmit with acceptable characteristics in terms of input impedance, pattern, beamwidth, polarization, side lobe level, gain, beam direction and radiation efficiency. To determine what is acceptable, there are some specifications given by standards, but they depend upon each use. Since the parameters mentioned above do not necessarily vary in the same manner or are critically affected by the frequency, usually a distinction is made between pattern bandwidth and impedance bandwidth. The pattern bandwidth is associated with the beamwidth, polarization, side lobe level, gain, beam direction while the impedance bandwidth is associated with the input impedance and the radiation efficiency.

1.1.9 Quality factor

The quality factor Q of an antenna is a common and simple way to quantify its potential bandwidth. It is defined as the quotient between the power stored in the reactive field and the radiated power [12]. There are several attempts to express the Q factor in the impedance of the antenna. Bandwidth of a series or parallel RLC network is well known to be equal to the inverse of Q under the condition of half power bandwidth [11]. However for many practical antennas this expression offers little usefulness, since we are more interested in the bandwidth defined by the VSWR. This parameter, denoted as FBW_V, is the bandwidth provided by the return loss along the transmission line feeding the antenna. The exact quality factor of a self-resonant antenna at a frequency ω_0, where the reactance $\mathrm{X}(\omega)$ of the antenna is equal to zero, in terms of the ratio of internal energy, $W(\omega_0)$, and accepted power, $P_A(\omega_0)$ is defined as it is shown in equation 1.15 [13]. The accepted power includes power associated to both radiated and loss.

$$Q(\omega_0) = \frac{\omega_0 |W(\omega_0)|}{P_A(\omega_0)} \tag{1.15}$$

In [13], Yaghjian and Best has approximated the quality factor by equation 1.16 .This expression was derived using a frequency dependent model of a general antenna [14].

$$Q(\omega_0) \approx Q_z(\omega_0) = \frac{\omega_0}{2R(\omega_0)} |Z'(\omega_0)| = \frac{\omega_0}{2R(\omega_0)} \sqrt{R'(\omega_0)^2 + (X'(\omega_0) + \frac{|X(\omega_0|}{\omega_0})^2} \tag{1.16}$$

where Z'(ω), R'(ω) and X'(ω) are the frequency derivatives of the untuned antenna's impedance, resistance, and reactance, respectively.

However, we seek to a definition which relates Q and VSWR bandwidth over a specific part of the spectrum, in the resonant narrow bands. A suitable relation between these two parameters is shown in equation 1.17 and it has been derived in [13] under the condition that $\frac{1}{2}$-power matched

VSWR bandwidth is not too large and that the antenna exhibits a single resonance within its defined operating bandwidth. The VSWR is denoted by s.

$$Q(\omega_0) \approx \frac{2\sqrt{\beta}}{FBW_V(\omega_0)}, \sqrt{\beta} = \frac{s-1}{2\sqrt{s}} \leq 1 \tag{1.17}$$

In [15] the author has analyzed the limitations of the expression presented in equation 1.17. In this analysis, numerical results validating the expression has been presented for a number of antennas including the electric dipole and several electrically small designs, which are on the scope of this thesis. The main conclusion is that the inverse relationship between Q and matched VSWR bandwidth is known to hold very well for antennas that exhibit narrow bandwidths and single resonances within the operating band. In case of wide band antennas, the expression only holds for small values of s.
Therefore, the expression is suitable over narrow-multiband scenarios where the different bands are far away from each other. Since, according with the bandwidth specifications that will be defined in subsection 2.1.1, the assumptions of the approximation presented are fulfilled, an algorithm to calculate the Q factor based on this criterion is detailed in the Appendix A.2.

1.2 Fano-Bode's criterion

The most desirable goal in a communication system is to design an antenna which provides a perfect matching with the widest bandwidth possible. However, empirical realizations show that this is not possible. This means that it should exists a theoretical limit that constrains the performance of an impedance matching network. Then, it is necessary to model mathematically the trade-off between matching and bandwidth. This model is explained in the Bode-Fano criterion [16],[17], which provides, for any type of canonical load impedances, the theoretical limit of the minimum reflection coefficient Γ_m, which can be obtained in a certain matching network with bandwidth $\Delta\omega$. Thus, this criterion provides an upper bound of the performance of the antenna in terms of matching. The general formula for any kind of load impedance is given by equation 1.18

$$\int_0^\infty ln\frac{1}{|\Gamma(\omega)|}\mathrm{d}\omega \leq K \tag{1.18}$$

Hence, if we focus the study on the bandwidth we are interested to match, it can be assumed that the reflection coefficient for the frequencies outside this bandwidth is equal to 1. Then, the general expression of equation 1.18 can be simplified as it is shown in equation 1.19.

$$\int_0^\infty ln\frac{1}{|\Gamma_m|}\mathrm{d}\Omega = \Delta\omega ln\frac{1}{\Gamma_m} \leq K \tag{1.19}$$

By developing the previous expression we can easily achieve the next equation:

$$\Delta\omega \leq K + ln(\Gamma_m) \tag{1.20}$$

It is well known that the lower is Γ_m, then the lower is $ln(\Gamma_m)$, and therefore, the lower is the achievable bandwidth. Then, coming back to the motivation of the section, from equation 1.20

can be concluded that the only bandwidth $\Delta\omega$ which provides a perfect matching (zero reflection coefficient) is $\Delta\omega = 0$. Since $1/|\Gamma|$ is proportional to the return loss in dB, then it can be interpreted that the bandwidth achievable to match at a certain reflection coefficient requires that the area between the return loss curve and the $|\Gamma|$=1 axis is less than or equal to a constant. [11]

1.3 Performance in small mobile terminals

One of the aims of small antennas engineers is to build a terminal with a good performance. But first of all it is necessary to define what is a good performance. In fact it depends upon the application of the antenna. In general the radiation pattern gives an overall overview of all the antenna characteristics and it has a very high relevance in traditional fixed antennas. However, for small mobile terminals the radiation pattern is not so relevant. This is mainly due to two facts: the target of the antenna and the size of terminal. The target of the antenna in mobile phones is to transmit and to receive energy from a wide variety of directions, the signal can come from any direction and hence, there are not unwanted directions. This means that engineers aim to design a low directive antenna. Thus, it is needed an electrically small antenna in order to produce low directivity. In the case of small mobile terminals working at low frequency, the space is an important constraint. Then, mobile phone antenna engineers always design antennas with low directivity. Thus, since the radiation pattern is so less directive, then it does not provide a lot of information since for these devices the performance cannot be based on the field radiated in a certain position, as both the size and polarization will change dependent on the direction [6].

There are several metrics which are specially relevant to study the performance of the small mobile terminals. The Total Radiated Power (TRP) and the Total Isotropic Sensitivity (TIS) are also very important parameters since they are the basis of the two standards which are being developed nowadays to estimate the performance of this kind of devices. These standards also provide the possibility to later include the Mean Effective Gain (MEG) and diversity. Besides, one of the most important drawback when a small mobile terminal is designed is to deal with the trade-off between TRP and SAR. As it was commented above, the TRP is proportional to the antenna efficiency and it is desirable to be as high as possible. However, the higher is the TRP , the higher is the absorption of a human body which is in the surrounding, i.e. the higher is the SAR, but this parameter cannot be higher than a certain value (check [18] for specifications). Thus, the goal is to be able to design a terminal with the lowest ratio SAR to TRP within the size and volume specifications.

Therefore, there are several aspects to deal with while designing an antenna for small devices. It can be concluded that an antenna has a good performance if it provides wide bandwidth, low directivity and low ratio SAR to TRP. Another relevant parameter to determine the performance of an antenna is its efficiency, that is explained in the next subsection. In this thesis, the two main parameters analyzed to quantify the performance are the bandwidth provided and the total efficiency.

1.3.1 Antenna efficiency

The total antenna efficiency e_0 takes into account not only the losses within the structure of the antenna but also losses at the input terminals. The overall efficiency of the antenna can be expressed as:

$$e_0 = e_r e_c e_d \tag{1.21}$$

where e_r is the reflection efficiency, e_c is the conduction efficiency and e_d is the dielectric efficiency. The conduction-dielectric efficiency presented in subsection 1.1.4.

The reflection efficiency represents the mismatch losses, i.e. the percentage of the input power which is absorbed by the load. Let consider that the reflection coefficient of the antenna is given by $\Gamma=(Z_{in}-Z_0)/(Z_{in}+Z_0)$, where Z_{in} is the antenna input impedance and Z_0 is the characteristic impedance of the transmission line. Then, the reflection efficiency is function of the return power loss $|\Gamma|^2$ as it is expressed in equation 1.22

$$e_r = 1 - |\Gamma|^2 \tag{1.22}$$

The conduction and conductive losses are very difficult to compute and they are usually lumped together to form the conduction-dielectric efficiency e_{cd}. This efficiency, also called the antenna radiation efficiency, is the percentage of the input power which is radiated by the radiation resistance R_r. The conduction-dielectric losses are dissipated in the resistance R_L. Then, the radiation efficiency can be written as: [9]

$$e_{cd} = \frac{R_r}{R_r + R_L} \tag{1.23}$$

Then, the total efficiency expression written in equation 1.21 can be reformulated as:

$$e_0 = e_{cd}(1 - |\Gamma|^2) = \frac{R_r}{R_r + R_L}(1 - |\Gamma|^2) \tag{1.24}$$

Since Γ is different depending upon the direction where the antenna is oriented, then the efficiency is also different for each direction and thereby it does not provide a lot of information. Therefore, the best way to characterize the quality of the antenna and the overall system is to measure the efficiency as the spherical integrated power over the incident power. Two different efficiencies can be distinguished depending upon the external environment. If there are not external objects in the surrounding of the antenna, it is called the free-space efficiency. However, when there are external objects in then surroundings (typically near-field region) like a human head, the efficiency has a different absolute value. Thus, to characterize an antenna using efficiency typically, it requires measurement of the free-space efficiency and the efficiency measured next to the head of the user [19]. In order to get an accurate value of the antenna efficiency, measurements have to take place in an anechoic chamber (see subsection 3.3.1).

1.3.2 Efficiency in MIMO

Nowadays current mobile phones are used to work in several frequency bands in order to support communications over different standards. For this reason it is important to specify the definition of the efficiency when there are many antennas. Assuming N closely located antennas connected to N transmission lines, each of them having the real-valued characteristic impedance Z_c , the pattern obtained when the antenna n is fed with a matched voltage generator and the rest are matched with load impedance equal to Z_c can be notated as F_n. In general this pattern is referred to the active or embedded pattern, i.e. the influence of the N-1 surrounding antennas is taken into account in contrast to the isolated patterns. Then the radiation efficiency of the port n is calculated by the integration over all the solid angles Ω [20].

$$\eta_n = \frac{1}{4\pi} \oint |F_n|^2 \mathrm{d}\Omega \tag{1.25}$$

When the antenna radiates in free space and there are no incident fields, then the incident V^+ and reflected waves V^- are related as function of the scattering matrix [S] as follows

$$V_n^- = \sum_{m=1}^{N} S_{mn} V_m^+ \tag{1.26}$$

In the far-field region the power radiated is given by

$$P_{rad} = \frac{1}{Z_c} r^2 \oint |E|^2 \mathrm{d}\Omega = \frac{1}{Z_c} [\sum_{m=1}^{N} |V_n^+|^2 - \sum_{m=1}^{N} |V_n^-|^2] \tag{1.27}$$

From last equations the following expression for the radiation efficiency can be derived

$$\eta_n = \sum_{m=1}^{N} 1 - |S_{mn}|^2 \tag{1.28}$$

In MIMO systems, correlation in a scattering environment is an important parameter for diversity reception [21]. The efficiency can be calculated as function of the correlation coefficient ρ_{lm} between the signals V_l^- and V_m^+-, as follows

$$\rho_{lm} = \frac{\oint F_l F_m^* \mathrm{d}\Omega}{\sqrt{\oint |F_l|^2 \oint |F_m|^2 \mathrm{d}\Omega}} = -\frac{\sum_{m=1}^{N} S_{nm} S_{nl}^*}{\sqrt{\eta_m \eta_l}} \tag{1.29}$$

When there are losses present in the medium, the previous equations might be not valid. The losses can be incorporated in additional fictive ports N_f that are never excited. Then, the radiation efficiency is given by the expression

$$\eta_n = 1 - \sum_{m=1}^{N+N_f} |S_{ni}|^2 \tag{1.30}$$

Efficiency for the two antennas case

Despite it is clear than increasing the number of antennas used for MIMO improves the performance, in general small terminals work with two antennas due to the spatial constraint intrinsic to these devices. Then it is interesting to stand out both the radiation and the total efficiency when there are two antennas working on the terminal. Assuming a lossless medium, it is possible to extract the efficiency expression by developing the general expression shown in equation 1.28 with N=2. Therefore the total efficiency in one of the ports is given by 1.31 and 1.32, respectively

$$\eta_1 = 1 - |S_{11}|^2 - |S_{21}|^2 \tag{1.31}$$

$$\eta_2 = 1 - |S_{22}|^2 - |S_{12}|^2 \tag{1.32}$$

Assuming a symmetric geometry, expressions 1.31 and 1.32 are the same.

In order to extract the radiation efficiency, it is necessary to take the reflection efficiency out from the formula of the total efficiency shown in equation 1.31. By doing the mathematical development shown in 1.33

$$\eta_1 = 1 - |S_{11}|^2 - |S_{21}|^2 = (1 - |S_{11}|^2)(1 - \frac{|S_{21}|^2}{1 - |S_{11}|^2}) \tag{1.33}$$

it is possible to achieve easily the expression for the radiation efficiency given by

$$\eta_{rad} = 1 - \frac{|S_{21}|^2}{1 - |S_{11}|^2} \tag{1.34}$$

1.3.3 Total radiated power

The TRP is a measure of how much power is radiated by the antenna when it is connected to any transmitter. It is calculated as the total received power when a certain power is output by the transmitter, and hereby this is the TRP. Then, it could be thought that the TRP is equivalent to the antenna efficiency measured in an anechoic chamber, but in fact it is not. The antenna efficiency is a metric of the antenna by itself. It assumes that the transmitter is matched to the characteristic impedance of the transmission line. However, the TRP takes also the transmitter characteristics and the connection between transmitter and antenna into account. Then, this parameter returns a different value for each kind of scenario and that is why companies do not care about the antenna efficiency when they public their requirements but they do about the TRP, since it is a measure of the real performance of antenna the system [9].

1.3.4 Total isotropic sensitivity

In order to understand the physical meaning of the TIS, it is necessary first to define what the sensitivity is. The sensitivity is defined as the smallest amount of power which can be input by the receiver while keeping a reliable communication. The TIS is defined as the power that reaches the antenna integrated through all the directions [22].
It could be thought that the TIS can be figured out by looking at the radiation pattern of the antenna but this statement is wrong because the radiation pattern only takes the antenna characteristics into account while the TIS also the receiver module, and the noise environment in which the measurement is performed in.

1.3.5 Mean effective gain

The MEG is the basis of a criterion to estimate the performance and which consists in calculating the average received power. The MEG is calculated by summing the products of the resultant radiation pattern and the incoming power in a typical environment, for all directions and both polarizations [6]. The MEG parameter was presented some years ago [23], [24] and it is the power received by the UE in a typical environment relative to a reference [25]. This reference is a model which has to be created after doing a large amount of experimental measures.

1.3.6 Discussion

The TRP and TIS parameters are very relevant in order to analyze the performance of a small mobile terminal. These two parameters together determine the maximum range at which a User Equipment (UE) can operate from a BTS with a certain level of performance [22]. In fact, it is usual that the standards only include TRP and TIS tests. However, the transmitted and received fields cannot be described only by these two parameters, the typical usage and the environment where the UE is located have to be taken into account in order to calculate a correct performance. A basic way to include the usage and the environment is by looking at the MEG parameter. Then, it is clear that calculating the MEG parameter requires more information and it is more complicated than the TRP and TIS parameters since its outcome depends not only on the UE but also on the surroundings [6]. In the case of the mobile phones, these surroundings refer typically to the head of the user but also to people, buildings and any kind of object which are in the vicinity of the UE and which affects to its transmitted and received signals. Thus, a model of the type of channel under study should be introduced in the analysis of the performance. In some experiments presented in [26], it has been demonstrated that the variations of the MEG parameter can be up to 10 dB depending upon the kind of the antenna.

1.3.7 Ground plane effects

One of the biggest complexities for antenna designers is to deal with the impact produced by the Ground Plane (GP) on the performance of the antenna. This is the reason why it is important to know what are the basics of the influence of the GP. First of all, it is necessary to point out that the transition between the feed line and the antenna input can be affected by the GP, since it has to be within a certain size in order to get reasonable current values running through the wire used as transition in the measurement process. This eventual high current leads to difficulties in determining the antenna performance and may indicate problems in integrating the antenna with other components.
The size of the GP plays a main role in the antenna characteristics. A small antenna placed beneath a GP acts as a dipole and parameters such as gain, bandwidth, efficiency, input impedance and resonant frequency are affected by the GP size. For example, it was demonstrated in [27] that if the GP size is under a certain threshold, then the resonant frequency will be significantly affected. The effect of the GP arises from the fact that the ground current is one of the most dominant factor in determining the small antenna radiation properties and the input impedance, since the ground plane is highly dependent on the GP size [28]. The radiation efficiency is also dependent on the GP size, so a compromise between desired efficiencies and a large GP [29] is needed. Moreover, it was demonstrated in [27], that another parameter affected by the GP size is the gain, since the gain increases as the GP size increases, reaching a maximum limit for an infinite ground plane. In [30] it was shown that whenever the GP size is decreased, the efficiency increases and the radiation pattern becomes more omni-directional. This effect is produced due to the fact that removing the GP from beneath the antenna reduces the surface wave loss and makes the electric fields to be propagated easier into the space. In [30], the GP size effects were analyzed over a meander line. It was shown that by truncating the GP, the bandwidth increases. As the GP size increases, the resonant frequency decreases, since the antenna becomes electrically larger, until the point where the ground plane extends to the full physical length of the antenna, where increasing the GP size has a minimal impact on the resonant frequency.

As summary of the GP effects we can conclude that by truncating the GP, the maximum return loss, the peak gain, the radiation efficiency and the bandwidth are increased, while the directivity is

decreased. Finally, it was shown in [30] that the ground plane has a critical impact on the antenna performance and experimental results lead to the conclusion that it is required a GP size at least five times the substrate thickness in order to mitigate the GP size related problems.

1.4 Inverted-F Antenna (IFA)

1.4.1 Definitions

The inverted-F antenna as the name indicates has the geometry of a returned F. This antenna is a variant of a dipole called monopole and the ground plane supplies the other pole of the antenna. This design is the evolution of the Inverted-L Antenna (ILA) to which was added to the feed a parallel inductance just to match. The IFA is composed of three wires, the feed, the short and the upper-arm that radiates. To get good impedance matching with the IFA, the position of the feeding point is simply adjusted. [1] An IFA can be considered as a monopole antenna that has been folded at some point so the upper-arm of this antenna become parallel to the ground plane. The feed and the short are located between the ground plane and the upper-arm. The length of these wires represents the height of the antenna.

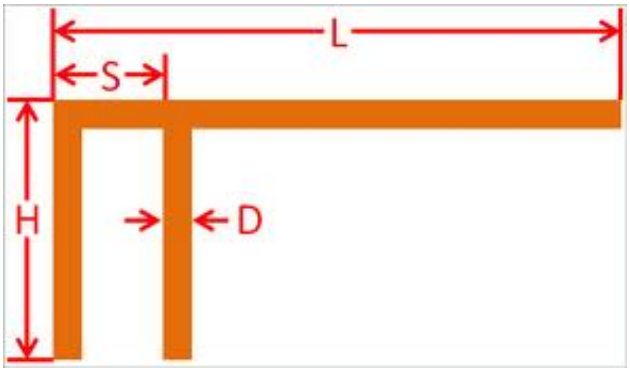

Figure 1.3: Inverted-F Antenna, [31]

1.4.2 Characteristics

The IFA is vertically or horizontally polarized when it is placed on the edge of the PCB with respectively the lower or upper elevation angles. The radiation pattern expected will have a donut shape and represents the ”changes in the antenna’s performance properties as a function of the ground plane size and location of the antenna on the ground plane” [1].
The height of the IFA above the PCB does not really affect the impedance or the radiation if it represents a small part of the total wavelength. Where the transmission line is short-circuited, the voltage and current are 90 degrees out of phase and it creates an inductive reactive component. Where the upper-arm of the antenna is open, it creates a capacitive component. We need to find the right place for the feed where the inductance and the capacitance cancel each other out. Thus, we obtain the effective resistance or radiation resistance, a good field strength indicator. The relation between the radiation resistance and the power of the field can be found in the equation 1.35.

$$R = \frac{P}{I^2} \tag{1.35}$$

1.4.3 Antenna design

When we design the feed from the ground plane we need to insert another wire in direction of the upper arm to make the connection. The short can be design at the edge of the ground plane and the feed needs to be closer to the short than the open part of the upper arm in order to obtain a good matching. For an IFA, the length of the upper-arm is approximately a quarter of the wavelength. To obtain the desired resonance frequency it is possible to increase or decrease this total length. The relation between the length and the frequency is the following:

$$L = \frac{c}{4f} = \frac{\lambda}{4} \tag{1.36}$$

L: Length of the antenna (m); c: Vacuum light speed $3x10^8$ (m/s); f: Frequency (Hz)

In order to be realistic, we can simulate an IFA antenna by designing the upper arm with a brick in the FDTD software. The height of the ground plane needs to be at least a quarter of a wavelength. If we reduce the height of the ground plane, the bandwidth and the efficiency will slowly decrease.

1.4.4 Bandwidth performances

The VSWR bandwidth of the IFA is measured at the input of the transmission line and it is calculated when the system has at least 5% of reflection coefficient. "In many applications, the bandwidth of the inverted-F antenna is not sufficient to cover the desired operating frequency range". [1]
In order to increase this bandwidth, the volume of the conductor can be extending. If the horizontal conductor is planar, the antenna is called Planar Inverted-F Antenna (PIFA) but this configuration will not be implemented in this thesis since for tuning applications a large bandwidth is not required so the main goal is not to improve the bandwidth.

1.4.5 Dual band IFA

There are different possible designs for dual-band IFA operations such as spiraled IFA but the interest will be focus on the design of an IFA combined with a folded ILA. In the inverted-FL antenna there are two resonances and the performance of a simple IFA are enhanced. Longer is the IFA and lower is the resonance frequency, shorter is the ILA and higher is the resonance frequency, [1].

To conclude this section, the inverted-F antenna is a well-known indoor antenna, low profile, cheap and easy to manufacture. IFA can provide good impedance matching and also create electromagnetic fields in either the horizontal or vertical polarizations. The main advantage of this antenna is the flexibility of the design by reducing the space consumption on the ground plane. Indeed, IFAs are integrable in small phone and easy to design compare to PIFAs. Without modifying the design, the IFA can be tuned and fit perfectly most of the wireless applications. [32]

1.5 Mutual coupling

1.5.1 Definitions

In telecommunications, the antenna elements are designed in a closely spaced array and the interaction that occurs between them is called mutual coupling and can degrade the overall system performance and radiation pattern like explained in [33]. Most of the cases, the coupling is prejudicial in the antenna operations but it can be sometimes profitable. A lot of researches have been done on the mutual coupling in antenna arrays in order to analyze its impact. The area concerned in our case will be the reduction of the mutual coupling in MIMO systems and different techniques will be implemented in Chapter 3. Coupling represents the transfer of energy from one port to another. The feed source in the first antenna creates current and electromagnetic fields running through this antenna but it also results in electromagnetic fields on the second antenna. The electromagnetic fields created by the second antenna feed source are also coupled to the first antenna. The following quote illustrated perfectly the mutual coupling: "The power accepted by the input port of one element is fed as a reverse wave back into the feeding transmission lines connected to other element ports instead of radiating to the far field." [34]

1.5.2 Characteristics

The pattern of an antenna in the presence of another element differs from the isolated pattern. The total radiation patterns and the input impedances of both antennas are thus affected and also the current distributions. The induced current on the non-excited element disturbs the radiation pattern of the system. To maintain a good radiation pattern, one technique presented in [34] is to calculate first the excitation current and then the generator voltage that is necessary.
Concerning the input impedance, the strong effects of mutual coupling are explained in [35].

The current distribution is an important and useful parameter directly affected by mutual coupling. "One approach to explain the cause of the electromagnetic coupling between the IFAs located closely is to draw the intensity of the excited surface current distribution and analyze its magnitude level." [36] The current distribution is affected in MIMO due to the poor isolation between the excited and the non-excited antenna creating an important surface of current.

1.5.3 Mathematical modeling

- Microwave network theory

Using microwave network theory, we can represent the coupling between two antennas using the most common two-port network to calculate the input current at each antenna port. The scattering parameters $|S_{21}|$ or $|S_{12}|$ are useful to model the scattering matrix (S-matrix) by calculating the amplitude of the reverse voltage at one port. $|S_{12}|$ represents the reverse voltage gain and $|S_{21}|$ is the forward voltage gain. The mutual impedance is also an important formula where the total voltage can be calculated by multiplying the $|S_{21}|$ and $|S_{12}|$ by the total current. Using the paper [34] , those two matrixes can be expressed by the following formula:

$$S = \frac{(Z - Z_0 I)}{(Z + Z_0 I)} \tag{1.37}$$

where S is the scattering matrix, Z_0 is the characteristic impedance of the transmission line and Z is

the load impedance.

- Mutual coupling compensation

The ideal element pattern without coupling can be written as X_{ideal} but in the presence of another element the output of the all system becomes X_{actual}. Thanks to the linearity of Maxwell's equations, we can apply the formula presented in [37]

$$X_{actual} = CX_{ideal} \tag{1.38}$$

We can express those parameters by using the mutual coupling compensation formula in [37].

$$C = \frac{Z_A + Z_L}{(Z + Z_L.I)} \tag{1.39}$$

where Z_A is the element impedance in isolation, Z_L is the load impedance in each element and C is the mutual coupling matrix. The mutual impedance matrix Z can also be extracted from this formula. To calculate the impedance match, the complex conjugate of Z_A should be calculate.

Chapter 2

Antenna Design Background

2.1 Industry requirements

2.1.1 Bandwidth requirements

The aim of the antenna design is to provide a 4G service. The standard used in 4G is LTE and hence, it is necessary to look at the characteristics of this standard in order to set the bandwidth specifications. Figure 2.1 shows all the FDD bands. This work does not aim to cover all the spectrum used by a manufactured mobile phone since the frequency requirements will be requested by the manufacturers for a specific device. The goal is to demonstrate that the designed antenna can work in multi-band and that it can be tuned to lower operation frequencies by applying tuning techniques. Therefore, two LTE frequency bands will be selected, one in low band and another in high band. Over these bands, it will be shown that they can work simultaneously and despite the fact that the bandwidth to cover is quite big, by using precise capacitor tuning techniques, all the spectrum within these bands can be covered. These tuning techniques lead the antenna to switch its operation frequency to lower bands. Once the goal proposed in this thesis is achieved, the concept could be extrapolated in order to manufacture a real mobile terminal. In this thesis bands 7 and 8 have been chosen for high and low band respectively as examples. Band 7 is the band that operators are using nowadays to provide 4G service in Europe, while band 8 is the widely used standard which provides 2G service in all around the world, this standard is called Extended Global (EGSM900).

Figure 2.2 shows the maximum number of non-overlapping channels for each band and bandwidth. Thus, for band 7 it is necessary to cover at least 20 MHz of bandwidth while for band 8 it is enough to cover 10 MHz of bandwidth in order to fulfill with the channel requirements. Then, the specifications for bands 7 and 8 in terms of bandwidth are the following:

- Band 7: Matching at frequency close to 2.690 GHz and, by applying capacitor tuning techniques, going down until 2.5 GHz while having at least 20 MHz of bandwidth every time the capacitor value is changed and while covering all the different sub-bands.
- Band 8: Matching at a frequency close to 960 MHz and, by using capacitor tuning techniques, going down until 880 MHz while having at least 10 MHz of bandwidth every time the capacitor value is changed and while covering all the different sub-bands.

Once it is demonstrated that bands 7 and 8 are covered by the antenna, it is also interesting to know the tuning range reachable.

Band Number	Uplink, (MHz)	Downlink, (MHz)	Band Gap (MHz)	Duplex Separation (MHz)	UMTS Usage	LTE Usage
	$F_{\text{UL low}}$–$F_{\text{UL high}}$	$F_{\text{DL low}}$–$F_{\text{DL high}}$				
1	1920–1980	2110–2170	130	190	Y	Y
2	1850–1910	1930–1990	20	80	Y	Y
3	1710–1785	1805–1880	20	95	Y	Y
4	1710–1755	2110–2155	355	400	Y	Y
5	824–849	869–894	20	45	Y	Y
6	830–840	875–885	35	45	Y	Y
7	2500–2570	2620–2690	50	120	Y	Y
8	880–915	925–960	10	45	Y	Y
9	1749.9–1784.9	1844.9–1879.9	60	95	Y	Y
10	1710–1770	2110–2170	340	400	Y	Y
11	1427.9–1452.9	1475.9–1500.9	23	48	Y	Y
12	698–716	728–746	12	30	Y	Y
13	777–787	746–756	21	31	Y	Y
14	788–798	758–768	20	30	Y	Y
17	704–716	734–746	18	30	N	Y

Figure 2.1: UMTS and LTE frequency bands for FDD, [38]

2.1.2 Voltage standing wave ratio

According to the Cellular Telecommunications and Internet Association (CTIA) specifications [39], the requirement is VSWR$\leq$3 (see definition in Appendix A.1).

2.1.3 Antenna efficiency

Typical values for the total antenna efficiency are in the range between 70% and 80% [19].

2.1.4 Gain

One of the weak points of the small antennas is its low gain compared to the traditional fixed antennas used for reception of television and radio. Due to the fact that the directivity and therefore the gain are proportional to the size of the antenna, for small antennas typical values of the gain are around 1.76 dBi. It means that the sensitivity in the direction of maximum propagation is only around 1.5 times greater than for an isotropic antenna with the same input power.

2.2 State of the art

The rapid development of electronics and wireless communications have led to an ever-increasing demand for mobile devices that can operate in different standards such as GSM850 (824-894 MHz), GSM900 (880-960 MHz), Global Positioning System (GPS) (1575 MHz), Digital Communication System (DCS) (1710-1880 MHz), Personal Communications Service (PCS) (1850-1990 MHz), UMTS (1920-2170 MHz), the Local Area Network (LAN) (2400-2484 MHz) or LTE (2500-2690 MHz). The latter has become a very popular standard nowadays since users demand multimedia services and low latency and LTE provides the high data rate required for this goal. This is achieved by using MIMO systems with spatial multiplexing. However, MIMO antenna design is a big challenge due to spatial limitations. Firstly, antennas must not occupy the entire PCB since it has to be space available to place other components. Secondly, mutual coupling introduced by closely MIMO antennas must be minimized since it degrades the total efficiency of the system. As reminder of the problem definition, the goal is to design an antenna that is

LTE band	Downlink bandwidth	Channel bandwidth (MHz)					
		1.4	3	5	10	15	20
1	60	—	—	12	6	4	3
2	60	42	20	12	6	[4]	[3]
3	75	53	23	15	7	[5]	[3]
4	45	32	15	9	4	3	2
5	25	17	8	5	[2]	—	—
6	10	—	—	2	[1]	X	X
7	70	—	—	14	7	4	[3]
8	35	25	11	7	[3]	—	—
9	35	—	—	7	3	[2]	[1]
10	60	—	—	12	6	4	3
11	25	—	—	5	[2]	[1]	[1]
12	18	12	6	[3]	[1]	—	X
13	10	7	3	[2]	[1]	X	X
14	10	7	3	[2]	[1]	X	X
...							
17	12	8	4	[2]	[1]	X	X
...							
33	20	—	—	4	2	1	1
34	15	—	—	3	1	1	X
35	60	42	20	12	6	4	3
36	60	42	20	12	6	4	3
37	20	—	—	4	2	1	1
38	50	—	—	10	5	—	—
39	40	—	—	8	4	3	2
40	100	—	—	—	10	6	5

Figure 2.2: Number of supported non-overlapping channels in each frequency band and bandwidth. [38]

spatially efficient, highly decoupled and tunable for any kind of mobile device format. Since mobile phones usually need to operate on two or more bands simultaneously, these three challenges have to be fulfilled for a multiband system with two simultaneous operating bands as it was detailed in section 2.1.1. In the next subsection several published techniques to deal with the three issues introduced before will be presented in the chronological order followed until reaching the final design.

2.2.1 Chronology of the system based on scientific papers

In this paragraph, it is presented the procedure followed until the final models were achieved. The details of these models will be presented and detailed in section 2.3.

Shrinking techniques over horizontal designs

The first attempt for designing an antenna usually consists on trying to implement a basic IFA on the top of the PCB, with the GP beneath the antenna. With this kind of design the bandwidth requirements presented in section 2.1.1 are fulfilled. It is well known from section 1.4, that the resonant part of the antenna has to be approximately $\lambda/4$ to make the antenna resonate at the desired frequency. This is an important constraint when designing the antenna, since for low frequencies and small size devices, the antenna has to be shrunken, otherwise it will not fit in the PCB dimensions. An antenna can be shrunken by folding it while keeping the same physical length. As it was presented in section 1.4, a straight IFA has a RLC Thevenin circuit associated, so every time the antenna is folded, the effect in the Thevenin circuit is equivalent to have another RLC circuit in series with the previous. Thus, every time the antenna is folded the Thevenin equivalent circuit is modified. Since the resonant frequency is given by equation 1.14, then folding the antenna affects not only the input impedance and therefore the reflection coefficient, but also the resonant frequency.

It is evident that the less the antenna is folded, the easier is to extract an equivalent circuit model. However, when the PCB acts as spatial constraint, then designers are forced to use shrinking techniques. IFA antennas with two or three arms can easily be modeled providing high bandwidth performance, but for low frequencies and small size formats both the spatial efficiency and the high decoupling goals are not complied. This leads designers to come up with multi-folded designs such as meandered lines; or lateral designs where straight IFA lines can be built without occupying the PCB surface.

It was shown in [40] that a Straight-Line Dipole Antenna (SLDA) resonates when the imaginary part of its input impedance is equal to zero. This occurs when the length of the line is slightly less than $\lambda/4$ at the frequency of operation. In [41], the authors have analyzed the impact of a meandered dipole antenna on the resonant frequency, by comparing a SLDA with a Meandered-Line Dipole Antenna (MLDA). Previously, other works like [42], [43], [44] had shown that bending the antenna while keeping the same mechanical length than the SLDA lowers the resonant frequency, but in [41] a further investigation in the evolution of the resonant frequency while bending the antenna is carried out. Even though the analysis was done for antennas operating in the Very High Frequency (VHF) band, it can be concluded that adding bends to SLDA producing a MLDA, is an effective way to lower the resonant frequency. However, the magnitude of the shifts diminishes with each additional fold. therefore in order to keep the same resonant frequency as the SLDA or a simple-folded antenna with few folds, the MLDA has to increased its mechanical length, but usually it still occupies less area than a simple-folded antenna.

Lateral designs

Recent studies have determined that antennas should be placed at the edges or the corners of the PCB. Since the electric field created by the PCB leads to maximal resonant modes, these positions are considered in [45], the best to investigate. The source of the antenna should then be in the corner and the straight resonating wire whose length is $\lambda/4$ should be placed along the PCB. The resonating arm has a better input impedance matching when it is design on the side of the PCB instead of the top. To respect the requirements of a small phone, the height of the antenna should not exceed a certain length. The difficulty with the lateral design is that the height of the antenna should be taken into account while calculating the width of the PCB. The implementation of the multiband in the lateral IFA antenna is required to support multiple performances and standards. Many studies were focused on the design of IFA for multiband operation in the mobile phone such

as [46] or [47]. The design of the multiband should respect the phone and antenna requirements but also the properties of the first designed band. The longest arm operates in the lower band and the shortest arm in the higher band. The next step after a multiband model is the implementation and analyze of MIMO to improve the performance of the system by adding another antenna on the PCB. The impact on antenna placement is analyzed in [48] and the best place to put these antennas is symmetrical to each other.

In the previous paragraphs it was described the different techniques considered to make the antenna spatially efficient. But in order to deal with the three main challenges presented before, tuning and decoupling techniques have to be added to the model.

Tuning techniques

As it was pointed out before, mobile devices demand that antennas operate at many frequency bands. It means that the antenna demands a reconfigurability. As the term suggest, reconfigurability employ some kind of variability. There are many ways of reconfiguring an antenna, including: [49]

- resonant mode switching/tuning (via shorting, reactive loading);
- feed network switching/tuning;
- mechanical reconfiguration (with moving parts)

In this work, we are interested in the resonant mode tuning. In the literature, it is possible to find many effective ways of tuning a multiband antenna such as adding parasitic elements to PIFA antennas [50],[51] or by adding more radiating elements share with the same feed and ground [52]. The main drawback of these techniques is that the overall antenna size is increased, so there is a tradeoff between extra operating bands and antenna size. However there are other works where extra frequency bands were achieved without decreasing the antenna size. For example, in [53] the author proposes a reconfigurable antenna that can reuse its entire volume to make the antenna resonate at different operating frequencies. The concept is that each operating band resonates on a portion of or the entire antenna geometry, without almost no extra antenna size needed. In [54] a tuning diode is placed in between the two radiating elements of the PIFA, so frequency shifts are achieved by varying the capacitance of the tuning diode with a wide tunable range since the frequency range simulated is equal to 55%. In [55], a slot is inserted in the antenna geometry and its effective length is controlled by PIN diodes located across the slot, so again, frequency shift is achieved without increasing the antenna size. Another solution of the same kind is presented in [56], where a group of antenna elements is arranged relative to a ground plane. Frequency shifts can be achieved by connecting or disconnecting one or more of these elements. Definitely, the alternatives presented before play either with the mechanical size or with the effective length of a slot. However, the main drawback of these techniques is that they are suitable for a single operating band only, and as it was explained, we aim to find suitable solutions for multiband systems.

In [57], Mak presents two suitable solutions for multiband systems over PIFA antennas. One solution consists on switching different feeding locations of the antenna (switched feed) while the other one consists on switching or breaking of the antenna's connection to the ground (switched ground). In the switched feed design, the overall antenna consists of an antenna element with a slot (PIFA antenna), a GP, and an switching network, which can select the position of the feed. The concept is that depending upon the position of the feed, the excited modes are different and therefore the resonant frequencies too. With this method, three different frequency bands can be

achieved, the lower frequency is always the same regardless the position of the feed while the higher frequency is shifted. In the switched ground design, the concept is similar, but in this case the different modes are arisen depending upon whether the connection between antenna elements and GP is broken or made. Again, the lower resonant frequency is the same regardless the connection, while the higher resonant frequency depends on the slot length when the connection is made and on the shorter arm length when the connection is broken.

Finally, in some other works like [58], [59], Langley proposes tunable matching circuits, which can provide extra tuning range with impedance match improvement. These tuning circuits are based in capacitive fed plates to build a reconfigurable antenna. The antenna can be either multi-port or single-port and both of them were verified to be suitable for the aim of this thesis. For simplicity, we focus the tuning techniques design in single-port capacitive circuits.

Decoupling techniques

When we insert another antenna on a small mobile phone equipments, the questions that comes directly to our mind are: How can you isolate one antenna from the other ? What are the parameters to study for knowing the effects of two closely spaced antennas ? What is the minimal distance that can be achieved between two antennas in order to avoid the coupling ?
There are different techniques to improve the isolation between antennas, some researchers present in [60] one of them but this will not be the main issue in this thesis. However, to obtain a good isolation or a low mutual coupling, the separation distance between a two-antennas system should be at least one half of the wavelength in free space. Since usually this configuration is not possible due to the small size of the phone, the effort will be concentrated on the reduction on mutual coupling instead of improving the isolation. An uncountable number of scientific papers have been published on how to reduce the mutual coupling between two antennas but not all of them can be applied in this thesis. Before explaining some of the techniques, it is important to define the parameters that will be analyzed. The first criteria is the scattering parameter S_{21} or S_{12}, respectively the forward and reverse voltage gain in dB. The last parameter is the total efficiency defined in subsection 1.3.1. It represents the relation between the power delivered by the source in the system and the power radiated after losses due to coupling.

The reduction of mutual coupling represent a hard task and most of the scientific papers are about a specific configuration regrouping different bands and a special type of antenna but there are some very interesting papers about simple decoupling techniques that will be presented here in three different groups.

The first group is about the techniques where the antennas are directly concerned. The connecting strips is a technique presented in [61] where the goal is to link a suspended wire with particular length or width between the two antennas by connecting together either the two shorting or feeding points like in [62]. Several antenna configurations have been examined and the conclusion is that the shorting strip is beneficial for reducing the coupling only if the antennas have a large frequency separation like DCS and UMTS in [63]. A novel similar technique suitable for a two-antennas very compact system consist in connecting each antennas to the ground plane with a strip as explained in [64]. Instead of going straight from one antenna to another, the current is now forced to take another path which will isolated the feeding points. Through these folded wires on each side of the antennas, this paper presents a solution of neutralization which is more relevant for isolation than reduction of coupling between antennas but sometimes mutual coupling can be beneficial for diversity performance like in [60]. Alternatives from different groups to reduce the coupling are presented in [65] and have the same results. Whether there is an interconnection

between the antenna ports and a matching network or whether a parasitic antenna is placed in the middle of the coupled antennas, the obtained decoupling results will be the same. This leads to a synthesis technique explained in [66] that significantly reduced mutual coupling by replacing all antennas by a S-matrix. Each antenna is reduced to a two-port circuit by connecting them together with coupling path, the reduction of the coupling is significant.

The second group includes the decoupling techniques related to changes in the ground plane. Instead of connecting the antennas together or to the PCB, researches have been made about the modification of the ground plane and it is possible to reduce mutual coupling by using a T-shape slot on the PCB and a decoupling slot like in [67]. In this paper, a T-shape slot is indeed inserted to transform the impedance of the decoupling slot. This method can be applied to multiband MIMO systems using a folded L-shape slot, which can be matched thanks to the T-shape slot which is, tuning the L-shape slot impedance. Defected ground planes presented in [68] and [69] is a technique which comprises inserting in the middle of the PCB, several pairs of slits having different widths and lengths and separated with metal strips for the conduction. A good reduction of coupling is obtained in these papers by combining capacitance and inductance between the slits. A novel design for reducing mutual coupling in handset antennas is also explained in [70]. The innovation concern the double slots of a quarter wavelength each designed on the PCB to block the current and then reduced the coupling. The problem is that the antennas need to be retuned by placing capacitors between the ground plane and each antenna. The encountered problem with these ground plane modifications is that despite the reduction of mutual coupling, the impedance bandwidth is significantly decreased and the technique uses a lot of space on the PCB.

The last group concerns the reduction of decoupling by inserting parasitic elements of different length and thickness on the ground plane. Even though the parasitic elements are not directly connected to the antennas, they can still provide good decoupling fields like in [60]. The same idea is developed in [71] with parasitic scatterer, this time the author used a loaded parasitic antenna acting like a protection shield between the two antennas. The coupling is truly reduced by tuning all the parasitic and antenna elements but the bandwidth also decreased which is not a good compromise. Parasitic element are also used for isolation enhancement between antennas like in [72] or bandwidth enhancement like in [73] but our attention will be concentrated in [74] with a parasitic element that creates reverse coupling to cancel mutual coupling. These parasitic elements generate two coupling paths, the original and the double-coupling one. With the expression of the coupling current, they obtained the coupling coefficients for this double-coupling path. By respecting the configurations of the system and changing the coupling coefficients, the created reverse coupling reduces the mutual coupling. Parasitic elements can be a good alternative to resolve the coupling even though they occupied a more or less important space between antennas.

2.2.2 Background of our investigation: IEEE Published methods selected

Shrinking techniques over horizontal designs

As it was discussed in 2.2.1 we concentrate on designing a MLDA since it is one of the best approaches to minimize the mechanical antenna size. One of the most relevant features of these kind of antennas is that they decrease the resonant frequency compared to a SLDA with the same mechanical size [41]. Previous works like [75] proposed Electrically Small Antenna (ESA) designs based on Meander Line Antennas (MLA) but they are not suitable for low frequency bands under 1 GHz. In [76], a single MLA designed to resonate around 850 MHz and with at least 100 MHz of bandwidth is presented. The geometry of the single MLA is shown in Figure 2.3. Antenna dimensions were optimized by using a software. The antenna was proved to be very spatially efficient

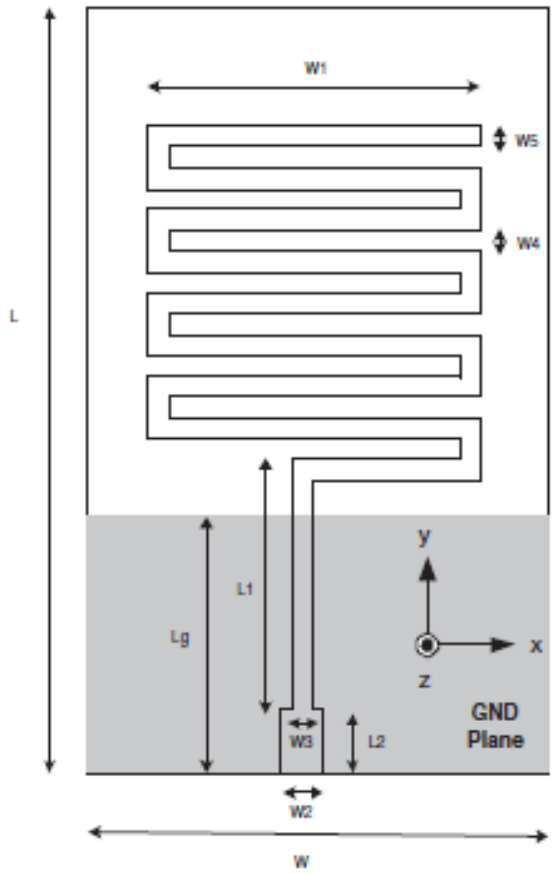

Figure 2.3: Geometry of the single meander line ESA, [76]

since it only consumes 1/4 of a regular mobile terminal. This aspect is capital, in order to provide MIMO capability. With the single antenna it was measured a bandwidth under $|S_{11}|$=-10 dB equal to 185 MHz at resonant frequency equal to 897 MHz. In the MIMO configuration measurements do not provide the same results in both antennas due to the tolerances of the connectors used but in average it provides a bandwidth under $|S_{11}|$=-10 dB around 150 MHz at resonant frequency around 830 MHz.

Lateral design

The characteristics of the lateral IFA design was detailed in the section 1.4 as low-profile, low-cost, efficient and easy to manufacture. Once the antenna designed, the goal is to implement a MIMO system by finding the lowest coupling position for the second identical antenna.

The configurations presented in [68] are really close to our requirements. Indeed, this paper relates a diversity system with two IFAs resonating at 5.2 GHz with flexible tuning and a large bandwidth. During the simulations where one antenna was fed and the other was open-circuited, the effect of four different antenna placement presented in Figure 2.4 was analyzed to understand the impact on the performance of the system. With the figures 2.4(a) and 2.4(b), deeper resonances are obtained. Moreover, if the distance d increases in 2.4(b), the electrical length between antennas will decrease.

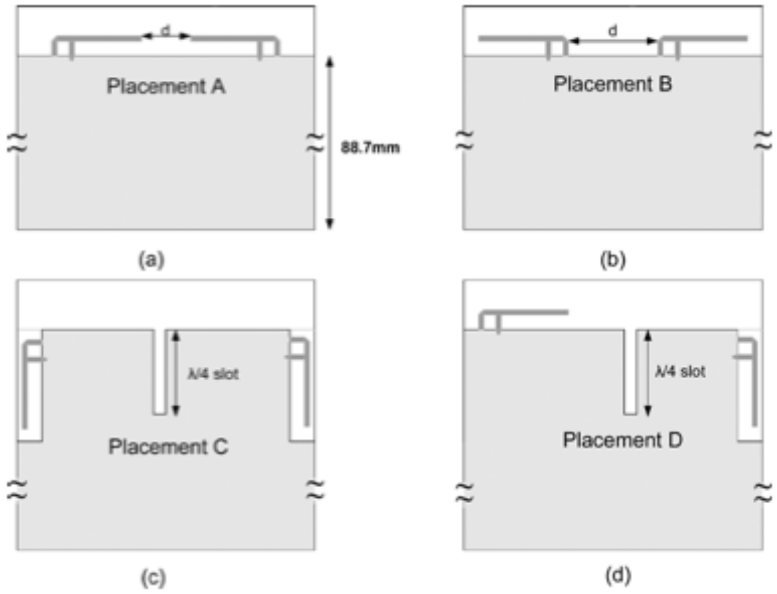

Figure 2.4: Placement of IFA antennas in MIMO system, [68]

The $|S_{21}|$ values shows that Figures 2.4(c) and 2.4(d) are preferable options, especially Figure 2.4(c) which achieve the lowest coupling coefficient. The antenna place is indeed a really important parameter and the impact on the system performance is not negligible.

Tuning techniques

As it was introduced in 2.2.1, the implementation of tuning techniques with capacitive circuits is one of the main goals, since they are simple to implement, but also effective to fulfill the bandwidth requirements. Figure 2.5 represents a sketch of resonant mode tuning over a PIFA by using a variable capacitor. When the capacitance increases, the antenna resonant frequency decreases with the penalty of reduced bandwidth. The capacitor is located at the point on the antenna where the electric field is the highest, which gives the highest possible resonant frequency tuning ratio for a given capacitance variation [77]. In [58], Langley shows the good tuning performance of a Microelectromechanical Systems (MEMS) switching structure mounted over a PIFA antenna.

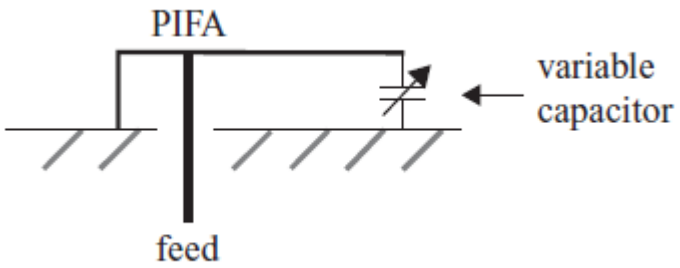

Figure 2.5: Sketch of a PIFA tuned by a variable capacitance, [77]

The geometry of the antenna can be observed in Figure 2.6. The switching configuration consists on four MEMS, two (1 and 2) mounted on two shorting strips, and other two (3 and 4) mounted on the main plate. By controlling the four MEMS switches seven different frequency bands were achieved, as observed in the $|S_{11}|$ parameter graph shown in Figure 2.7.

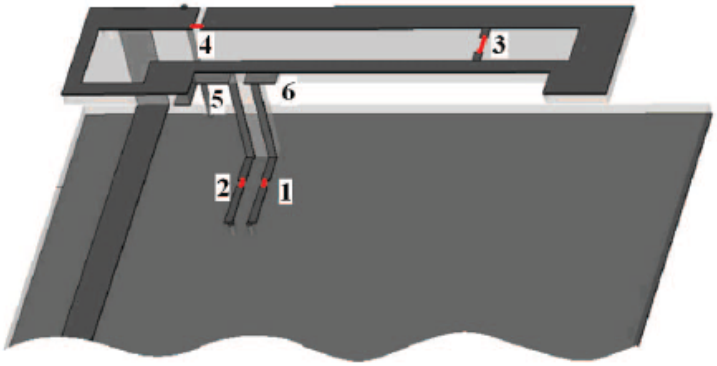

Figure 2.6: MEMS switching reconfigurable PIFA geometry, [58]

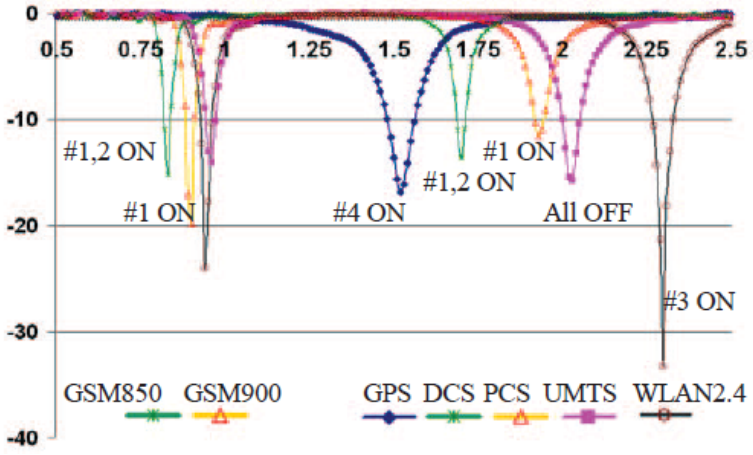

Figure 2.7: Simulated reflection coefficient for reconfigurable PIFA and switching combinations [58]

In applications where a large tuning range is needed, like for example, the integration of a Digital Video Broadcasting - Handheld (DVB-H) antenna into a mobile phone terminal, Langey presented in [58] and [59] a suitable solution which consists of a single-port reconfigurable PIFA antenna with tunable capacitive matching circuit. In Figure 2.8 this geometry can be observed. The matching circuit is composed by a variable capacitor across one gap of the patch which can tune the electrical length of the antenna obtaining the large tuning range required. It was tested that the antenna, created to resonate around 2 GHz by itself, provides a tunable frequency range over 75% with tuning capacitor range values from 1.5 pF to 42 pF. However the challenge is to develop a circuit requiring a lower range of variable capacitance. That is the reason why in the geometry shown in Figure 2.8, a solid wire was used to achieve the largest capacitance in test since variable capacitors with such a large tunability are not still commercially available.

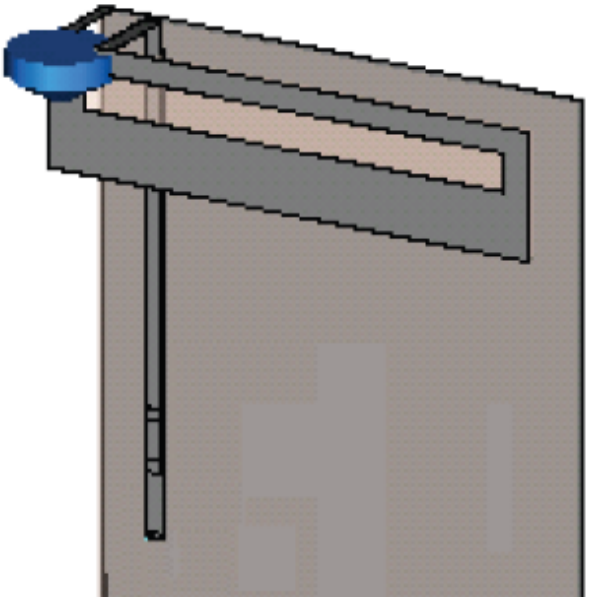

Figure 2.8: Geometry of tunable handset antenna, [59]

Decoupling techniques

A selection of good decoupling techniques were classified in 2.2.1 into three groups namely connecting antennas, modified ground plane and parasitic elements. The techniques about the isolation between antennas or the decoupling using a defected ground plane will not be detailed further due to the impact on the bandwidth and the complexity in terms of manufacturing and measurements in the laboratory. To respect the requirements of our design, only the techniques using a connecting strip or a parasitic element will be developed in this section.

Some decoupling techniques that seems promising for multiband MIMO design are presented in [61] and consists of connecting either the two shorting or feeding points together with a suspended wire. This paper is dealing with two PIFAs operating in the DCS1800 and UMTS bands. To analyze the coupling, the two PIFAs are place on the top of the PCB where there is the lowest coupling. The configuration of the antennas varies with either the shorting or the feeding strips facing each other, see Figure 2.9. By inserting a line between the antennas feeding or shorting points, the idea was to generate an opposite coupling in order to compensate the one already existing. The short or the source are chosen for two reasons, first these points are far away from the open-arm of the antenna where the impedance is low and second, the intensity of the currents is maximum around those points. Moreover, the resonant frequencies and the bandwidths of these antennas are not affected. In order to achieve a low mutual coupling at a given resonance frequency, the parameters such as the width or the length of the connecting wire have to be perfectly chosen.

This connecting strip is a wire which neutralizes a part of the UMTS signal and carry it back to the DCS band producing a reverse coupling which reduce significantly the $\mid S_{21} \mid$ parameter, the graph in Figure 2.10 presents the results.

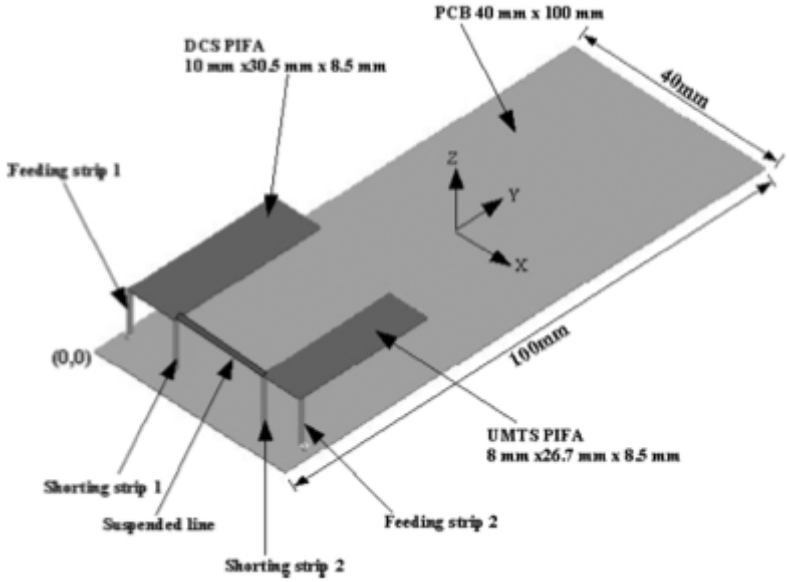

Figure 2.9: PIFAs when the shorting strips are facing and connected with suspended wire, [61]

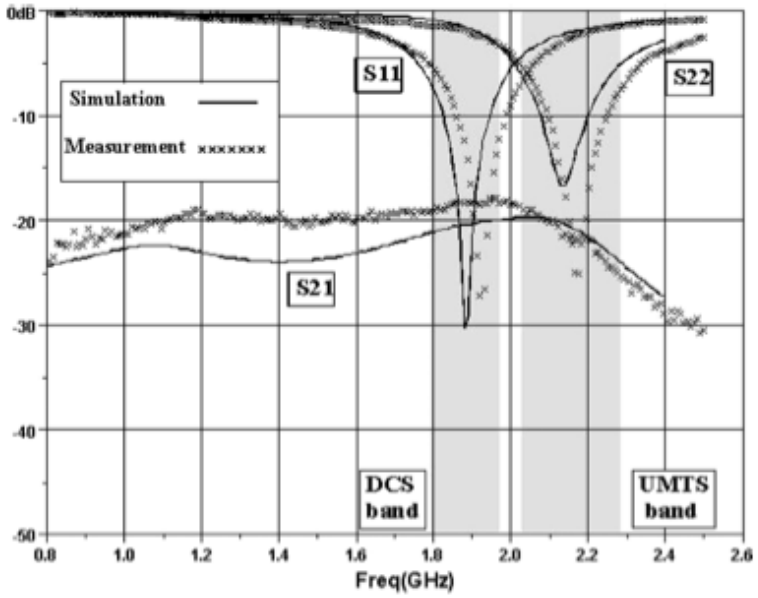

Figure 2.10: Simulated and measured $\mid S_{11} \mid$, $\mid S_{22} \mid$ and $\mid S_{21} \mid$ of the PIFA when the shorting strips are facing and linked by a suspended wire, [61]

With the shorting strips method, the $\mid S_{21} \mid$ curve is flat for the measurements and always under the coupling requirements of -20dB instead of a maximum value of -10dB without decoupling technique. For the same design with and without a shorting wire, the total efficiencies improve from 10% and 15.8% for the DSC and UMTS respectively. As an improvement for small ground planes in term of decoupling, this technique is very interesting, simple to design, efficient and low-cost. Another published method in [74] could be relevant for designing our system, the technique is using parasitic elements to reduce the coupling between antennas. The principle exposed in Figure 2.11 is simple and could be applied easily for a two-IFA system.

At first, two close antennas are designed in 2.11(a), antenna 1 is excited by a current I_0 and antenna 2 is coupled in the same time by the same current I_0, multiplied by a coupling coefficient a.

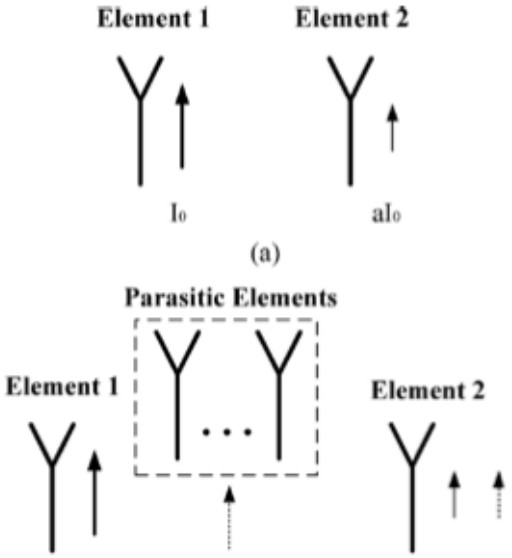

Figure 2.11: Simplified model for reducing mutual coupling, [74]

Some parasitic elements are then added between the antennas for the decoupling model, as it is shown in Figure 2.11(b). Two coupling paths are now formed, the original coupling path aI_0 and the double-coupling path. In the double-coupling path, the current is coupled from antenna 1 to the parasitic elements and then from the parasitic elements to antenna 2. The mutual coupling can then be expressed in the equation 2.1.

$$aI_0 + b^2 I_0 = 0 \tag{2.1}$$

where b is the average coupling coefficient, bI_0 is the equivalent coupling current and $b^2 I_0$ is the coupled current on antenna 2.

This technique is very useful to calculate the mutual coupling and then reduce this coupling by using parasitic elements to create a reverse coupling.

2.3 Presentation of the models selected

In order to isolate and understand fully the contribution of the tuning and decoupling techniques, each of them will be tested by separate over the two different models achieved. Therefore, tuning techniques will be tested over the meandered line design, while the decoupling techniques will be tested over the lateral design. The reason why this selection was chosen will be explained in the next chapter.

2.3.1 The requirements

The goal of this master thesis is to create and implement a tunable and decoupled antenna design on different size of communication equipments. The final antenna's design needs to deal with different requirements:

- Design: Small inverted-F antenna in terms of structure volume and space consumption on the PCB but also efficient radiation properties.
- Multi band and MIMO: The system should access to multiband operations and the characteristics of MIMO systems must be respected.
- Tunable: The bandwidth coverage must be as wide as possible by using tuning techniques.
- Decoupled: The current running from one antenna to another must be reduced by using decoupling techniques, to achieve a good performance.

2.3.2 The methods

It was introduced in previous sub-sections in this chapter that the PCB size is a big constraint specially for low frequency operating bands and small size formats. This is considered to be the worst scenario possible, due to the fact that the bigger is the surface occupied by the antennas on the PCB, the less is the space available to place other components. Moreover, for finite ground planes, even though it cannot be always ensured that the further the antennas are from each other the less coupled they are, the tendency of the decoupling level as function of the ground plane size is decreasing. MLAs were proved to be an efficient solution for these kind of systems, since they can reach the same resonant frequency as a Straight Line Antenna (SLA) occupying less mechanical section . However, for high band systems the PCB size is not used to be a big challenge since the antennas are electrically smaller. Therefore, an hybrid design will be implemented in this thesis.

Shrinking and tuning techniques

The design consists of a meander line and a two-arm line for the low band operating frequencies and high band operating frequencies, respectively. The motivation for selecting this design is due to the aim to find a solution which can deal the spatial efficiency while fulfilling the industry requirements presented in section 2.1.The antenna is fed by a single port and it consists of two lines; a meander line for the low frequency operating band and a two-straight-arms line for the high frequency operating band. These two lines have to be reasonably far away from each other since otherwise the coupling produced between them will contaminate the high resonant frequency band. But it can occur that in the worst case, the PCB size is so small that the meander line has to be folded back towards the straight line in order to deal with reasonable separation requirement.

The geometry proposed is also composed of three capacitive elements, one placed across the meandered line and the other across the straight line. They are fix-value capacitors, but in fact they represent variable capacitors, such as MEMS, which are proved to provide very good performance in mobile phones antennas, so from now on the capacitors represented in the geometries can be assumed to be MEMS. These capacitors provide tunability to the antenna. One MEMS placed across the meandered line tunes the low frequency operating band to other lower frequency operating bands while the other one is placed across the straight line tunes the high frequency operating band to other lower frequency operating bands. The biggest challenge while tuning is to deal with the multiband aspect. Frequency bands are required to be shifted simultaneously. Thus, the aim is to find the proper place where to place the capacitor on both lines and to achieve the largest tuning frequency range possible with the lowest capacitance range possible since too large capacitor values are not commercially available.

Lateral design and decoupling techniques

Before providing our lateral design, it was important to read as much scientific papers as possible related on multiband IFA and MIMO. Our design will be based on the papers presented in section 2.2.1. The lateral configuration was selected because it is the emplacement were the coupling is the lowest, [68]. To create a multiband antenna, the high band arm was added to the low band arm already existing and the idea for this design was inspirited by [78].

Reducing the mutual coupling between antennas requires a good knowledge about antenna design; many different techniques will be implemented based on the papers cited in section 2.2.1. The first technique is the connecting strip and consists in connecting together the two feeding or shorting points of the antennas in order to intercept the current running from one antenna to the other. The goal is to use the connection with the first antenna to cancel out the mutual coupling with the second antenna. The strip have approximately the same length as the width of the PCB and the height of this suspending wire is 2mm. This technique is effective in our lateral design but not for both frequency bands that is why another technique will also be implemented, the defected ground plane. The principle is simple and consists in creating a slot in the middle of the PCB with a specific length but the space consumption of this method is slightly compromised since the slot can not be covered by metal, so no other components can be added. The last technique that seems really promising for our lateral antenna is the parasitic elements and consists in adding on the PCB a parasitic element composed of two linked wires, the short and the resonance part and the goal is to find the perfect matching between the parasitic element and the resonance frequency of the band we want to decoupled.

Chapter 3

Simulations

3.1 Simulations parameters

3.1.1 Software

Designed on the FDTD software, the simulations are running on the Matlab FDTD kernel. For the designs with maximum two sources, the program chooses automatically the parallel Fortran kernel *fdtdpar.exe* running on Aalborg University's hybrid cluster *Fyrkat*.
The first step after designing the model is to save a *.in* file and **Deploy**, then this file is added on the *tasklist.txt* and the next step **Submit to queue** consists in submitting this file to the scheduler queue. Once the simulation has been compiled, the *.in* file disappears from the *tasklist.txt* and an *.out* file is created by the Fortran kernel. The last step **Collect** permits to load this *.out* file into Matlab and locked the data. Different software parameters presented in Figures 3.1(a) and 3.1(b) can be modified before launching simulations. In Figure 3.1(a), the Perfectly Matched Layers (PML) parameters are defined such as the depth of the PML 8 cells but also the grading order and the maxima of *sigma*, *kappa* and *a*. In Figure 3.1(b), the cell size is fixed to 1mm and represents the dimensions of the Yee cube. The frequency resolution is 1MHz and represents the smallest step of the frequency domain results for the S_{11} parameter. The termination condition influences the running time and the accuracy of the results. The maximum time steps are fixed at 200000 and the simulation will stop after both the energy in the source or the total energy excluding the source drops under -60dB. Other parameters such as the excitation pulse and the domain boundaries can also be modified. The last parameters concern the activity during the FDTD simulation by enabling the near fields, far fields and the computation of energy with a step of 100.

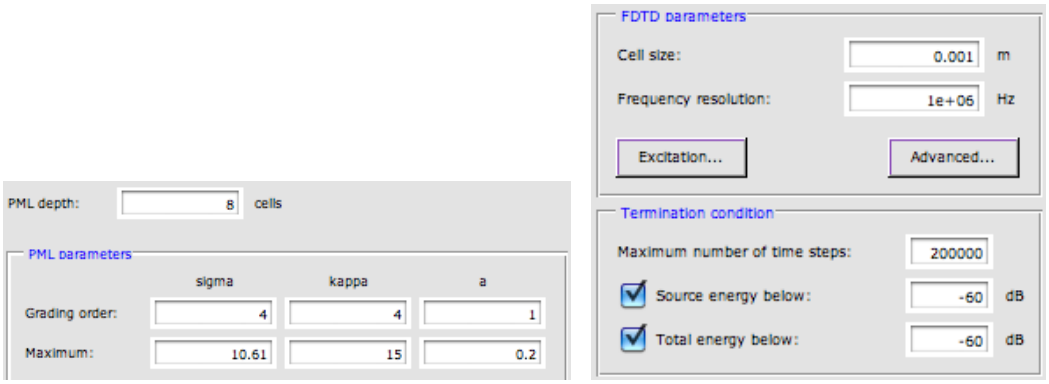

(a) Perfectly Matched Layer (b) FDTD Parameters

Figure 3.1: Simulations parameters (a) and (b)

3.1.2 Antenna models

Designs

This section introduces the final designs of our antennas in Figures 3.2(a) and 3.2(b). The models are resonating at the same frequencies in order to compare their efficiencies and performances. To build these antennas, wires with Perfect Electric Conductor (PEC) are used to obtain lossless simulations.

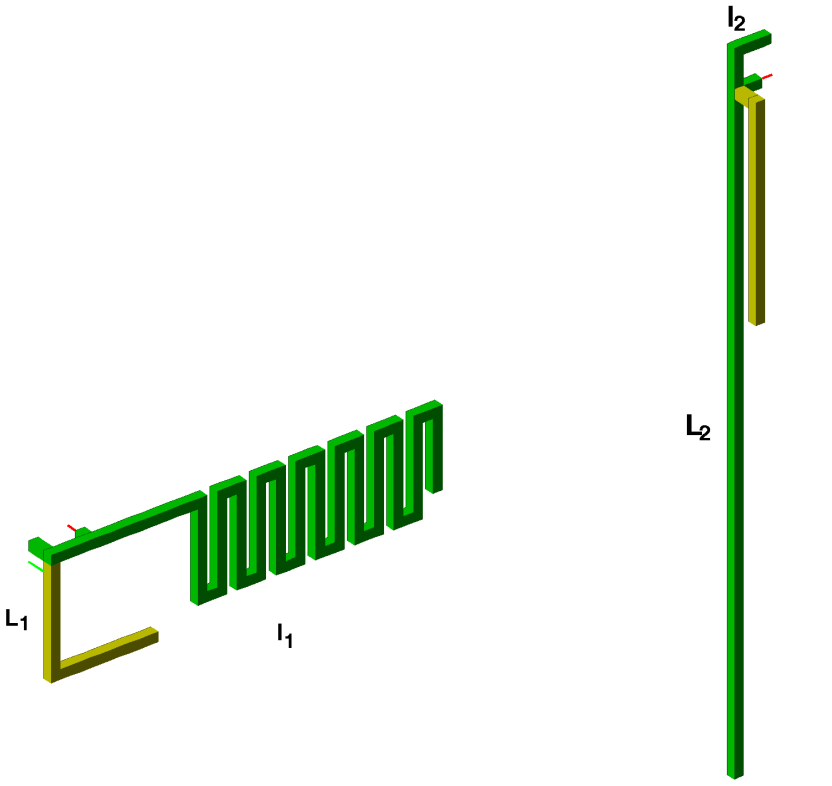

(a) meander antenna design (b) Lateral antenna design

Figure 3.2: Three dimensional view of the meander design (a) and the lateral design (b)

As it was commented in previous chapters, the terminal size is a big challenge for small devices which are supposed to operate at low frequencies. An antenna is considered to be good not only if it provides good antenna properties but also if it is spatially efficient. Then, manufacturers have more space to place other components on the PCB.

Definitely, the aim of finding a compact antenna leaded us to consider a meander design as the one shown in Figure 3.2(a). The height of the antenna (distance between antenna and PCB) is equal to 2mm, while the distance between short and source is equal to 3mm. The green wires represent the low band arm with a resonant part of 151mm, composed of six meander sections of 9x3mm each and separated by 1mm between them. The yellow wires represent the high band arm with a resonant part of 22mm, composed by two orthogonal wires of 12mm and 10mm respectively. Therefore, the total section occupied by the entire antenna is l_1=40 x L_1=12mm. Since the antenna system works in MIMO with two antennas, it means that 9.6cm^2 (4.8cm^{2}x2) out of the entire PCB area cannot be used to place other components.

The Figure 3.2(b) portrays a lateral antenna of 3mm height and 3mm between short and source. The green wires represent the low band arm with a straight resonance part of 67mm and the yellow orthogonal wires of 22mm and 2mm are for the high band with a resonance part of 24mm. The space between the two bands is 2mm to maintain the radiation performances and the matching of the low band. The total section occupied by this model l_2=4mm x L depends on the length L of the PCB presented later in Figures 3.5(a) and (b).

Basic conclusions

Despite several investigations already developed in the literature, a particular investigation about the impact of the IFA geometry on its performance has been conducted. There are three main parameters in the IFA antennas that affect the performance of the antenna: distance between short and source, total length and height. The goal is to optimize the performance once the desired resonant frequency has been achieved by changing the length of these parameters. Table 3.1 summarizes the effects of those three parameters on the resonance frequency but also the real and imaginary impedances of the antenna at resonance. The table shows the proportionality between the parameters. The behavior of the reflection coefficient and therefore, of the antenna bandwidth, can only be understood by looking at the input impedance evolution. Each PEC piece is equivalent to a RLC circuit. Whenever the geometry of this piece is modified, their RLC components are also affected. Depending on how much are these components affected, the impact on the antenna performance varies.

	$max\ (Re(Z_{in})$	$max\ (Im(Z_{in})$	$min\ (Im(Z_{in})$	f_r
Antenna Length	I	I	I	I
Antenna Height	D	I	I	I
Distance Short-Source	D	D	I	=
Capacitor	D	D	I	I

I: Inversely proportional; D: Directly proportional

Table 3.1: Basic conclusions of the antenna parameters

Besides the three main parameters mentioned, also the effects of mounting a capacitor between the antenna and the PCB are analyzed. Placing a capacitor is sometimes a smart solution in order to enlarge the bandwidth and also, as it was introduced before, it is one of the ways widely used to tune operating frequency bands. In order to understand better the evolution of the resonance frequency it is important to keep in mind the expression given by equation 1.14.
In the following, the effects of all these parameters will be explained in more detail:

- Antenna length: To study the effects of the length of the antenna, the height and the distance short-source will remain the same. When the length of the antenna increases, then the antenna impedance evolves toward the admittance-capacitive part of the Smith Chart at resonance. It means that the resonance frequency observed in Figure 3.3(b) is reduced, as consequence of an increase of the capacitance of the antenna. The maximum value of the real part of the impedance decreases while the range of the imaginary part is kept the same, but with lower average.

- Antenna Height: To study the effects of the height, the length and the distance short-source will remain the same. When the height of the antenna decreases, the resonance frequency

observed in Figure 3.3(c) increases, as consequence that the antenna impedance evolves toward the resistive-capacitive part of the Smith Chart at resonance. The maximum of the real part of the impedance increases while the range of the imaginary part is kept the same. The most relevant aspect of this parameter is its influence into the Q-factor and therefore, the bandwidth achievable by the antenna. The higher is the antenna, the lower is its Q-factor and consequently, the wider is its bandwidth. Figure 3.3(c) also shows this effect.

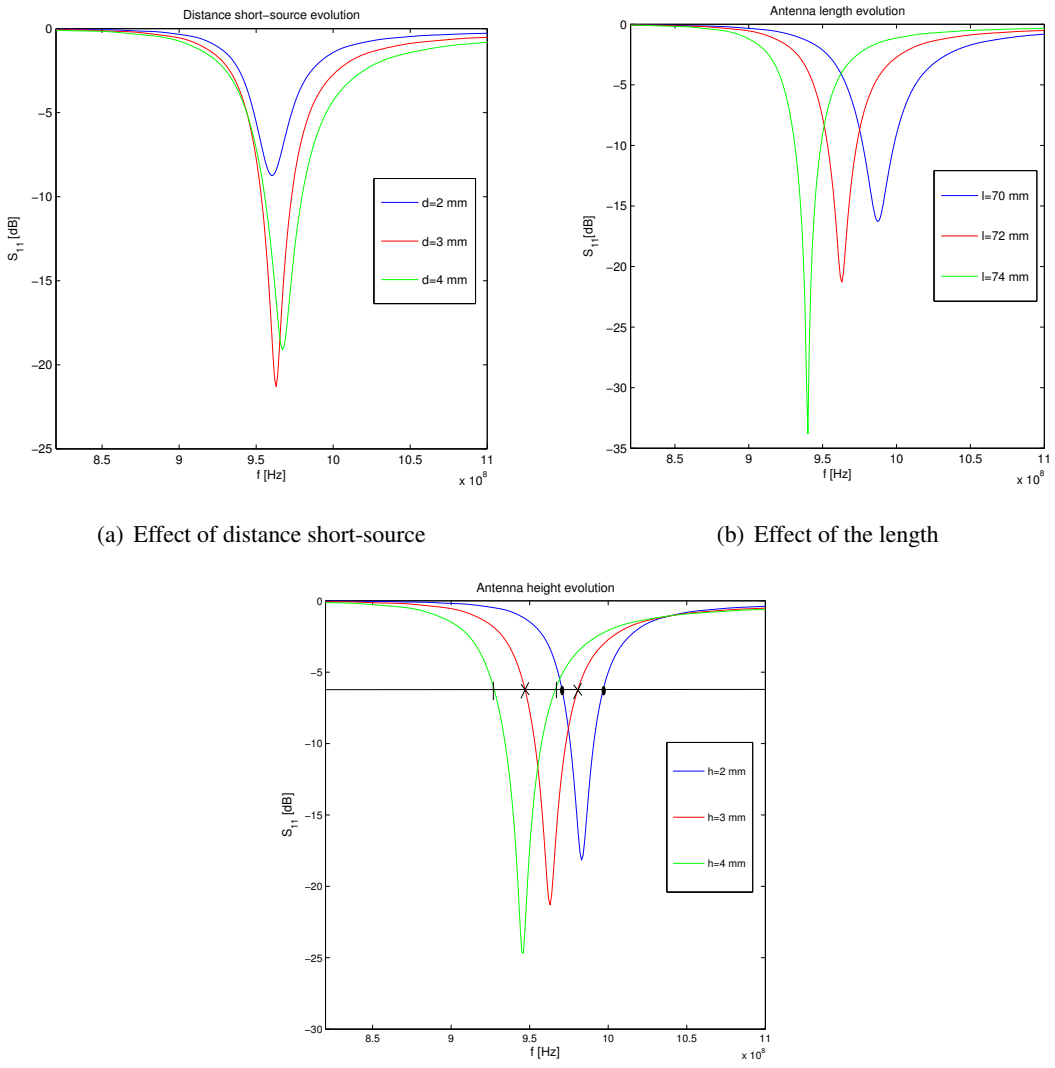

(a) Effect of distance short-source

(b) Effect of the length

(c) Effect of the height

Figure 3.3: S_{11} parameters of an IFA with distances short-source, lengths or heights different

- Distance Short-Source: To study the effects of the distance between the feeding point and the ground point, the height and the length of the antenna will remain the same. When the source is far away from the ground point, the resonance frequency observed in Figure 3.3(a) is higher, as consequence of a reduction of the length of the resonant antenna part. The distance between short and source is used to match the antenna as much as it is required, within the antenna bandwidth limitation given by its Q factor. While increasing this distance, the absolute value of the input impedance is also increased. It means that the circle of complex input impedances over the Smith Chart becomes bigger.

- Adding a Capacitor: If a capacitor is added into the antenna structure, the resonance frequency is decreased as consequence that the antenna impedance evolves toward the resistive-capacitive part of the Smith Chart at resonance. Both the maximum range values of the real and imaginary part of the input impedance are increased.

Parametric investigation of antenna position on the platform

In order to choose the proper position of one antenna on the PCB, an investigation was conducted with all possible positions for the models with SISO configuration. The most relevant criteria to make the decision was the bandwidth achieved. Figure 3.4 shows the evolution of the bandwidth when the antenna is placed in the twenty closer positions from the left superior corner over the models analyzed in section 3.2. Vertical and horizontal orientations of the PCB can be observed in Figures 3.5(a) and 3.7, respectively. Indeed, in the left superior corner the bandwidth is always the highest one. The investigation results over all the different positions where the antenna can be placed are presented in Appendix B.1, leading to the same conclusion.

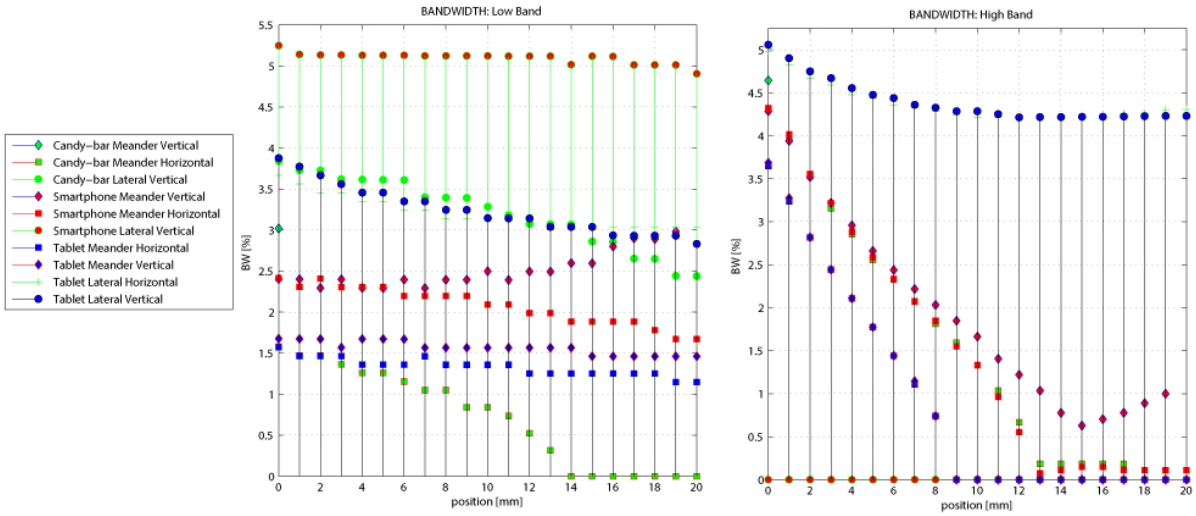

Figure 3.4: Evolution of the bandwidth for the first 20 positions of the antenna emplacement

Antenna orientation for MIMO

Once it is clear where to place the antenna for each of all the possible configurations, it is necessary to develop an analysis in order to optimize the performance over MIMO systems with two antennas. PCB can be oriented either in the horizontal or the vertical position while antennas can be placed either in mirror or opposite configurations. The mirror configuration is symmetrical with respect to a vertical axis placed in the middle of the PCB, while the opposite one is symmetrical with respect to an axis that matches the right superior corner with left inferior one, as is depicted, again, in Figures 3.5(a) and 3.7, respectively. Then, it is possible to make a decision on the final configuration selected for each PCB format. It is well known that the efficiency is function of the S_{11} and S_{21} parameters. The criteria chosen to select the configuration are not always the same, it can change depending upon the device. High bandwidth, high efficiency and low spatial consumption are the three main desired parameters. However, very rarely all of them can be achieved. This is the reason

why antenna designers have to prioritize according to the constraints of the systems. For instance, in small devices the most important constraint is the space, since an antenna with good performance is useless if it cannot be built within the PCB dimensions together with the rest of the components. When the space is not a big constraint, the criterion is chosen depending on the specifications of the device, but always dealing with the minimum requirements of bandwidth and efficiency in order to get a reliable communication. Thus, for devices which do not need to provide a wide bandwidth, the selection can be made in order to optimize the efficiency and vice versa. This is the reason why the configurations selected can be switched by others if the specifications requested deal better with them. The results of this analysis, presented in Appendix B.2 for both antenna models, lead to the following selected configurations:

- Meander antenna over Candybar format: vertical position and mirror configuration.
- Lateral antenna over Candybar format: vertical position and mirror configuration.
- Meander antenna over Smartphone format: horizontal position and opposite configuration.
- Lateral antenna over Smartphone format: vertical position and mirror configuration.
- Meander antenna over Tablet format: horizontal position and opposite configuration.
- Lateral antenna over Tablet format: vertical position and mirror configuration.

3.2 Parametrical studies

This section can be divided in two main parts presenting the results of parametrical studies about our antenna models. First, each model will be simulated in three different sizes of PCBs, taking into account the best positions and orientations of the antennas presented in Appendices B.1 and B.2 for each model. This section will also introduces a comparison table of both models device by device, but also an analysis about the impact of the form factor.

3.2.1 Initial model: Candybar

The Candybar format L=100 x W=40mm in Figures 3.5(a) and (b), is the smallest device to analyze and therefore the most difficult in terms of performance and efficiency since the antennas are really close to each other.

Designs

For the Candybar platform, the antennas are placed on the upper corner of the PCB with a mirror MIMO configuration for both models. The meander antennas in Figure 3.5(a) are horizontally oriented. The lateral antennas in 3.5(b) are straight along the side of the PCB.

As it was introduced in section 1.4, the total length of the IFA implemented is around $\lambda/4$, which is a large value for the low resonance frequencies except for meander designs, where the antennas have longer physical length, as it was presented in subsection 2.2.2. The expected resonance frequency is 970 MHz for the low band, then according to the theory, the length of the resonant part of the lateral antenna has to be around 77mm. If the antennas are very close to each other the mutual coupling might be high, then the best solution is to place them as further as the PCB size allows. In this case one antenna will be place on the top while the other one will be placed on the bottom. If the spatial

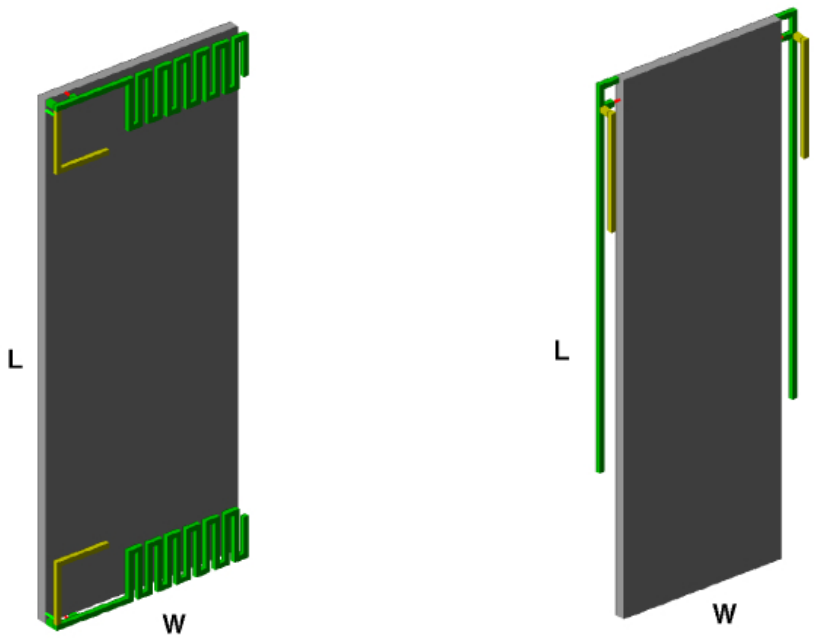

(a) Meander antennas implemented on the Candybar (b) Lateral antennas implemented on the Candybar

Figure 3.5: Three dimensional view of the meander design (a) and the lateral design (b)

efficiency is defined as the percentage of the PCB area that can be used to place other components, then the spatial efficiency of the meandered antenna over the Candybar format is equal to 76%, since 9.6cm^2 out of the 40cm^2 whole PCB area cannot be used to place other components. For the lateral model in the Candybar, one antenna occupies L=100 x $l_2 = 4mm$. The spatial efficiency is then equal to 80% since 8cm^2 out of the 40cm^2 whole PCB area cannot be used to place other components.

S-parameters

The S parameters for the meandering model are plotted in Figure 3.6 with the light blue and red curves for S_{11}, S_{22} and S_{21}, S_{12}, respectively. It can be observed that for both bands, the bandwidth requirements are fulfilled since 20 MHz are covered for the low band and 125 MHz for the high band, wider than 10MHz and 20MHz respectively. In term of decoupling, one of the strongest points of this model is the low coupling for high bands, with the $\mid S_{21} \mid$ under -20dB. Therefore, there is no need to implement any decoupling technique for the high band, which is an appreciable aspect for this model where the space is a big constraint. However, the weak point of this model is that for the low band, both antennas are badly decoupled. Thus, a strong decoupling technique should be implemented for the low band.

The S parameters of the lateral antenna model are plotted in Figure 3.6 with the green and dark blue curves for S_{11}, S_{22} and S_{21}, S_{12}, respectively. It can be observed that for both bands, the bandwidth requirements are fulfilled since 37MHz are covered for the low band and 258MHz for the high band, wider than 10MHz and 20MHz respectively. For the low band, the mutual coupling $\mid S_{21} \mid$ and $\mid S_{12} \mid$ are close to the acceptable decoupling threshold of -10dB and concerning the high band, the transmission coefficients $\mid S_{21} \mid$ and $\mid S_{12} \mid$ are not under the acceptable decoupling threshold of -20dB.

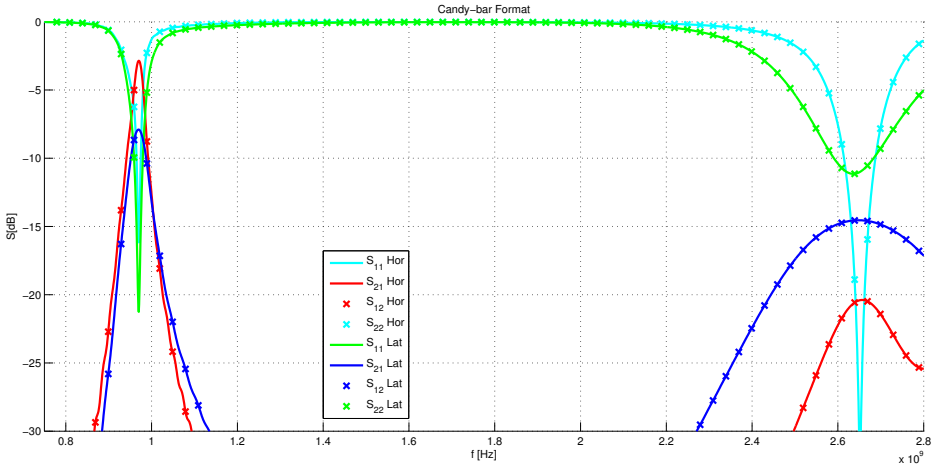

Figure 3.6: S-Parameters of both models implemented on the Candybar

Conclusions

Even-tough the two models resonate around the same frequencies in the low band and the high band, the Figure 3.6 reveals other parameters that can impact on the choice of a model. The meander design is interesting regarding the matching and the decoupling level of the high bands. If this model is selected, the mutual coupling of the low band only should be strongly reduced using a decoupling technique and, since the bandwidth for the high band is narrow, the coverage of a maximum range of frequencies using a tuning capacitor will be longer. The lateral design is interesting since the bandwidths are wider for both low bands and high bands so the coverage of different frequencies using a tuning capacitor will be easier. Moreover, the reduction of the coupling for the low band using a parasitic element will be easier since the mutual coupling level is close to the acceptable threshold.

3.2.2 Smartphone

The Smartphone format with L=119 x W=59mm (based on Figures 3.7 and 3.5(b)) is nowadays the most common used in the industry, with a touchscreen of the size of the PCB.

Designs

For the Smartphone platform, the antennas are placed on the upper corner of the PCB with an opposite MIMO configuration for the meander model and mirror configuration for the lateral one. The meandered antennas are horizontally oriented and the lateral antennas are placed along the side of the PCB. The spatial efficiency of the meandered antenna over the Smartphone format is equal to 86.3%, since 9.6cm^2 out of the 70.2cm^2 whole PCB area cannot be used to place other components. For the lateral model in the Smartphone, one antenna occupies L=119 x $l_2 = 4mm$. The spatial efficiency is then equal to 86.4% since 9.52cm^2 out of the 70.2cm^2 whole PCB area cannot be used to place other components.

S-parameters

The S parameters for the meander model are plotted in Figure 3.8 with the light blue and red curves for S_{11}, S_{22} and S_{21}, S_{12}, respectively. It can be observed that for both bands, the bandwidth

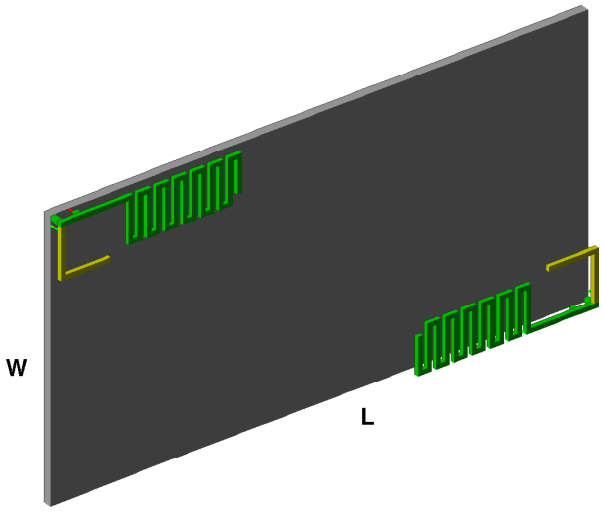

Figure 3.7: Meander antennas implemented on the Smartphone

requirements are fulfilled since 16MHz are covered for the low band and 111MHz for the high band, wider than 10MHz and 20MHz respectively. However, decoupling requirements are not fulfilled since for both bands, the mutual coupling between antennas has to be improved in around 4dB to reach the threshold. Thus, for this design, decoupling techniques should be implemented for both bands.

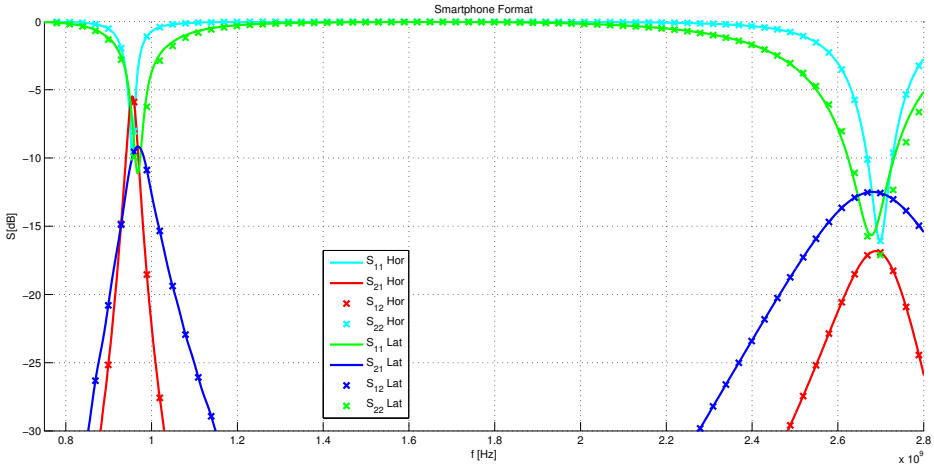

Figure 3.8: S-Parameters of both models implemented on the Smartphone

The S parameters of the lateral antenna model are plotted in Figure 3.8 with the green and dark blue curves. For the low band, the matching is slightly worst so the mutual coupling coefficients $|S_{21}|$ and $|S_{12}|$ are closer to the acceptable decoupling threshold of -10dB but the bandwidth is still wide. Concerning the high band, the matching improved, the bandwidth gets narrower but the transmission coefficients $|S_{21}|$ and $|S_{12}|$ are still not under the acceptable decoupling threshold of -20dB.

Conclusions

The two models are not exactly resonating around the same frequencies (ΔFr=13MHz in the low band and 20MHz in the high band) but they are still comparable by looking at the Figure 3.8. The meander design is interesting regarding the decoupling level of the high bands. If this model is selected, the mutual coupling of the low band only should be strongly reduced using a decoupling technique and, since the bandwidth for the high band is narrow, very precise tuning techniques are required to cover an acceptable bandwidth. The lateral design is interesting since the bandwidths are still wider for both low band and high band so the coverage of different frequencies using a tuning capacitor will be easier. Moreover, the reduction of the coupling for the low band using a parasitic element will not be hard since the decoupling level is close to the acceptable threshold but the high bands should be much more decoupled using parasitic elements.

3.2.3 Tablet

The tablet format L=240 x W=186mm (based on Figures 3.5(a) and 3.5(b)), also has a tactile touchscreen taking the total size of the PCB and can be considered as a mobile computer without keyboard or mouse. Our simulations will focus on a tablet that can connect directly to the Internet via a cellular network 3G or 4G: LTE or UMTS.

Designs

For the Tablet platform, the antennas are paced on the upper corner of the PCB with a mirror MIMO configuration for both models. The meander antennas are horizontally oriented and the lateral antennas are still along the side of the PCB. The spatial efficiency of the meandered antenna over the Tablet format is equal to 97.8%, since 9.6cm^2 out of the 446.4cm^2 whole PCB area cannot be used to place other components. For the lateral model in the Tablet, one antenna occupies L=240 x $l_2 = 4mm$. The spatial efficiency is then equal to 95.7% since 19.2cm^2 out of the 446.4cm^2 whole PCB area cannot be used to place other components.

S-parameters

The S parameters for the meander model are plotted in Figure 3.9 with the light blue and red curves for S_{11}, S_{22} and S_{21}, S_{12}, respectively. As it can be observed, both the bandwidth and decoupling requirements are fulfilled. The bandwidth is equal to 14MHz for the low band, and 114MHz for the high band, wider than 10MHz and 20MHz respectively. The $\mid S_{21} \mid$ and $\mid S_{12} \mid$ parameters are below -10dB for the low band and below -20dB for the high band. Thus, no decoupling techniques are needed for this model over the Tablet format.

The S parameters of the lateral antenna model are plotted in Figure 3.9 with the green and dark blue curves for S_{11}, S_{22} and S_{21}, S_{12}, respectively. It can be observed that for both bands, the bandwidth requirements are fulfilled since 43MHz are covered for the low band and 212MHz for the high band, wider than 10MHz and 20MHz respectively. Concerning the high band, the matching improved again, the bandwidth gets narrower and the transmission coefficients $\mid S_{21} \mid$ and $\mid S_{12} \mid$ are getting even closer to the acceptable decoupling threshold of -20dB.

Conclusions

The two models are not exactly resonating around the same frequencies (ΔFr=22MHz in the low band and 26MHz in the high band) but they are still comparable by looking at the Figure 3.9.

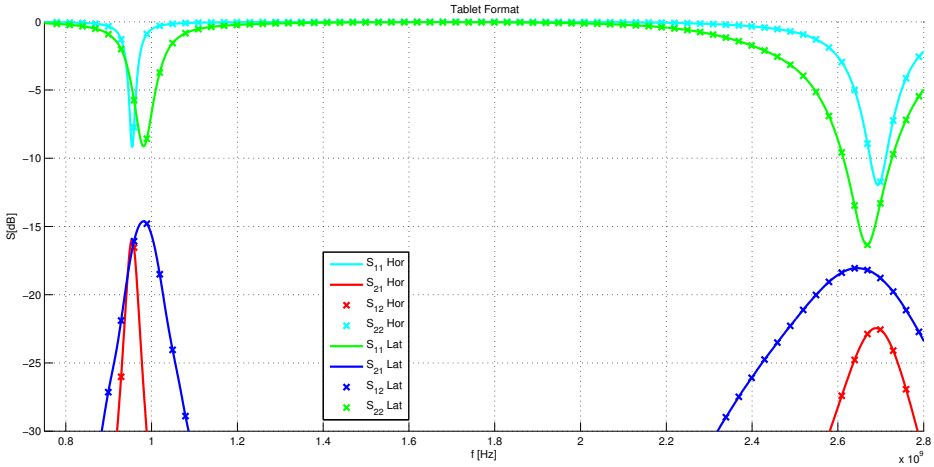

Figure 3.9: S-Parameters of both models implemented on the Tablet

The meander design is interesting regarding the decoupling level of both low band and high band represented by the red curve. If this model is selected, the mutual coupling in both bands is under the acceptable threshold so none of the decoupling techniques will be used but since the bandwidth for the high band is still narrow, very precise tuning techniques are required to cover an acceptable bandwidth. The lateral design is interesting since the bandwidths are still wider for both frequency bands so the coverage of different frequencies using a tuning capacitor will be easier. Moreover, only the high band will need to be slightly decoupled since the low band is already under the acceptable threshold of -10dB.

3.2.4 Performance of reusable antenna models on different devices

Comparison of each model on all the devices

In the previous subsections 3.2.1, 3.2.2, 3.2.3, each device has been presented but also the results of our models implemented on each of them. In this section, each model will be compared from the Candybar to the Smartphone and then from the Smartphone to the Tablet. In order to follow the chronology of the table 3.2 for both models, each band will be studied separately. A good indication on the model that provides the best performances on all devices will be given.

The first paragraph will concern the analyze of the meander design from the Candybar to the Smartphone, and from the Smartphone to the Tablet for each band. In the low band, when the size of the PCB increases, the bandwidth decreases from 2.1% to 1.7% to 1.5% and in respect with this reduction of the bandwidth, the Q increases until a really high value of 95.7. The efficiency of the low band increases of 50% from the Candybar to the Smartphone and over 40% from the Smartphone to the Tablet with a minimum efficiency of 44.3% in the Candybar format. The decoupling of the low band in the meander design is really bad especially in the Candybar even-though the $|S_{21}|$ doubled in the Smartphone and tripled in the Tablet with a final decoupling of -16dB under the acceptable threshold.
In the high band, when the size of the PCB increases, the bandwidth decreases from 4.7% to 4.1% then increases slightly to 4.2%. With respect to this small reduction of the bandwidth, the Q increases slowly until reaching 42.1 which is less than the half of the Q in the low band. The efficiency of the high band is already high in the Candybar and increases of 6% in the Smartphone

		Candybar		**Smartphone**		**Tablet**	
		Meander	*Lateral*	*Meander*	*Lateral*	*Meander*	*Lateral*
Low Band	*Fr (MHz)*	970	970	955	968	955	977
	S11 (dB)	-16.17	-21.26	-9.9	-11.12	-9.17	-11.34
	S21 (dB)	-2.85	-7.9	-5.48	-9.17	-15.96	-13.73
	Bandwidth (%)	2.06	3.81	1.67	3.62	1.46	4.30
	Q	74.76	28.58	95.7	19.4	95.7	18.12
	Efficiency (%)	44.28	82.74	61.43	79.94	85.68	88.83
High Band	*Fr (MHz)*	2652	2636	2698	2678	2693	2667
	S11 (dB)	-31.56	-11.14	-16.08	-15.66	-11.8	-15.87
	S21 (dB)	-20.4	-14.56	-16.9	-12.5	-22.47	-17.31
	Bandwidth (%)	4.71	9.79	4.11	7.88	4.23	8.14
	Q	26.80	7.78	32.92	11.55	42.10	11.50
	Efficiency (%)	91.46	90.35	97.34	93.23	96.31	97.59

Table 3.2: Devices and designs comparisons

and decreases to 96.3% in the Tablet. The decoupling of the high band in the meander design is really good especially in the Candybar with -20.4dB but except for the Smartphone where the value of the $|S_{21}|$ stays below the acceptable threshold of -20dB. This behavior in the Smartphone can be explained by the fact that the orientation of the PCB changed from vertical to horizontal and the orientation of the models in MIMO changed from a mirror to an opposite configuration affecting the distance between the antennas and thus, the mutual coupling.

The second paragraph will present the analyze of the lateral design from the Candybar to the Smartphone, and from the Smartphone to the Tablet for each band. In the low band, when the size of the PCB increases, the bandwidth decreases slightly in the Smartphone but increases again in the Tablet from more than 0.5% compare to the Candybar. With respect to this increase of the bandwidth, the Q is reducing to 18.1 which is the lowest value presented in the low band. The efficiency of the low band is already superior to 80% in the Candybar and decreases slightly in the Smartphone before increasing again in the Tablet with the maximum value obtained in the low band, 88.8%. The mutual coupling of the low band in the lateral design is averaging around the acceptable threshold and gets better when the PCB increases until the distance between the antennas exceeds $\lambda/4$ in the Tablet.
In the high band when the size of the PCB increases, the bandwidth decreases of less than 1% in the Smartphone and increases slightly in the Tablet. With respect to this small reduction of the bandwidth the Q increases slowly from 7.8, the lowest value achieved in the high band, to 11.5 in the Tablet. The efficiency of the high band is already high in the Candybar with 90% and keep increasing of 3% to reach 97.59% in the Tablet, the best efficiency achieved. The mutual coupling of the high band in the lateral design is less than average especially in the Smartphone, even-though the distance between antennas get longer when the PCB increases, the value of the mutual coupling is still under the acceptable threshold of -20dB and the maximum $|S_{21}|$ obtained is -17.3dB in the Tablet.

To summarize this part, the overall performances of both models over the three devices can be presented briefly, a deeper analyze will be given later in section 4.1. Despite the good decoupling of the high band in the meander design, this model encounter some weaknesses concerning the decoupling of the low band, the bandwidth, and the efficiencies on the different devices. For the

lateral design, despite the good bandwidth and the efficiencies better than the meander design except only in the low band for Candybar and Smartphone formats, the mutual coupling between antennas is under average and a strong decoupling technique is needed to decouple properly this model. Since it is a bigger challenge, in subsection 3.2.5 and 3.2.6, the tuning will be analyzed on the meander design having a smaller bandwidth and the decoupling will be implemented on the lateral design having the smaller mutual coupling value. This selection will also be confirmed in the following part with the impact of increasing the form factor.

Impact of increasing the form factor

As it was presented in previous sections, the PCB size plays a main role regarding the antenna performance. This aspect has been tested over three specific formats. Thus, an investigation on the impact of the size of the form factor over some antenna parameters has been developed in order to know what are the expectations of the two different models presented in this work over different formats. Simulations have been tested over 147 different formats, from the Candybar format 100x40mm until the 256x46mm format, increasing 1x1 mm the size in every iteration. For each of the formats, two different MIMO configurations, mirror and opposite, have been tested for each model, four configurations in total. The four parameters tested are: bandwidth, S_{11}, S_{21} and total efficiency.

- **Bandwidth**

  Figure 3.10 shows the evolution of the bandwidth in both low and high bands. Two main aspects can be observed regardless the size of the PCB. Firstly, the bandwidth achieved by the lateral model is always wider than the one achieved by the meander model. Secondly, the bandwidth range achieved in the high band is much higher than in the low band, regardless the size of the PCB. However, within both models, the two different MIMO configurations do not evolve in the same way. For the meander model, both configurations provide similar bandwidth, but in most of the positions mirror is better. The evolution of the bandwidth follows a sinusoidal wave with higher dynamic range (difference between maximum and minimum values) for small PCB formats and lower frequency for low bands. Regarding the dynamic range, it can be also observed that it is higher for opposite than for mirror configurations. In the lateral model, the opposite configuration provides wider bandwidth for all formats bigger than 130x70mm but for smaller devices there are some sizes where the mirror configuration provides wider bandwidth.

- **S-parameters**

  Figure 3.11 shows the evolution of the $|S_{11}|$ and $|S_{21}|$ parameters for both low and high bands. Only these two S-parameters are plotted in this section, but since all the configurations are symmetrical, it can be assumed that $|S_{11}|$ is equal to $|S_{22}|$ and $|S_{21}|$ is equal to $|S_{12}|$. The $|S_{11}|$ parameter follows a sinusoidal wave. It can be observed that, for small devices, the $|S_{11}|$ varies dramatically for small size increase. However, when the device is becoming bigger, then the sinusoidal looks more constant but always decreasing its dynamic range. The frequency of this sinusoidal is higher in high bands while for low bands the $|S_{11}|$ parameter tends to a constant value when the device is big. Regarding the $|S_{21}|$ parameter, the wave is long-term decreasing, but with short-term fluctuations. It can be observed that, in the

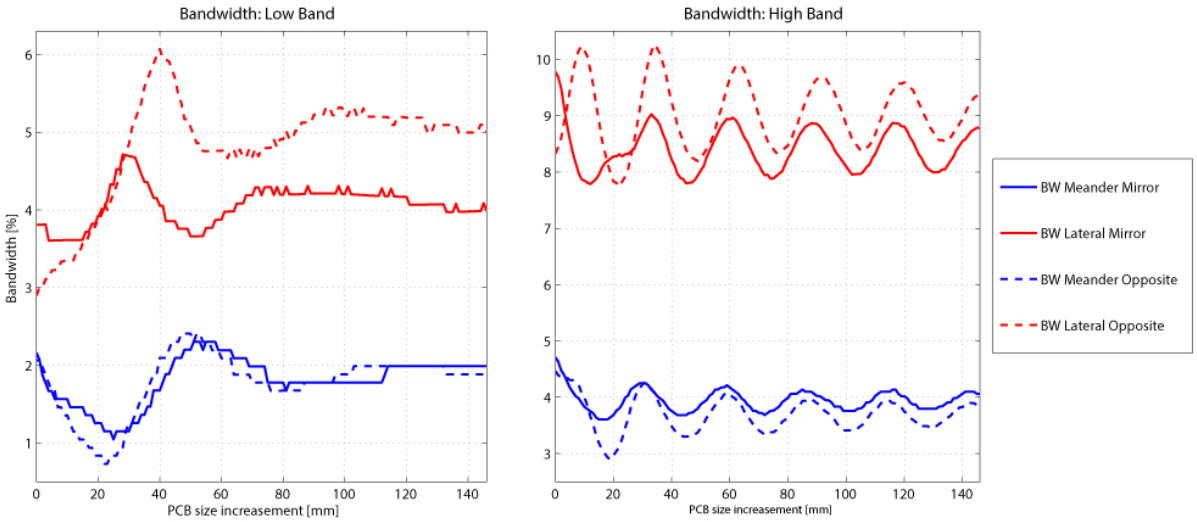

Figure 3.10: Bandwidth evolution for different PCB sizes

opposite design $|S_{21}|$ decreases faster since the antennas are further away from each other. The frequency of these fluctuations is higher for the high bands and the closer are the antennas to each other, the more critical are the changes in the $|S_{21}|$ parameter.

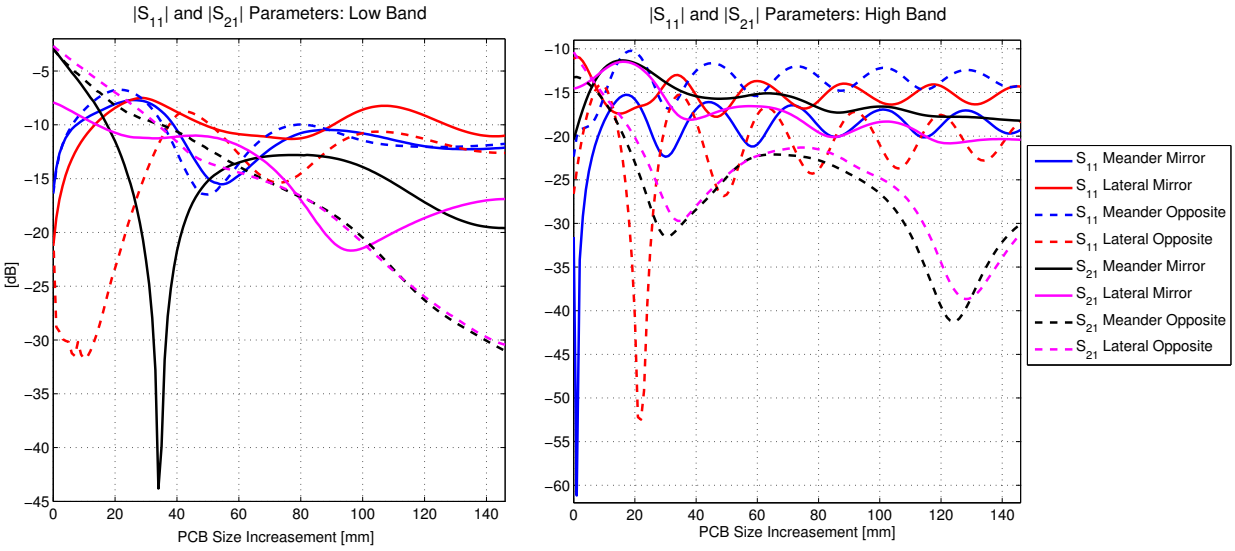

Figure 3.11: S-Parameters evolution for different PCB sizes

- **Total efficiency**

Figure 3.12 shows the evolution of the total efficiency parameters for both low and high bands. It can be observed that the efficiency in the high band is higher than in the low band for each size. Since the total efficiency is function of both the S_{11} and the S_{21} parameters, and as it was commented in the previous paragraph, they vary in a critical way when the antennas

are close to each other, consequently the total efficiency also suffer critical variations during the first increases of the analysis. For big devices, as it occurred with the other parameters, the wave becomes sinusoidal with higher frequency for the high bands. For the low band the best configuration changes depending upon the format used, while for the high band the best model for all the formats bigger than 152x12mm is lateral in opposite configuration.

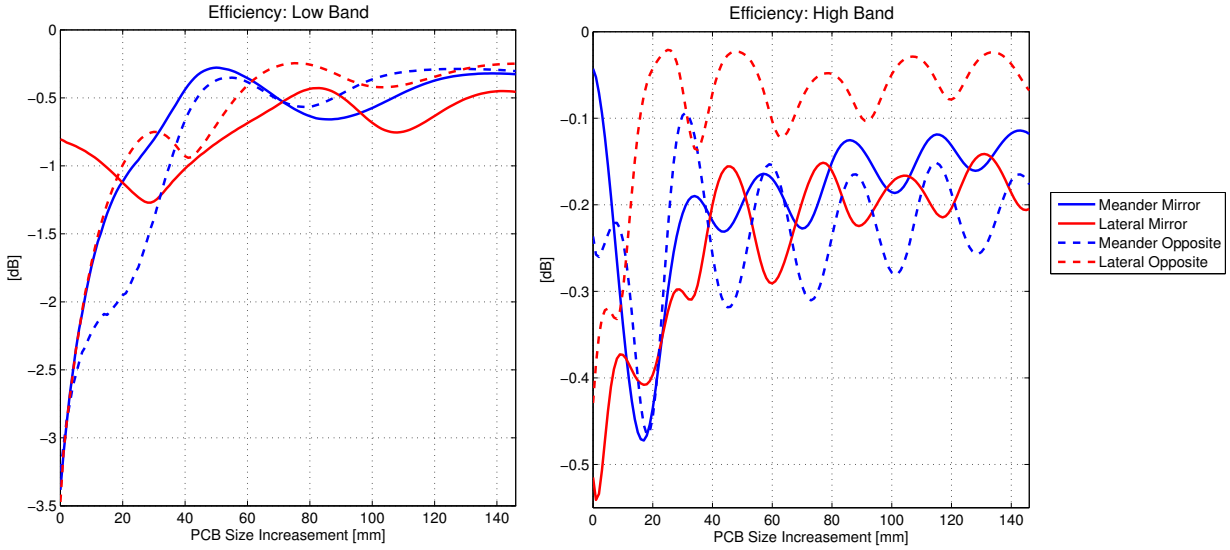

Figure 3.12: Efficiency evolution for different PCB sizes

3.2.5 Tuning techniques

Tunability of the antenna is one of the main issues of this work. Nowadays, most of the electronic devices work at several operating bands simultaneously. In order to provide this feature, several tuning techniques currently used in the industry were presented in subsections 2.2.1 and 2.2.2. In this work, the tuning technique is performed by using two MEM capacitors placed in the low band line and high band line, respectively. There are two main parameters that determine the performance of the tuning: the position where the capacitor is placed and its nominal value. It is well known that the resonant frequency can be decreased either by placing the capacitor further from the source while keeping its nominal value, or by increasing its nominal value while keeping the capacitor placed in the same position. The further is the capacitor placed away from the source, the longer is the tuning scope achieved. However, the distance between the covered bands is also increased for a given number of iterations. This number is determined by the minimum step achievable in the nominal value of the MEMS. A MEMS consists of two parallel plates: one plate is fixed and the other one is suspended using a mechanical spring that controls the voltage difference between the plates [79]. This voltage determines the capacitance value of the MEMS. Then, it exits a compromise between achieving a large tuning range and covering all the sub-bands under the -6 dB bandwidth criteria. The optimal solution is to find a position where all the sub-bands of interest are covered while achieving a tuning range as maximum as possible. Another important requirement to take into account is to deal with the maximum channel bandwidth within the bands selected as example to test the performance of the antennas in this work. Therefore, the goal is to cover bands 7 and 8 simultaneously, where all the sub-bands covered by the different capacitor iterations have to be wider than 20MHz for band 7 and wider than 10MHz for band 8 (see section 2.1.1).

Meander model

Figure 3.13 shows the geometry of the meander model when the tuning technique is implemented. Two extra capacitors, C_1 and C_2, to tune the low band and high band respectively, can be observed with respect to the original design shown in Figure 3.5(a), while the matching capacitor (C_3) is kept at the same fixed value as before (2.4pF). Both bands are tuned at the same time by placing a capacitor with certain nominal value between PCB and antenna. The frequency shift of each band has to be absolutely independent of the shift in the other.

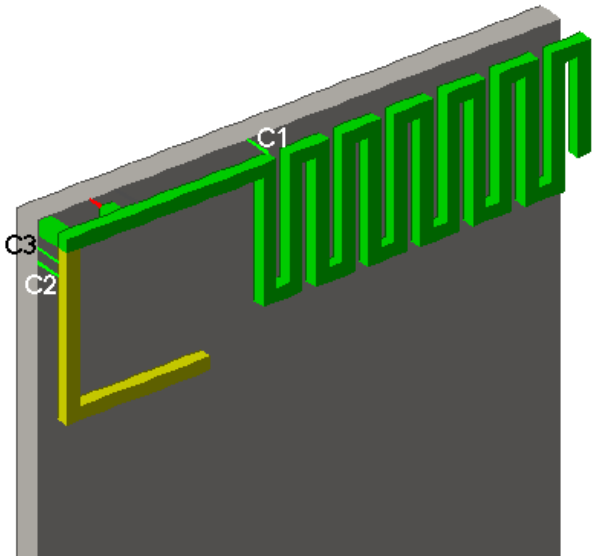

Figure 3.13: Additional capacitors added to implement tuning techniques

This principle is depicted in the example shown in Figure 3.14, where C_1 is set to 0.125pF and C_2 vary its nominal value from 0 to 1.375pF covering several frequency bands. Band 7 is covered only with two combinations (0 and 0.5pF). The scope of the tuning in the high band in this example is equal to 312MHz, providing a tuning range equal to 12%.

In order to determine all the different frequencies achieved by this antenna model, all possible combinations for C_1 and C_2 has been tested for three of the formats under study, with a capacitor value step equal to 0.125pF. Tables 3.2.5, 3.2.5 and 3.2.5 show the sub-bands covered over the desired bands 7 and 8 by the meander model, for the three different formats. As it can be observed in those tables, band 8 can be always covered for the Candybar and Smartphone format, regardless of the value of C_2. However, as the reader can notice, for the Tablet this band cannot be completely covered. This arises from the fact that the original bandwidth for the tablet without tuning is very small (14MHz), so the sub-bands covered while implementing tuning techniques need to be very close to each other. This can be implemented by placing C_1 closer to the source as it will be explained in subsection 4.2.1. Another relevant aspect which can be observed in the tables is that band 7 cannot always be covered due to the impact of the harmonic.

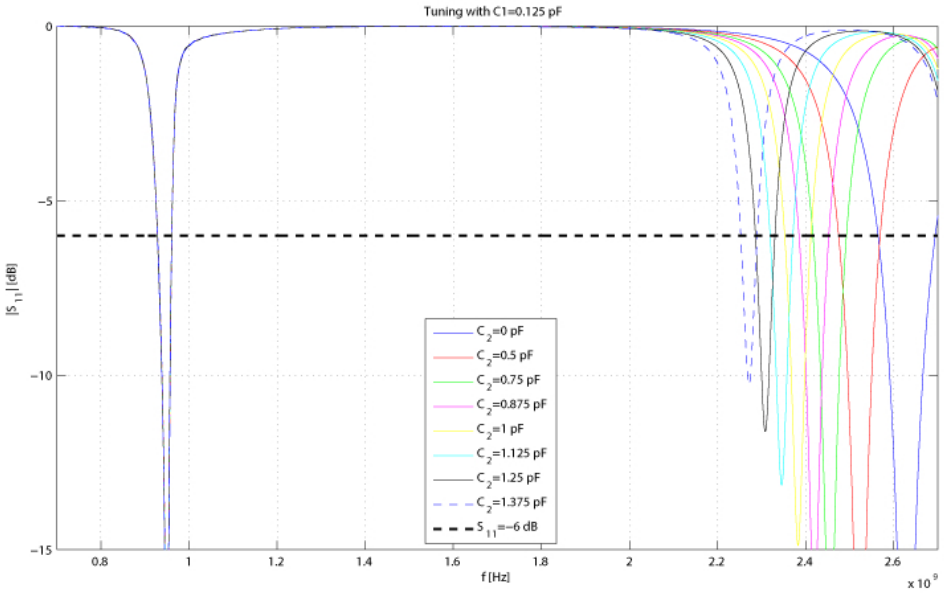

Figure 3.14: Example of the tuning technique in Candy-bar format with C_1=0.125pF

Low Band		High Band	
C_1 (pF)	Bandwidth (MHz)	C_2 (pF)	Bandwidth (GHz)
0.125	929-961	0	2.565-2.694
		0.5	2.475-2.569
0.25	907-942	0	2.531-2.648
		0.5	2.461-2.558
		1	2.648-2.703
0.375	887-916	0.125	2.477-2.574
		1.125	2.588-2.615
0.5	870-892	0	2.433-2.506
		1.5	2.502-2.526

Table 3.3: Relevant frequency bands covered in the Candybar format

Challenge of the harmonic

As it was commented in the previous section, a good tuning technique requires independence between all different bands to be tuned. It means that the frequency shift of one of the bands should not interfere in the shift of the others. In the techniques implemented in this work, a necessary condition to deal with this requirement is that the value of the capacitor placed across the low band arm does not interfere into the high band and vice versa. This aspect was properly fulfilled. However, the high band is still dependent of the low band. This is due to the fact that the low band resonating at around 970MHz has a third order harmonic associated resonating at triple frequency, i.e. around 2.9GHz, which is close to the 2.7GHz band covered by the high band arm. These harmonics do not cause any problems for single-band systems since they are very far away from the band of interest. However, in multiband systems, like the one under analysis, it could occur that the harmonic resonates at a frequency close to the resonance of the antenna itself. Then, the resulting

Low Band		High Band	
C_1 (pF)	Bandwidth (MHz)	C_2 (pF)	Bandwidth (GHz)
0	947-962	0.125	2.617-2.721
		0.375	2.561-2.648
		0.625	2.496-2.567
		0.75	2.461-2.525
0.25	934-948	0	2.538-2.607
		0.5	2.477-2.551
0.5	921-934	-	Nothing
0.625	913-927	-	Nothing
0.75	905-920	-	Nothing
1	893-905	-	Nothing
1.125	885-896	-	Nothing
1.25	878-896	-	Nothing

Table 3.4: Frequency bands covered in Smartphone format

Low Band		High Band	
C_1 (pF)	Bandwidth (MHz)	C_2 (pF)	Bandwidth (GHz)
0	946-961	0	2.620-2.708
		0.375	2.557-2.635
		0.5	2.518-2.594
		0.625	2.475-2.547
0.125	936-949	0	2.600-2.666
		0.375	2.532-2.606
0.25	924-937	0.25	2.511-2.537
		0.5	2.466-2.515
0.375	914-925	-	Nothing
0.5	902-913	-	Nothing
0.625	891-901	-	Nothing

Table 3.5: Frequency bands covered in Tablet format

resonant frequency will be affected due to the interference caused by the harmonic associated to another resonant band.

Sometimes can occur that the harmonic cannot be easily distinguished by looking at the S_{11} graph since the resonant band produced by the antenna and the one produced by the harmonic might be merged into one resonant band. In such case, it can be affirmed that the harmonic is helping the antenna to increase its bandwidth over that specific band. This increase of bandwidth might also exceed the theoretical bandwidth constraint given by the Q-factor, since the harmonic is an extraordinary factor which is not taken into account while calculating this parameter. Thus, first of all, the harmonic has to be identified. In our case, the harmonic was identified from the beginning

since there is a band resonating at around 2.9GHz over the high band produced by the antenna. Since both bands are quite close, they are interfering to each other. Then, the procedure followed to find out the resonant frequency produced by the high arm of the antenna was to shift the harmonic far away from the high band area while placing a high capacitor in the low band arm, C_1=2.5pF. Then, once the real resonant frequency is found out, the effects of the harmonic can be predicted. Thus, what occurs in our model is that for some specific shifts of the low band, by changing the value of C_1, the harmonic is also shifted towards lower frequencies interfering strongly the high band resonant frequency. Actually it can be observed in tables B.1, B.2, B.3 and B.4 that when the harmonic is shifted away from the high band influence area, as consequence of a big shift in the low band, then the bands covered in the high band are approximately the same, for a given value of the tuning capacitor C_2. This is the reason why it is not possible to cover both bands 7 and 8 at the same time.

This problem leads to the importance of dealing with the harmonics, every time a multiband antenna is designed. That is the reason why nowadays engineers come up with innovative publications about harmonic's suppression, as the one presented in [80]. However, for the specific case under consideration, bands 7 and 8 over the LTE standard are never used at the same time and hence, the challenge of the harmonic is not a big issue anymore in this specific case. Thus, whenever the operating band in the high one, the value of C_1 should be high, 2.5pF for instance, in order to shift the harmonic away from the high band of interest. Then, the independence achieved between low and high bands allows the high band to be tuned without any problem.

3.2.6 Reduce mutual coupling

Selected technique: Parasitic elements

To reduce the mutual coupling in the lateral design between two antennas placed on the same PCB, different decoupling techniques presented in 2.2.1 are implemented. In Appendix B.4, the techniques of connecting strips and defected ground plane are presented but also the reasons why none of these techniques are effective for our design. Therefore, this section will present the results of the simulations concerning only the selected decoupling techniques known as parasitic elements. The principle is simple and consists in creating a reverse coupling to cancel out the mutual coupling. For this, the parasitic element should resonate at the same frequency than the band that needed to be decoupled in order to reduce the S_{21} and S_{12} parameters.

The figures 3.16(a), 3.16(b) and 3.16(c) explain this principle with different length of the parasitic element for the low band. The antenna is resonating at the same resonant frequency on all the figures and the resonance frequency of the element is decreasing when its length is increasing, making the $\mid S_{21} \mid$ curve shifting to the left. The Figure 3.16(b) is the exact matching between the resonant frequency of the low band antenna and the parasitic element, the $\mid S_{21} \mid$ value at the exact resonance frequency is excellent.

In the Figure 3.15(a), two parasitic elements with a 2mm height are added in the lateral design, the blue and pink elements with a respective resonant part of 76mm to reduce the coupling of the low band and 27mm to reduce the coupling of the high band. The Figure 3.15(b) represents the magnetic H fields of the design 3.15(a) with two parasitic elements and is useful to observe the current running from one antenna to the other through the parasitic elements. The magnetic H fields are shown with a mirror effect with respect to the design, indeed, a high concentration of current is visible on the top right corner of the ZX and XY planes whereas the parasitic elements

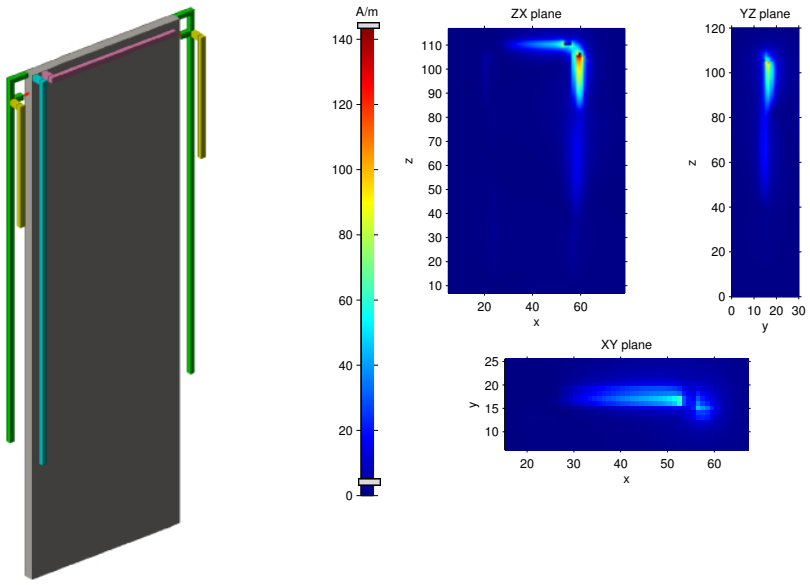

(a) Design (b) H fields

Figure 3.15: Two parasitic elements design (a) and magnetic H fields (b)

are placed on the top left corner of the design. The H fields are really important to understand this decoupling technique and how the mutual coupling can be reduced. In the ZX plane, the current is running from the first antenna on the left of 3.15(a) to the parasitic elements and thanks to those elements, almost no current flows in the second antenna which allows a very low $\mid S_{21} \mid$, -43dB in the low band and -21dB in the high band. The decoupling in the low band is considerably good from the first antenna with -35dB of improvement against -6dB in the high band compare to the lateral model without any decoupling technique.

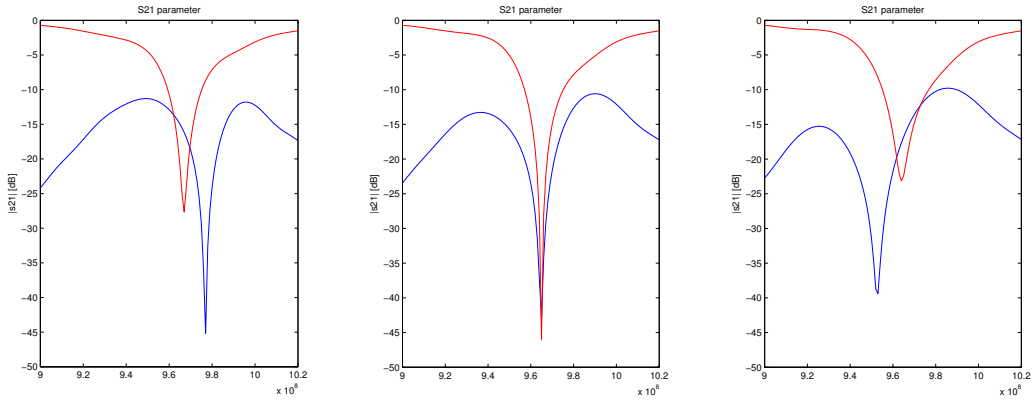

(a) Length = 76mm (b) Length = 77mm (c) Length = 78mm

Figure 3.16: Zoom of the S-parameters with different parasitic elements length for the low band

The problem with this design is the S-parameters from the second antenna port, plot in light green in Figures 3.18(a) for the low band and 3.18(b) for the high band. Since the parasitic elements are placed near the first antenna, the resonance frequency of the low band is shift and the coupling in

the second antenna is higher for the low band with -10.5dB but still under the acceptable threshold of -10dB with -2,67dB of improvement. However, the resonance frequency of the high band plot in light green in Figure 3.18(b) improves with -28.6dB corresponding to -14dB of improvement. Since the decoupling of the low bands in the design 3.15(a) were really effective, the goal is to improve the S_{21} of the low band in the design with two parasitic elements and maintain a good decoupling in the high band.

One solution is presented in 3.17(a) and consists in adding two other parasitic elements this time near the second antenna, in order to create a symmetrical design and obtain better results. Two parasitic elements are implemented near each antenna, one blue and one purple to reduce respectively the decoupling in the low band and the high band. The purple elements for the high

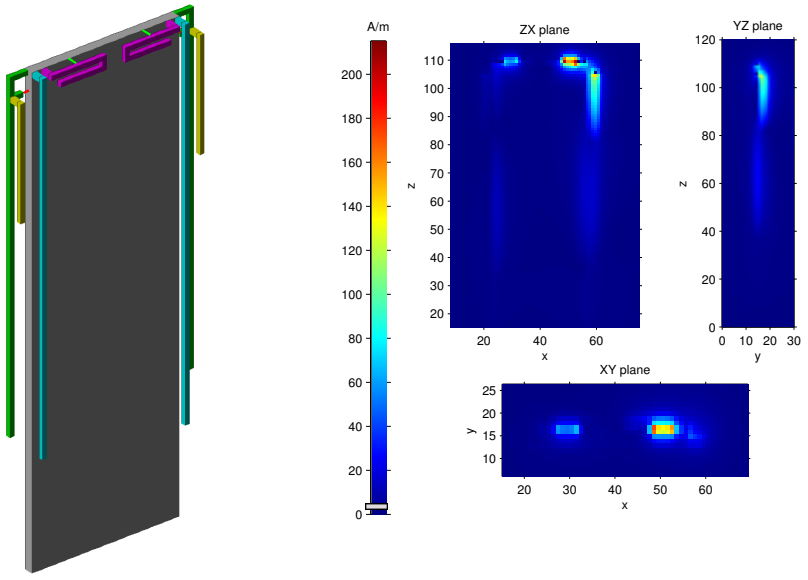

(a) Design (b) H fields

Figure 3.17: Four parasitic elements design (a) and magnetic H fields (b)

band are now meander and symmetrical for both antennas with a resonance part of 23mm, a 2mm height and a capacitor of 0.820pF placed at 5mm from the short of both elements. For the low band, the blue elements are also symmetrical but with a different resonance length, 76mm for the first antenna and 80mm for the second antenna.

The Figure 3.17(b) represents the magnetic H fields of the design 3.17(a) with four parasitic elements and is useful to observe the current running from one antenna to the other through the parasitic elements. In the ZX plane, the current is running from the first antenna to the parasitic elements near the first antenna and then through the parasitic elements near the second antenna to the second antenna. Thanks to those elements, more current flows in the purple wires and less in the second antenna which allows a good reduction of the $\mid S_{21} \mid$ in the high band to -28.6dB. The decoupling in the high band improved in the first antenna from -6.5dB and -4.6dB in the second antenna whereas the improvement of the coupling in the low band are respectively -2.9dB and -1.4dB. The problem with this design is the S-parameters from the second antenna port, plot in light blue in Figure 3.18(a) for the low band and 3.18(b) for the high band, the values of $\mid S_{12} \mid$ for both bands are below their respective thresholds.

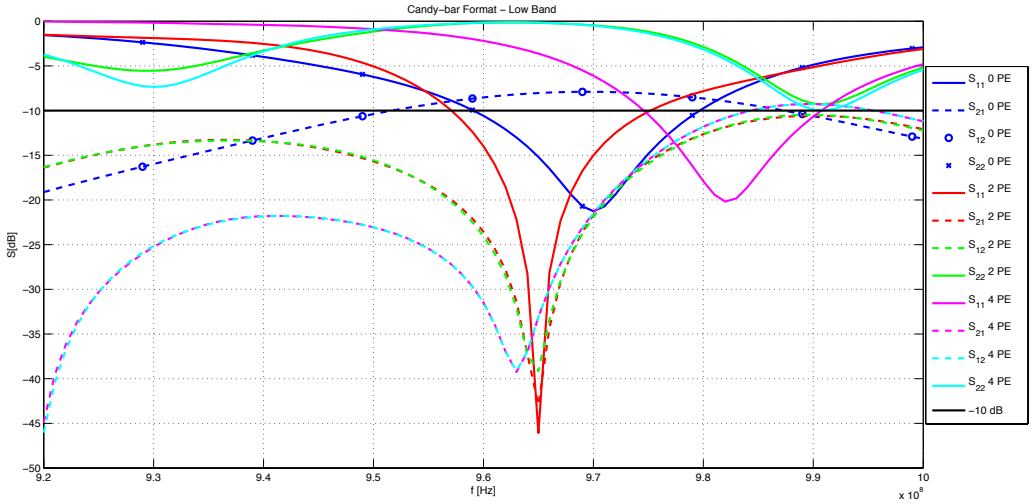

(a) Low band

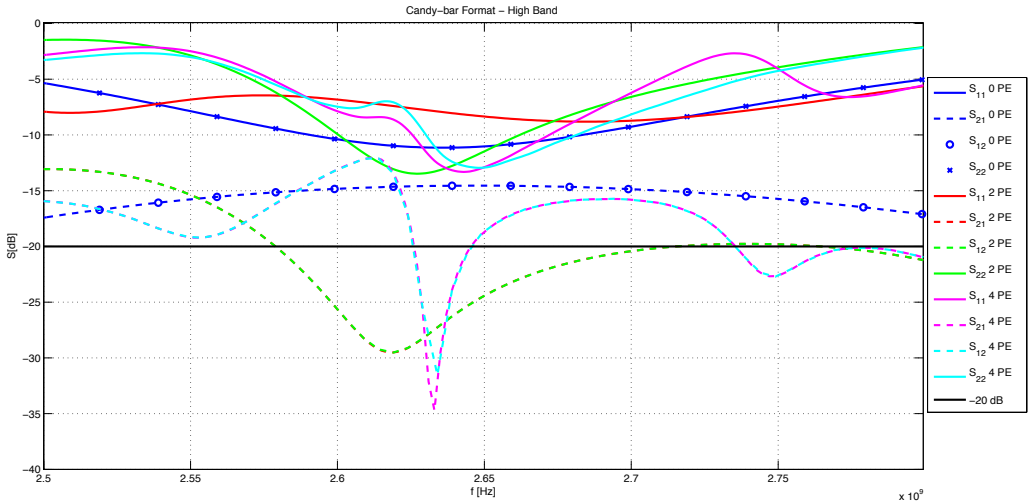

(b) High band

Figure 3.18: S-parameters of the lateral design with and without parasitic elements (PE) in the low band (a) and the high band (b)

To conclude this decoupling part, the strength of the design with two parasitic elements is the really good decoupling improvement for the low band and the decoupling of the high band just under the acceptable threshold of -20dB. But the weakness concerns the low band of the second antenna port due to a shift of frequency. However, this design is easier to create for laboratory measurements than the one with four parasitic elements and two capacitors. The main problem encountered with the four parasitic elements design concerns the resonance frequencies. Since there are two parasitic elements and two antenna arms resonating around the same frequency, all the $\mid S_{11} \mid$ curves merge with each other and distorts the real resonance frequency. Also, the conception of this design for measurements in laboratory is much longer than the design with only two parasitic elements. The efficiencies of those models using this decoupling technique are better for the low band when there is only two parasitic elements with 100% for the first antenna and 79% for the second antenna while for the high band, the design with four parasitic elements is more efficient with 96% for the

first antenna and 95% for the second one. The bandwidth is also better when there is two parasitic elements, with 3.6% for the first antenna in the low band and 8.5% in the high band.

3.3 Preliminary measurements

After becoming familiar with the software and the different parameters to design an IFA antenna, our precursor lateral antenna design at the end of the first semester was implemented on the Candybar (100x40mm) and measured in an anechoic chamber in the laboratory. In the following, the functionality of an anechoic chamber is introduced and the measurements done are presented.

3.3.1 Anechoic chamber

As it was already introduced in subsection 3.1.1, the FDTD software simulates the fields until the energy computed over each cell is under the energy threshold fixed in the configuration settings. Simulations assume that the surroundings of the mobile device is an infinite free space region and this is the reason why the simulations takes place over a small cell since there is no computer which can store that large amount of data. However, this is not possible to be implemented in real life, since the mobile device has to be bounded by a real material. Then, it is necessary to bound the device with an absorbing material in order to make the scenario to be as similar as possible to the simulated one. Therefore, it is necessary to set some boundary conditions that permits all outward propagating numerical waves to exit as if the simulation is performed on a computational domain of infinite extent [81]. These conditions are called Absorbing Boundary Conditions (ABC) and consists on suppressing the reflections produced by the surrounded materials as much as possible in order to get no reflected wave. ABCs can be extracted by several algorithms which are out of the scope of this thesis.

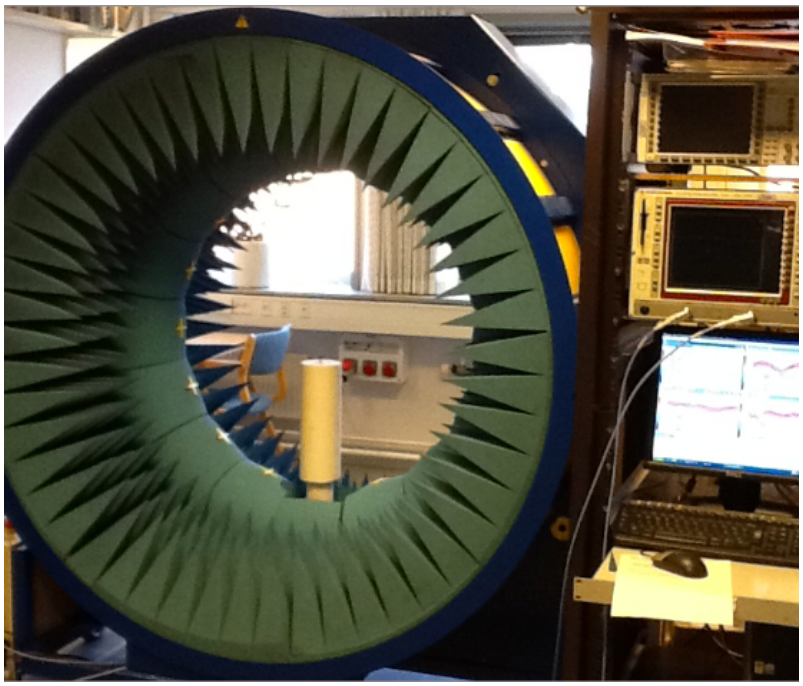

Figure 3.19: Circular SATIMO anechoic chamber

Measurements have been done in the laboratory by placing the mock up built inside the circular SATIMO anechoic chamber shown in Figure 3.19. The wall inside the circle is composed by special electromagnetic absorbing material. The jagged triangle shapes are designed so that what is reflected from them tends to spread in random directions, and what is added together from all the random reflections tends to add incoherently and is thus suppressed further [9]. The SATIMO chamber contains 16 patch antennas surrounding the center of the circle, as it can be observed in Figure 3.19. These antennas receive the radiation from the mock up terminal and the data are computed by a FDTD software program. Final results are computed in far-field despite measured fields are near-fields. Thus, the FDTD software includes a Near-to-Far-Field Transformation code based on the integration of the near fields weighted by the free-space Green's function over a virtual surface surrounding the antenna of interest [81].

3.3.2 Laboratory session

These preliminary measurements allowed us to validate our design and test the scattering parameters of our mock up presented in Figure 3.20 with 3mm height, 3mm between short and source and 71mm of resonant part. During the measurements, the antenna was welded to the PCB and maintained with polystyrene and special lossless duck tape. The antenna and the PCB were designed with copper.

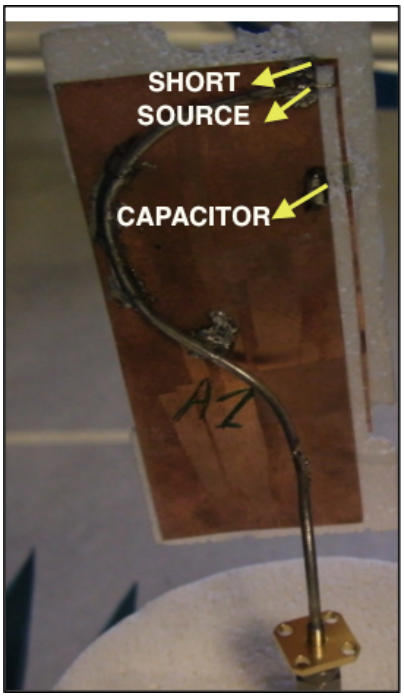

Figure 3.20: Mock up of the precursor lateral antenna design

The scattering parameter $|S_{11}|$ is presented in the Figure 3.21(a), the resonance frequency is 916MHz, the bandwidth is 3.7% and the efficiency is 89%. The bandwidth was narrower during the simulation with 2.8% but this difference is due to the deterioration of the matching in the measurements therefore, the efficiency decreases also. For a first laboratory session, those results were quiet successful and motivating.

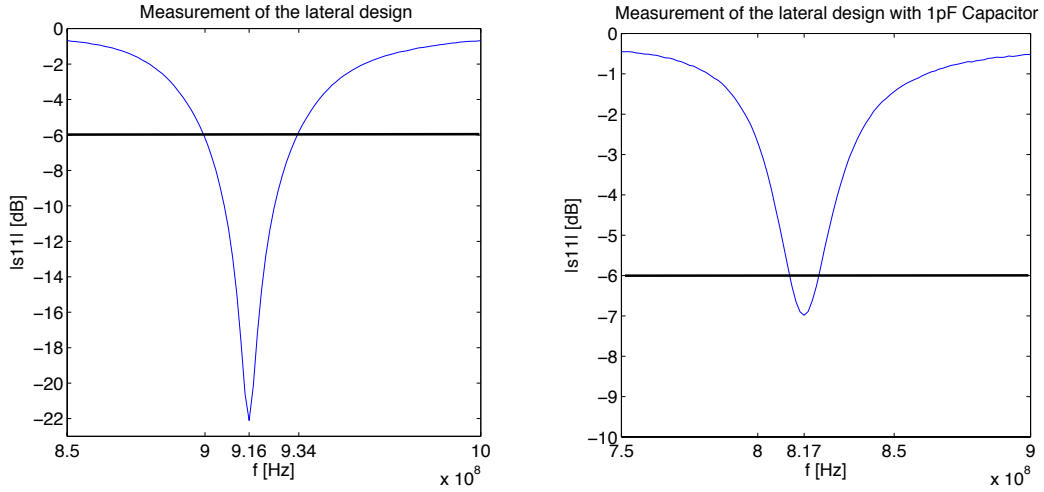

(a) (b) High band

Figure 3.21: S-parameters of the precursor lateral design in the low band (a) and with tuning capacitor (b)

During this session, the tuning with a capacitor of 1pF placed at 20mm from the source were also measured with the lateral antenna. The results of the scattering parameter are presented in Figure 3.21(b), the resonance frequency is reduced to 817MHz and the bandwidth decreases considerably to 0.97%. Further the capacitor is placed from the source and smaller is the resonance frequency and the matching, by consequences, the bandwidth tends to decrease.

Chapter 4

Discussion and future work

4.1 Discussion

This section is dedicated for the discussion about our meander and lateral designs and their behavior on different devices. For the comparison of these two models, the overall performances of each antenna should be exposed starting with a basic requirement in the phone industry, the space consumption on the PCB. Indeed, the meander design is more compact but since it is placed on the PCB, the surface occupied by the antenna is bigger, 9.6cm^2 instead of 8cm^2 for the lateral design. With those configurations, the percentage of free space to place other components on the PCB is 76% and 80% respectively, for the meander and lateral model over the candy-bar model. Depending on the size of the format this space can increase up to respectively 97.9% or 95.7% in the Tablet.

Another important parameter to analyze is the bandwidth for each antenna calculated at -6dB on the return loss curves. For the meander antenna, the maximum bandwidth achieved is found in the Candybar with respectively 2% and 4.7% for the low and high bands whereas for the lateral antenna, the maximum achievable bandwidth is twice greater with respectively 4.3% in the Tablet and 9.8% in the Candybar for both bands. These bandwidth values, as all the antenna parameters, depend upon the size of the PCB and the MIMO configuration selected. Then, the bandwidth in the low band can vary between 0.8% and 2.5% for the meander model and between 3 and 6.1% for the lateral one. In the high band, these ranges are 3%-4.8% and 7.8%-10.2%, respectively. Therefore, it can be affirmed that the bandwidth achieved by the lateral model is around twice the band achieved by the meander one, regardless the size of the PCB and the MIMO configuration selected.

On of the most important parameter for the phone industry is the efficiency achievable with the antenna. As it was presented in previous chapters, a good efficiency is achieved when both $|S_{11}|$ and $|S_{21}|$ parameters are close to zero in natural units. The behavior of these two parameters with respect to the PCB size is different. As it was observed in Figure 3.11, $|S_{11}|$ is not directed dependent on the PCB size, but $|S_{21}|$ presents a long term decreasing evolution when the PCB size is increased. Thus, it results logic that the best efficiencies obtained within the three formats analyzed were achieved over the tablet format. For the meander model the maximum efficiencies obtained are 85.7% in low-band and 97.3% for the high-band, whereas for the lateral model these values are 88.8% and 97.6%, respectively. Thus, in term of maximum efficiency achieved, both models present similar results. Moreover, as it was observed in Figure 3.12, in low band all models present very poor efficiency over small size terminals, except for the lateral model in mirror configuration in Figure 3.5(b). Thus these models, will not be used for small devices unless efficiency is improved after implementing decoupling techniques.

Another important indicator of performance concerns the level of mutual coupling between antennas in MIMO configuration. Indeed, if the values of the $| S_{21} |$ parameter are under the acceptable decoupling levels of -10dB and -20dB respectively for both bands, the antennas are considered well decoupled. As mentioned before in the former paragraph, the minimum value of the $|S_{21}|$ was found in the tablet format. For the meander model the minimum $| S_{21} |$ obtained is equal to -15.96dB in low band and -22.5dB for the high band, whereas for the lateral model these values are -13.7dB and -17.3dB, respectively. In the evolution of this parameter over different PCB sizes shown in Figure 3.11, a good decoupling level under -10dB can be achieved for the low-band by selecting mirror MIMO configuration for both meander and lateral model in formats bigger than 118x58mm. For the high-band, a good decoupling level under -20dB can be achieved for the low-band by selecting opposite MIMO configuration the meander model and mirror for the lateral one, in formats bigger than 120x60mm.

Tuning techniques are a smart solution for narrow band antennas which aim to provide wide-band services. Tuning techniques over multiband antennas can be performed by placing a capacitor across each of the resonating arms. There are two main parameters that determine the behavior of the tuning: the position of the capacitor and its nominal value. The further is the capacitor away from the source, the largest is the frequency shift for a fixed capacitor value. Nevertheless, the higher is the capacitor value, the largest is the frequency shift for a fixed capacitor position. Thus, the further is the capacitor away from the source, the more number of capacitor iterations are needed to cover all the sub-bands in between the range desired to achieve. From the values of the tables shown in Appendix B.3, it can be subtracted that by the application of this tuning technique, 156MHz, 84MHz and 47MHz can be covered for the low-band in the Candybar, Smartphone and Tablet format, respectively. The starting bandwidths without using tuning techniques for these three designs were 20MHz, 16MHz and 14MHz respectively. It means that the lower is the original bandwidth, the shorter is the tuning range achieved. One of the most relevant aspects shown in this work, is the problematic arising from the influence of the harmonics into the bands of interest. A harmonic is an intrinsic characteristic of the antenna that cannot be removed unless additional circuitry is used. Hence, in multiband systems, frequencies that are multiple of lower resonant bands are potentially problematic. Since the harmonic is tuned at the same time of the low-band that is associated to, if the antenna is required to be tuned and the harmonic resonates close to another resonance band, low and high resonant bands are not frequency independent anymore. This effect has been shown over the meander model. The antenna resonates in the high band at around 2.7GHz while the third-order harmonic of the low band was resonating at around 2.9GHz. When the low band is tuned, consequently the harmonic is also tuned and it distortions the resonance frequency and the bandwidth of the high band.

To maintain a good overall performances of the small antennas, the mutual coupling is an important issue and the implementation of a decoupling technique to reduce this coupling represent a good enhancement of our design. Many decoupling techniques were attempted but only the technique using parasitic elements provided a successful decoupling. The first conception of this technique used only two parasitic elements placed near the excited antenna and the results were really productive in the low band with an improvement of -35dB and -6.5dB in the high band compared to the minimum $| S_{21} |$ achievable without decoupling techniques presented earlier in this section. Therefore, an improvement of this technique were created by adding two other parasitic elements near the non-excited antenna in order to obtain symmetrical results. This conception was not really glaring with -2.9dB in the low band -6.5dB in the high band but it could be interesting to continue the investigation of a tunable parasitic element.

4.2 Future work

4.2.1 Tuning

As it was shown in section 3.2.5, two main problems were presented while implementing the tuning technique: the challenge of the harmonic and the problematic of tuning very narrow bands as it occurred in the tablet format. Thus, two enhancements are proposed in order to implement a more accurate multi-band tuning model. The first is to implement a technique that successfully remove the harmonics when they are present in one of bands of interest. The second one is to optimize the trade-off between large tuning range and covering all the sub-bands in between the range desired to achieve, by implementing a mechanical system that permits the capacitor to be moved dynamically to different positions. Therefore, depending on the bandwidth, the tuning capacitor can be moved closer to the source when the bandwidth is narrow in order to cover all the different sub-bands, and can be moved to further positions when the bandwidth is wide enough in order to increase the tuning range.

4.2.2 Decoupling

The decoupling technique integrating parasitic elements on the PCB has been implemented on the lateral model as results for the reduction of the mutual coupling between the MIMO antennas. The design with four parasitic elements could be improved in the future by reducing the length of the high band elements and increasing the value of the capacitor which will allow more accurate results and also make room on the PCB. Another improvement could be made in the low band elements by reducing the length of the resonant part to add a capacitor with a high value for higher precision. A deeper investigation could also be made about one of the biggest challenge of this decoupling technique, precisely the effect on the $\mid S_{11} \mid$ curves of many elements resonating at the same frequency.

4.2.3 Switching of the techniques

Since the bandwidth is twice larger than in the meander model, the tuning with a capacitor in the lateral model should need less values of capacitor to cover a bigger range of frequency bands and it could be an interesting and successful future work. Similarly, since the level of mutual coupling in the meander antenna is already very good in the high band, a future work could be to introduce a decoupling technique to decouple only the high band.

Conclusions

Device-independent antennas is a very promising field of study for the mobile communication systems since antennas are a major part of the communication reliability and the radio performances depend mainly on antennas. With a reusable antenna for different devices while keeping good performances, the researches made by antenna designers whenever the components or the size of the phone are modified could be significantly reduced.

Throughout this thesis, we presented and analyzed two different multi-band antenna designs but comparable to each other since they resonate at similar frequencies. The portability of those models were tested on three devices, the Candybar, the Smartphone and the Tablet formats and the results obtained were noteworthy and met the project requirements. Since the ground plane has an important effect on the antenna radiations, an interesting investigation was conducted for the impact of increasing the form factor in both designs to validate the portability of these antennas and estimate how much the ground plane size can be modified while keeping acceptable antenna performances. Once our two antennas were worth for multiple platforms, several enhancements have been implemented on the designs. The first improvement concerning the tuning techniques is to match the resonance frequencies, to cover a maximum range of bands and to meet the 4G throughput. This is possible with the support of MIMO systems, based on multiple antennas to improve wireless communications performance and applications efficiency but also to increase the data throughput without the need of a wider bandwidth. The second enhancement reduces the interaction between two closely smart antennas called mutual coupling by shorting on the ground plane some parasitic elements resonating at the same frequency than the one that needed to be decoupled. If the antennas are not correctly decoupled and isolated, the overall system performances can be seriously degraded.

If the meander model is selected, then the maximum channel bandwidth is fulfilled over the bands of interest presented in 2.1.1, for any PCB size, even though it is not really wide. This design has been proved to be the most efficient choice for narrow high band services over small devices as the Candybar. Moreover, for these small devices the decoupling level in the high band is so good that there is no need to implement any decoupling technique for this band. Consequently, the final spatial efficiency will be higher than other models that need to decouple both bands. If the field of interest are low-band services, this model provide a really high decoupling level, and therefore high efficiency, for some specific size formats within 120x70mm and 140x90mm of PCB size.

The selection of the lateral model should be based on the wider bandwidth and the smaller value of Q, over the requirements for both bands in multiple devices. This conception on the side of the PCB is very innovative in term of space consumption leaving free surface on the ground plane. Regarding the efficiency, this model always provide an efficient result respecting the industry requirements even when no decoupling technique is applied on the antenna. Moreover, the level of decoupling in the Candybar is the most difficult to reduce therefore, the selection of the lateral model could provide a coupling value approaching the acceptable threshold, thus requiring a smaller decoupling.

The strengths and the weaknesses of both models over the three devices can now be summarized in order to clarify the domain of performances of each model. In the meander antenna, except for the low coupling level of the high band that is performant, there are some other difficult issues about the narrow bandwidth generating a high value of Q and also the efficiency that is in most simulations inferior to the lateral one. The lateral design could be selected as the most performant model except for the level of decoupling in the high band but this could be fixed with a good decoupling technique.

As the results achieved with the meander and the lateral antennas were successful, the next step could be to measure the total efficiencies of those models in the anechoic chamber, thus the selection of a model could be done. If the measurements are satisfactory, the goal will be to write a scientific publication about the impact of the form factor on the same antenna design.

Bibliography

[1] D. A. Sanchez-Hernandez, Ed., Multiband Integrated Antennas for 4G Terminals. Reading, MA: Artech House, 2008

[2] Indrawati; Murugesan, S.; Raman, M.; , "3G Mobile multimedia services (MMS) utilization in Indonesia: An exploratory research," Technology and Society (ISTAS), 2010 IEEE International Symposium on , vol., no., pp.145-155, 7-9 June 2010

[3] www.streaminglearningcenter.com

[4] Abeta, S.; , "Toward LTE commercial launch and future plan for LTE enhancements (LTE-Advanced)," Communication Systems (ICCS), 2010 IEEE International Conference on , vol., no., pp.146-150, 17-19 Nov. 2010

[5] http://www.home.agilent.com

[6] Gert Frølund Pedersen. Antennas for Small Mobile Terminals. Aalborg Universitet. September 2003

[7] H. Bolcskei and A. J. Paulraj, Multiple-input multiple-output (MIMO) wireless systems, in The Communications Handbook. CRC Press, 2nd edition, 2002.

[8] Moray Rumney; Janine Whitacre, Analyze Antenna Approaches for LTE Wireless Systems, 2008

[9] Constantine A. Balanis. Antenna Theory, Analyses and Design, 2005, Third Edition, John Wileys and Sons Inc., ISBN ISBN-978-0-471-66782-7

[10] Annapurna Das, Sisir K. Das. Microwave Engineering, Tata McGraw-Hill Education, 2000

[11] David M. Pozar. Microwave Engineering, 2nd Edition. John Wiley and Sons, 1998

[12] Mats Gustafsson, Sven Nordebo. Bandwidth, Q factor and resonance models of antenna, 2005

[13] Yaghjian, A.D.; Best, S.R.; , "Impedance, bandwidth, and Q of antennas," Antennas and Propagation, IEEE Transactions on , vol.53, no.4, pp. 1298- 1324, April 2005

[14] Rashid, A.K.; Zhongxiang Shen; , "On the inverse relationship between quality factor and bandwidth of small antennas," Microwave Conference, 2009. APMC 2009. Asia Pacific , vol., no., pp.44-47, 7-10 Dec. 2009

[15] Best, S.R.; , "The inverse relationship between quality factor and bandwidth in multiple resonant antennas," Antennas and Propagation Society International Symposium 2006, IEEE , vol., no., pp.623-626, 9-14 July 2006

[16] H. W. Bode,"Network Analysis and Feedback Amplifier Design", Van Nostrand, N.Y., 1945

[17] R. M. Fano, "Theoretical Limitations on the Broad-Band Matching of Arbitrary Impedances," Journal of the Franklin Institute, vol.249, pp. 57-83, January 1950, and pp.139-154, February 1950

[18] Health Physics 74 (4): 494-522; 1998

[19] Compliance with TIS and TRP Requirements, May 2006. http://www.broadcom.com/collateral/wp/21XX-WP100-R.pdf

[20] Stjernman, A.; , "Relationship between radiation pattern correlation and scattering matrix of lossless and lossy antennas," Electronics Letters , vol.41, no.12, pp. 678- 680, 9 June 2005

[21] Hallbjorner, P.; , "The significance of radiation efficiencies when using S-parameters to calculate the received signal correlation from two antennas," Antennas and Wireless Propagation Letters, IEEE , vol.4, no., pp. 97- 99, 2005

[22] Salah I. Al-Mously, and Marai M. Abousetta. Users Hand Effect on TIS of Different GSM900/1800 Mobile Phone Models Using FDTD Method. World Academy of Science, Engineering and Technology 49 2009

[23] Andersen, J.B.; Hansen, F.; , "Antennas for VHF/UHF personal radio: A theoretical and experimental study of characteristics and performance," Vehicular Technology, IEEE Transactions on , vol.26, no.4, pp. 349- 357, Nov 1977

[24] Taga, T.; , "Analysis for mean effective gain of mobile antennas in land mobile radio environments," Vehicular Technology, IEEE Transactions on , vol.39, no.2, pp.117-131, May 1990

[25] Pedersen, G.F.; Nielsen, J.O.; , "Radiation pattern measurements of mobile phones next to different head phantoms," Vehicular Technology Conference, 2002. Proceedings. VTC 2002-Fall. 2002 IEEE 56th , vol.4, no., pp. 2465- 2469 vol.4, 2002

[26] Pedersen, G.F.; Nielsen, J.O.; Olesen, K.; Kovacs, I.Z.; , "Measured variation in performance of handheld antennas for a large number of test persons," Vehicular Technology Conference, 1998. VTC 98. 48th IEEE , vol.1, no., pp.505-509 vol.1, 18-21 May 1998

[27] Huynh, M.-C.; Stutzman, W.; , "Ground plane effects on planar inverted-F antenna (PIFA) performance," Microwaves, Antennas and Propagation, IEE Proceedings - , vol.150, no.4, pp. 209- 213, 8 Aug. 2003

[28] Horng-Dean Chen; , "Compact Broadband Microstrip-Line-Fed Sleeve Monopole Antenna for DTV Application and Ground Plane Effect," Antennas and Wireless Propagation Letters, IEEE , vol.7, no., pp.497-500, 2008

[29] P. Salonen, "Effect of groundplane size on radiation efficiency and bandwidth of dual-band U-PIFA," IEEE Antennas and Propagation Society International Symposium, vol.3, pp. 70-73, June 2003.

[30] Nassar, I.T.; Weller, T.M.; , "The ground plane effect of a small meandered line antenna," Wireless and Microwave Technology Conference (WAMICON), 2011 IEEE 12th Annual , vol., no., pp.1-5, 18-19 April 2011

[31] REMCOM article, Optimization of Inverted-F Antenna (PSO)

[32] C. Soras, M. Karaboikis, G. Tsachtsiris, and V. Makios, Analysis and Design of an Inverted-F Antenna Printed on a PCMCIA Card for the 2.4 GHz ISM Band, IEEE Antenna and Propagation Magazine, Vol. 44, No. 1, pp. 37-44, February 2002.

[33] I.J. Gupta and A. K. Ksienski, Effect of mutual couping on the performance of adaptive arrays, IEEE Trans. Antennas Propag., vol AP-31, pp.785-791, May 1983.

[34] Saunders, S.R. and Aragn Zavala, Antennas and propagation for wireless communication systems, pp. 66-69, 2007.

[35] Ray, K.P.; Chande, J.V.; Damle, S.H.; , "The mutual coupling effect on the input impedance and radiation pattern of Yagi antenna in an array environment," Microwave and Optoelectronics Conference, 1995. Proceedings., 1995 SBMO/IEEE MTT-S International , vol.1, no., pp.326-331 vol.1, 24-27 Jul 1995

[36] J.-F. Li and Q.-X. Chu, "Proximity-FED MIMO antenna with two printed ifas and a wideband t-shaped neutralization line," Progress In Electromagnetics Research M, Vol. 21, 279-294, 2011.

[37] Z. Huang and C.A. Balanis, Mutual coupling compensation in UCAs: Simulations and experiment, IEEE Trans. Antennas Propag., vol54, pp.3082-3086, Nov. 2006.

[38] Issam Toufik and Matthew Baker, "LTE The UMTS Long Term Evolution: From Theory to Practice. Stefania Sesia", 2009. John Wiley and Sons

[39] CTIA Certificate. Test Plan for Mobile Station Over the Air Performance. Method of Measurement for Radiated RF Power and Received Performance. December 2008.

[40] R. G. Brown, R. A. Sharpe, W. L. Hughes, and R. E. Post, Lines, Waves, and Antennas, 2nd ed. New York: John Wiley and Sons, 1973, p. 345

[41] Olaode, O. O.; Palmer, W. D.; Joines, W. T.; , "Effects of Meandering on Dipole Antenna Resonant Frequency," Antennas and Wireless Propagation Letters, IEEE , vol.11, no., pp.122-125, 2012

[42] Warnagiris, T.J.; Minardo, T.J.; , "Performance of a meandered line as an electrically small transmitting antenna," Antennas and Propagation, IEEE Transactions on , vol.46, no.12, pp.1797-1801, Dec 1998

[43] Endo, T.; Sunahara, Y.; Satoh, S.; Katagi, T.; , "Resonant frequency and radiation efficiency of meander line antennas", Electron. Commun. Jpn., Part II 83, 2000

[44] Puente, D.; Valderas, D.; Garcia, J.; Melendez, J.; Gomez, J.; Sancho, J. I.;,"Resonant frequency calculation of meander dipole antennas by TLM", Microw. Opt. Techn. Lett., vol. 50, no.6, Jun. 2008

[45] J. Villanen, J. Ollikainen, O. Kivekas, and P. Vainikainen. Compact antenna structures for mobile handsets. 1:4044 Vol.1, Oct. 2003.

[46] Li, Z. and Y. Rahmat-Samii, Optimization of PIFA-IFA combination in handset antenna designs, IEEE Trans. Antennas Propag., Vol. 53, 17701778, 2005.

[47] Jiang, B. T. and J. F. Mao, Design of a PIFA-IFA-monopole in dual-SIM mobile phone for GSM/DCS/Bluetooth operations, 2008 ICMMT Microwave and Millimeter Wave Technology, Vol. 3, 10501053, 2008.

[48] Karaboikis, M.; Soras, C.; Tsachtsiris, G.; Makios, V.; , "Compact dual-printed inverted-F antenna diversity systems for portable wireless devices," Antennas and Wireless Propagation Letters, IEEE , vol.3, no.1, pp.9-14, Dec. 2004

[49] Yi Huang and Kevin Boyle; Antennas: from Theory to Practice, 2008, John Wiley and Sons

[50] Young Jun Cho; Soon Ho Hwang; Seong-Ook Park; , "A dual-band internal antenna with a parasitic patch for mobile handsets and the consideration of the handset case and battery," Antennas and Wireless Propagation Letters, IEEE , vol.4, no., pp. 429- 432, 2005

[51] Song, C.T.P.; Mak, A.; Wong, B.; George, D.; Murch, R.D.; , "Compact Low Cost Dual Polarized Adaptive Planar Phased Array for WLAN," Antennas and Propagation, IEEE Transactions on , vol.53, no.8, pp. 2406- 2416, Aug. 2005

[52] C. Rowell, A. Mak, and C. L. Mak, "Isolation between multiband antennas," IEEE APS/URSI/AMEREM Int. Symp., Albuquerque, NM, Jul. 2006, pp.551

[53] A. Faraone and C. D. Nallo, " Mobile phone multi-band antenna employing a volume re-use concept", IEEE 2006, pp.561

[54] Virga, K.L.; Rahmat-Samii, Y.; , "Low-profile enhanced-bandwidth PIFA antennas for wireless communications packaging," Microwave Theory and Techniques, IEEE Transactions on , vol.45, no.10, pp.1879-1888, Oct 1997

[55] Fan Yang; Rahmat-Samii, Y.; , "Patch antenna with switchable slots (PASS): reconfigurable design for wireless communications," Antennas and Propagation Society International Symposium, 2002. IEEE , vol.1, no., pp. 462- 465 vol.1, 2002

[56] Corbett, R., "Antenna arrangement", U.S. Patent WO0 120 718

[57] Mak, A.C.K.; Rowell, C.R.; Murch, R.D.; Chi-Lun Mak; , "Reconfigurable Multiband Antenna Designs for Wireless Communication Devices," Antennas and Propagation, IEEE Transactions on , vol.55, no.7, pp.1919-1928, July 2007

[58] Langley, R.J.; Lu, L.; , "Electrically tunable handset antenna," Antennas and Propagation in Wireless Communications (APWC), 2011 IEEE-APS Topical Conference on , vol., no., pp.572-575, 12-16 Sept. 2011

[59] Liu, Luyi; Langley, Richard; , "Frequency-tunable mobile phone antennas with matching circuits," Antennas and Propagation (EuCAP), 2010 Proceedings of the Fourth European Conference on , vol., no., pp.1-4, 12-16 April 2010

[60] Mak, A.C.K.; Rowell, C.R.; Murch, R.D.; , "Isolation Enhancement Between Two Closely Packed Antennas," Antennas and Propagation, IEEE Transactions on , vol.56, no.11, pp.3411-3419, Nov. 2008

[61] Diallo, A.; Luxey, C.; Le Thuc, P.; Staraj, R.; Kossiavas, G.; , "Study and Reduction of the Mutual Coupling Between Two Mobile Phone PIFAs Operating in the DCS1800 and UMTS Bands," Antennas and Propagation, IEEE Transactions on , vol.54, no.11, pp.3063-3074, Nov. 2006

[62] Andersen, J.; Rasmussen, H.; , "Decoupling and descattering networks for antennas," Antennas and Propagation, IEEE Transactions on , vol.24, no.6, pp. 841- 846, Nov 1976

[63] K.-L. Wong, J.-H. Chou, C.-L. Tang, and S.-H. Yeh, Integrated internal GSM/DCS and WLAN antennas with optimized isolation for a PDA phone, Microwave Opt. Technol. Lett., vol. 46, no. 4, pp. 323326, Aug. 20, 2005.

[64] Chebihi, A.; Luxey, C.; Diallo, A.; Le Thuc, P.; Staraj, R.; , "A Novel Isolation Technique for Closely Spaced PIFAs for UMTS Mobile Phones," Antennas and Wireless Propagation Letters, IEEE , vol.7, no., pp.665-668, 2008

[65] Buon Kiong Lau; Andersen, J.B.; , "Unleashing multiple antenna systems in compact terminal devices," Antenna Technology, 2009. iWAT 2009. IEEE International Workshop on , vol., no., pp.1-4, 2-4 March 2009

[66] Shaker, G.; Rafi, G.; Safavi-Naeini, S.; Sangary, N.; , "A synthesis technique for reducing mutual coupling between closely separated patch antennas," Antennas and Propagation Society International Symposium, 2008. AP-S 2008. IEEE , vol., no., pp.1-4, 5-11 July 2008

[67] Zhang, S.; Lau, B. K.; Tan, Y.; Ying, Z.; He, S.; , "Mutual Coupling Reduction of Two PIFAs With a T-Shape Slot Impedance Transformer for MIMO Mobile Terminals," Antennas and Propagation, IEEE Transactions on , vol.60, no.3, pp.1521-1531, March 2012

[68] Karaboikis, M.; Soras, C.; Tsachtsiris, G.; Makios, V.; , "Compact dual-printed inverted-F antenna diversity systems for portable wireless devices," Antennas and Wireless Propagation Letters, IEEE , vol.3, no.1, pp.9-14, Dec. 2004

[69] Chi-Yuk Chiu; Chi-Ho Cheng; Murch, R.D.; Rowell, C.R.; , "Reduction of Mutual Coupling Between Closely-Packed Antenna Elements," Antennas and Propagation, IEEE Transactions on , vol.55, no.6, pp.1732-1738, June 2007

[70] Andrenko, A.S.; Yamagajo, T.; , "Novel design for reducing mutual coupling and signal correlation in diversity handset antennas," Microwave Conference Proceedings (APMC), 2010 Asia-Pacific , vol., no., pp.2095-2098, 7-10 Dec. 2010

[71] Buon Kiong Lau; Andersen, J.B.; , "Simple and Efficient Decoupling of Compact Arrays With Parasitic Scatterers," Antennas and Propagation, IEEE Transactions on , vol.60, no.2, pp.464-472, Feb. 2012

[72] Zhengyi Li; Zhengwei Du; Ke Gong; , "A dual-slot diversity antenna with isolation enhancement using parasitic elements for mobile handsets," Microwave Conference, 2009. APMC 2009. Asia Pacific , vol., no., pp.1821-1824, 7-10 Dec. 2009

[73] Nakano, H.; Suzuki, R.; Yamauchi, J.; , "Low-profile inverted-F antenna with parasitic elements on an infinite ground plane," Microwaves, Antennas and Propagation, IEE Proceedings - , vol.145, no.4, pp.321-325, Aug 1998

[74] Zhengyi Li; Zhengwei Du; Takahashi, M.; Saito, K.; Ito, K.; , "Reducing Mutual Coupling of MIMO Antennas With Parasitic Elements for Mobile Terminals," Antennas and Propagation, IEEE Transactions on , vol.60, no.2, pp.473-481, Feb. 2012

[75] Calla, O.; Singh, A.; Kumar Singh, A.; Kumar, S.; Kumar, T.; , "Empirical relation for designing the meander line antenna," Recent Advances in Microwave Theory and Applications, 2008. MICROWAVE 2008. International Conference on , vol., no., pp.695-697, 21-24 Nov. 2008

[76] Sharawi, M.S.; Faouri, Y.S.; Iqbal, S.S.; , "Design and fabrication of a dual electrically small MIMO antenna system for 4G terminals," Microwave Conference (GeMIC), 2011 German , vol., no., pp.1-4, 14-16 March 2011

[77] Huang, Y.; Boyle, K.; ."Antennas: From Theory to Practice", John Wiley and Sons, 2008

[78] Nakano, H.; Sato, Y.; Mimaki, H.; Yamauchi, J.; , "An Inverted FL Antenna for Dual-Frequency Operation," Antennas and Propagation, IEEE Transactions on , vol.53, no.8, pp. 2417- 2421, Aug. 2005

[79] Nieminen, H.; Ermolov, V.; Nybergh, K.; Silanto, S.; Ryhanen, T.; Microelectromechanical capacitors for RF applications, Journal of Micromechanics and Microengineering 12, number 2, pages 177-186. Institute of Physics Publishing, 2002

[80] Libo Huang; Russer, P.; , "Tunable antenna design procedure and harmonics suppression methods of the tunable DVB-H antenna for mobile applications," Microwave Conference, 2007. European , vol., no., pp.1062-1065, 9-12 Oct. 2007

[81] Computational Electrodynamics. The Finite-Difference Time-Domain Method. Allen Taflove, 1995. Artech House Publishers

Appendix A

THEORY

A.1 Introduction to relevant lossless transmission lines theory

In this section a brief introduction to lossless transmission lines theory will be presented in order to provide to the reader a better knowledge concerning some transmission line parameters used frequently in this thesis such as reflection coefficient or voltage standing wave ratio.
Let consider a lossless transmission line terminated in an arbitrary load impedance Z_L as can be observed in Figure A.1

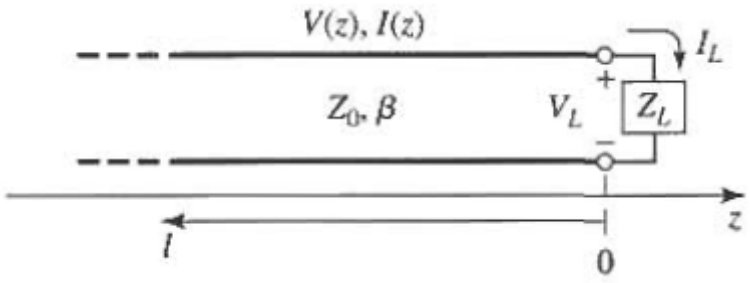

Figure A.1: A transmission line terminated in a load impedance Z_L, [11]

.

The incident wave generated by a source located at z < 0 is assumed to be of the form $V_0^+ \, e^{-j\beta z}$. The ratio between the voltage and the current while the wave is traveling through the transmission line is the characteristic impedance Z_0. However, since in general $Z_L \neq Z_0$, then the incident wave is reflected in the load and comes back towards the source with the form $V_0^- \, e^{j\beta z}$. Then, the total voltage on the line $V(z)$ can be written as the sum of incident and reflected waves as shown in equation A.1

$$V(z) = V_0^+ e^{-j\beta z} + V_0^- e^{j\beta z} \tag{A.1}$$

Similarly, the total current on the line is described by equation A.2

$$V(z) = \frac{V_0^+}{Z_0} e^{-j\beta z} - \frac{V_0^-}{Z_0} e^{j\beta z} \tag{A.2}$$

At z=0, the transmission line impedance is equal to the load impedance Z_L, and it is defined as the

ratio between voltage and current as described by equation A.3

$$Z_L = \frac{V(0)}{I(0)} = \frac{V_0^+ + V_0^-}{V_0^+ - V_0^-} Z_0 \tag{A.3}$$

Solving V_0^- gives

$$V_0^- = \frac{Z_L - Z_0}{Z_L + Z_0} V_0^+ \tag{A.4}$$

Defining the reflection coefficient Γ as the ratio between the amplitude of the reflected wave and the amplitude of the incident wave, the reflection coefficient in the load is described by A.5. From now on, the reflection coefficient will be denoted as S_{11} in order to be coherent with the rest of the report.

$$\Gamma = \frac{V_0^-}{V_0^+} = \frac{Z_L - Z_0}{Z_L + Z_0} \tag{A.5}$$

Thus, equation A.1 can be re-written as

$$V(z) = V_0^+ [e^{-j\beta z} + S_{11} e^{j\beta z}] = V_0^+ e^{-j\beta z} [1 + S_{11} e^{2j\beta z}] \tag{A.6}$$

From these equations, it can be concluded that both voltage and current through the line consist on a superposition of an incident and a reflected wave; such waves are called standing waves [11]. A measure of the mismatch of a transmission line is the VSWR, usually noted by s. It is defined as the ratio between the maximum and the minimum value of the standing wave, as it is defined by equation A.7

$$s = \frac{V_{max}}{V_{min}} = \frac{1 + |S_{11}|}{1 - |S_{11}|} \tag{A.7}$$

The VSWR can vary between 1 and infinite. The closer it reaches to 1, the better is the matching and the closer it reaches to infinite the worse is the matching.

A.2 Algorithm to calculate Q factor

As it was explained in section 1.1.9, formula 1.17 is suitable over single resonances within the operating bandwidth. In order to fulfill with this condition, a simple way to use the formula is to find the lumped components which provides perfect matching. It means that it is possible to design a matching network between the antenna and the characteristic impedance. Once these lumped components are found, it is possible to plot the S_{11} parameter over all the spectrum. As it was presented in equation A.7, s can be expressed as function of the S_{11} parameter. Therefore, expression 1.17 can be simplified as

$$Q(\omega_0) \approx \frac{1}{FBW_V(\omega_0)}, \tag{A.8}$$

whenever the condition shown in equation A.9 is fulfilled

$$\frac{1}{2} = \frac{s-1}{2\sqrt{s}} \tag{A.9}$$

Equation A.9 is fulfilled when s=2.57 which, by applying equation A.7, leads to a reflection coefficient equal to –7.06 dB. Thus, the inverse of the VSWR bandwidth under -7.06 dB is the Q factor at resonance.

The procedure followed to calculate the Q factor is given by the following steps:

- Determine whether the input impedance of the antenna Z_{in} at the resonance frequency is higher or lower than the characteristic impedance Z_0=50 Ω.
- Calculate the values of the lumped components which compose the matching network by using equations A.11, A.12 in case $Z_{in} \geq Z_0$ or by using equations A.14, A.15 in case $Z_{in} \leq Z_0$.
- Compute the S_{11} parameter with the matching network and calculate the bandwidth under -7.06 dB.
- The Q factor is just the inverse of the bandwidth calculated in the previous step.

A.2.1 Matching with lumped components (L networks)

In this paragraph, the procedure followed to find the different components of the matching network is explained.
One of the simplest type of matching network is the L section. It is composed by two reactive components connected to a transmission line. The two reactive components can be either inductance or capacitance depending upon the load impedance and the resonant frequency. Depending on whether the load impedance is higher or lower than the characteristic impedance, circuits shown in Figures A.2a and A.2b should be used respectively.

In reality, this type of networks are only feasible for frequencies up to around 1 GHz. There is a large range of frequencies where these circuits may not be realizable due to the fact that the size of components would be too big for being part of an integrated circuit. However, we do not look at this aspect since we do not use the matching network as a final product to be built, but it is a tool used to calculate the Q factor.

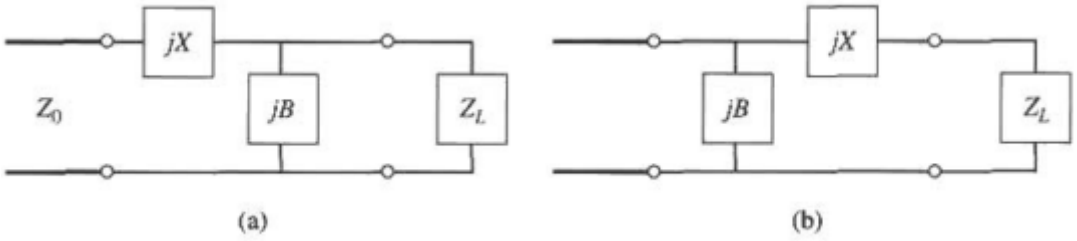

Figure A.2: L matching networks. (a) Network for $z_L \geq z_0$. (b) Network for $z_L \leq z_0$, [11]

Analytic Solutions

As it is well known, perfect matching is achieved when the impedance seen looking into the matching network is equal to the characteristic impedance Z_0. Therefore depending upon what kind of matching network is used, the impedance seen looking into the matching network is different.

In case that $Z_L \geq Z_0$, which implies that the normalized impedance Z_{LN}=Z_L/Z_0 is inside the (1 + jX) circle on the Smith Chart, then perfect matching is achieved if

$$Z_0 = jX + \frac{1}{jB + 1/(R_L + jX_L)} \tag{A.10}$$

where R_L is the load resistance and X_L is the load reactance.

By rearranging and separating real and imaginary parts in equation A.10, it is possible to get a quadratic equation for B

$$B = \frac{X_L \pm \sqrt{R_L/Z_0}\sqrt{R_L^2 + X_L^2 - Z_0 R_L}}{R_L^2 + X_L^2} \tag{A.11}$$

Then the series reactance can be found as

$$X = \frac{1}{B} + \frac{X_L Z_0}{R_L} - \frac{Z_0}{B R_L} \tag{A.12}$$

In case that $Z_L \leq Z_0$, which implies that the normalized impedance z_L is outside the (1 + jX) circle on the Smith Chart, then perfect matching is achieved if

$$\frac{1}{Z_0} = jB + \frac{1}{R_L + j(X + X_L)} \tag{A.13}$$

By rearranging and separating real and imaginary parts in equation A.10, it is possible to get quadratic equations for both B and X shown in equations A.14 and A.15, respectively

$$B = \pm \frac{\sqrt{(Z_0 - R_L)/R_L}}{Z_0} \tag{A.14}$$

$$X = \pm \sqrt{R_L(Z_0 - R_L)} - X_L \tag{A.15}$$

Appendix B

SIMULATIONS

B.1 Selection of the position of the antennas in SISO configuration

Simulations have proved that the position on the antenna on the PCB affects its radiation characteristics. In this section a deep analysis of the impact of the position has been carried out. In order to simplify the study, the analysis has been performed over SISO systems. Ten different configurations have been simulated in order to select the one that provides better bandwidth features. Three different configurations have been tested over the Candybar format, two for the meandering antenna design (horizontal and vertical orientation of the PCB) and one for the lateral antenna design (only vertical orientation since there is no space to place the antenna if the PCB is oriented in the horizontal position). Three different configurations have been tested over the candy-bar format, two for the meandering antenna design and one for the lateral antenna design. Four different configurations have been tested over the tablet format, two for the meandering antenna design and two for the lateral antenna design (horizontal and vertical). However, this study aims to go further and also the impact on the radiation frequency and the antenna impedance are also analyzed. The evolution of three antenna parameters with respect to the antenna shift from the upper left corner is analyzed. The shift is towards the right side of the PCB for the meander model and towards the bottom of the PCB for the lateral model. The three parameters analyzed are: resonant frequency, bandwidth and input impedance.

B.1.1 Resonant frequency

Figure B.1 shows the resonant frequency for both low and high bands for all the configurations presented. It can be observed that the resonant frequency oscillates within a specific range for all the configurations. In the low-band all the designs have a maximum of their resonant frequency on the last shift of the analysis, i.e. in the upper right corner for the meander model, and the bottom of the PCB for the lateral design.

B.1.2 Bandwidth

Figure B.2 shows the bandwidth for both low and high bands for all the configurations presented. Even though in some of the formats the evolution seems to be sinusoidal, in all the configurations a decreasing tendency can be observed. Thus, the maximum bandwidth will be always achieved by placing the antenna on the upper left corner of the PCB.

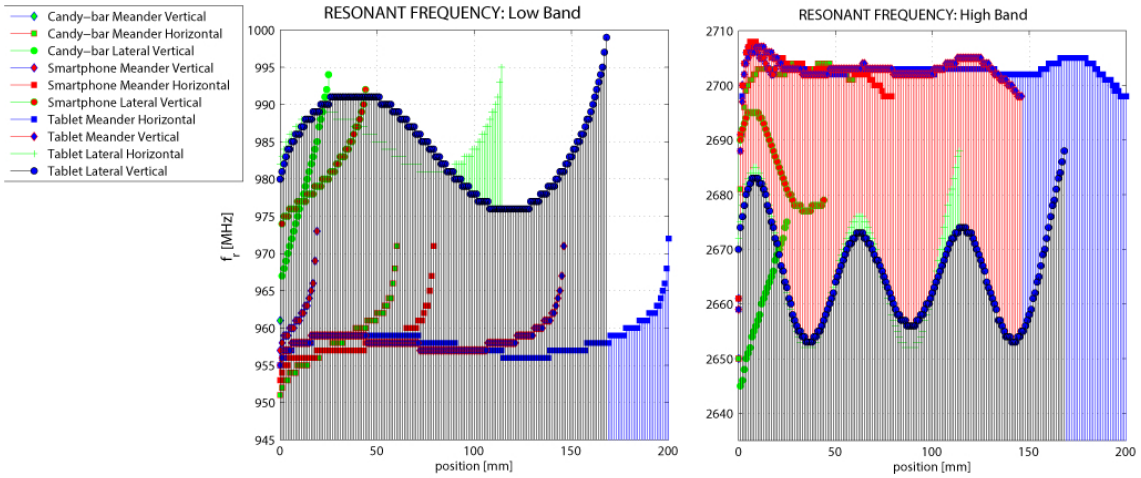

Figure B.1: Evolution of the resonant frequency with respect to the antenna shift

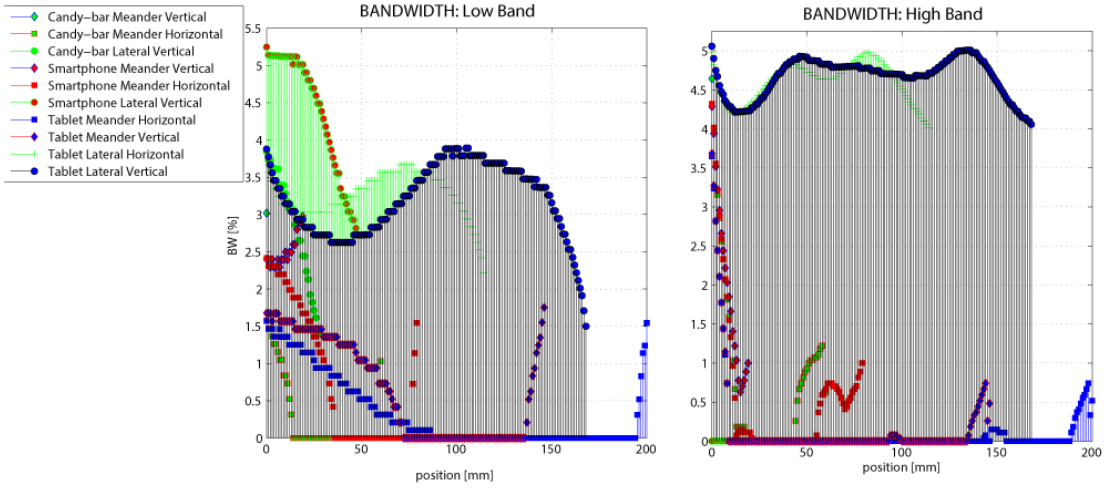

Figure B.2: Evolution of the bandwidth with respect to the antenna shift

B.1.3 Input impedance

Figures B.3 and B.4 show the normalized real and imaginary part of the antenna input impedance, respectively. This graphs are relevant in order to determine the quality of the matching of each configuration. It is well known that the perfect matching is given by an input impedance of 50 Ω. Since the graph represents the impedance normalized by 50, then a perfect matching is achieved if the real part of the impedance is equal to 1 and the imaginary part is equal to zero. By looking at the graphs it can be observed that the configuration that provides better matching are lateral configurations over the tablet format. This aspect is relevant for narrow-band application which requires really good matching at a certain frequency.

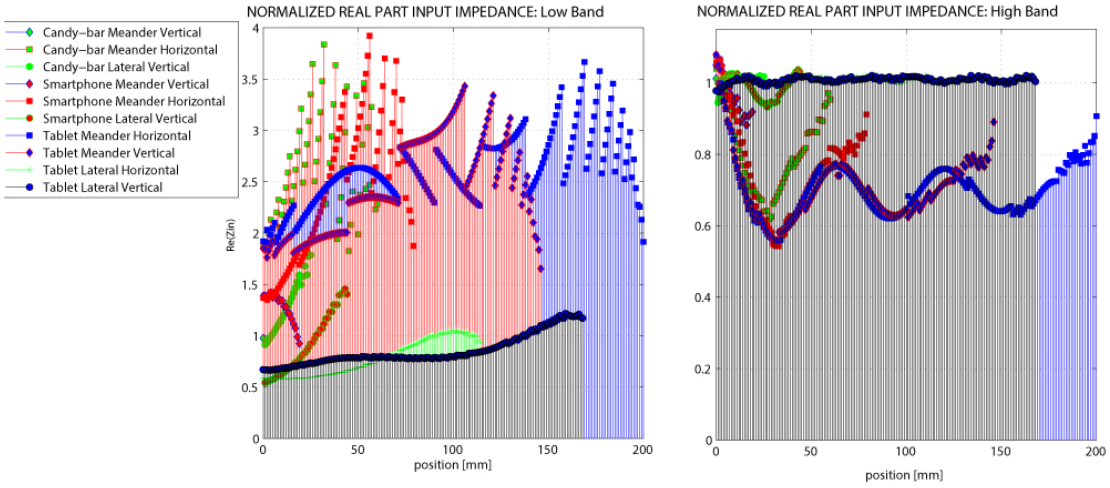

Figure B.3: Evolution of the real part of the antenna impedance with respect to the antenna shift

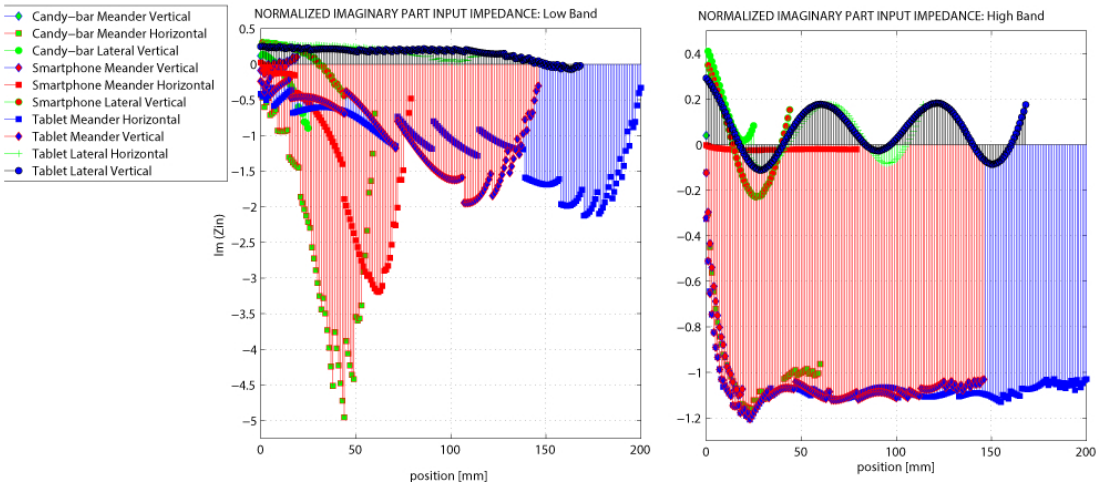

Figure B.4: Evolution of the imaginary part of the antenna impedance with respect to the antenna shift

B.2 Selection of the orientation of the antennas and MIMO configuration

The goal of this appendix is to show which configuration is the best over the two-antennas models in terms of efficiency. In the following, nine different figures are plotted. Three figures are shown for the Candybar format: meander antenna with the PCB oriented in vertical position (Figure B.5), meander antenna with the PCB oriented in horizontal position (Figure B.6) and lateral antenna with the PCB oriented in vertical position (Figure B.7). Three figures are shown for the Smartphone format: meander antenna with the PCB oriented in vertical position (Figure B.8), meander antenna with the PCB oriented in horizontal position (Figure B.9) and lateral antenna with the PCB oriented in vertical position (Figure B.10). Finally, three more figures are shown for the Tablet format: meander antenna with the PCB oriented in vertical position (Figure B.11), meander antenna with the PCB oriented in horizontal position (Figure B.12), lateral antenna with the PCB oriented in vertical position (Figure B.13). For each graph, both mirror and opposite MIMO configurations are depicted.

The meander model over the candy-bar format is very bad decoupled for the low-band in all models except for mirror configuration with the PCB oriented in horizontal position. However this configuration is rejected since the bandwidth in the low-band does not deal with the maximum channel bandwidth specifications presented in subsection 2.1.1. Within the other configurations, the mirror configuration with the PCB oriented in vertical position is the one which provides the best decoupling properties, presenting a decoupling level under -20 dB for the hig-band. Then, this model was selected based on the low decoupling level for the high-band but also on low spatial consumption, since by choosing this configuration, decoupling for high-band should not be implemented. For the Smartphone and Tablet models, the configurations selected was opposite with the PCB oriented in horizontal position, based on the best compromise possible between bandwidth and decoupling level. Decoupling techniques should be implemented for both bands in the Smartphone but for the design selected for the tablet, no decoupling techniques should be implemented.

For the lateral model, the same configuration was selected for all the different formats. This configuration is mirror with the PCB oriented in vertical position. This design was selected because it is the best decoupled for the low-band, the band which usually is the hardest to decouple.

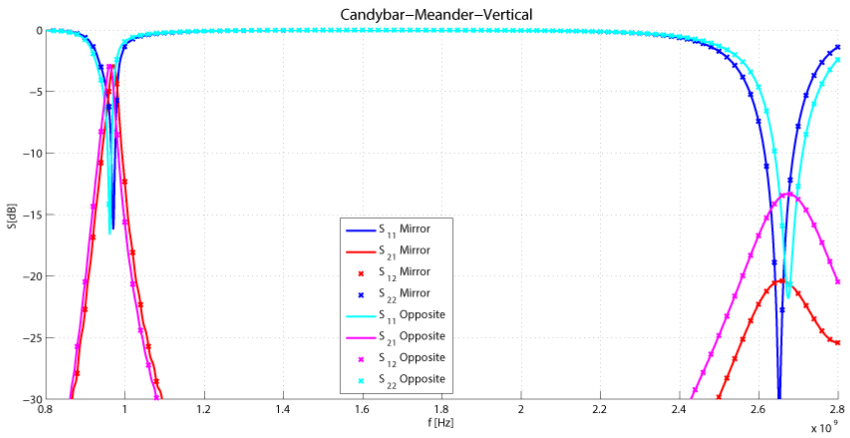

Figure B.5: S-Parameters of the meander model over Candybar with the PCB oriented in vertical position

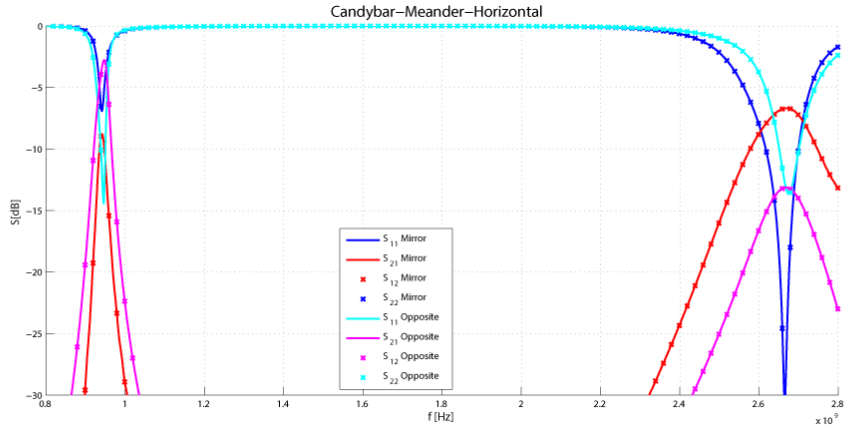

Figure B.6: S-Parameters of the meander model over Candybar with the PCB oriented in horizontal position

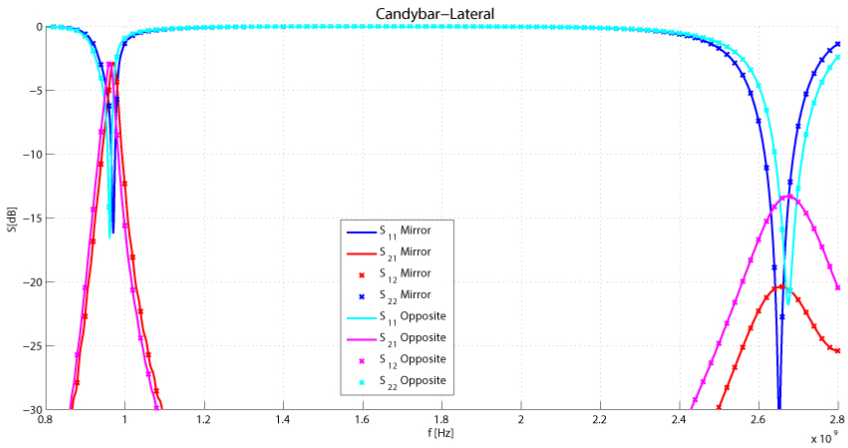

Figure B.7: S-Parameters of the lateral model over Candybar with the PCB oriented in vertical position

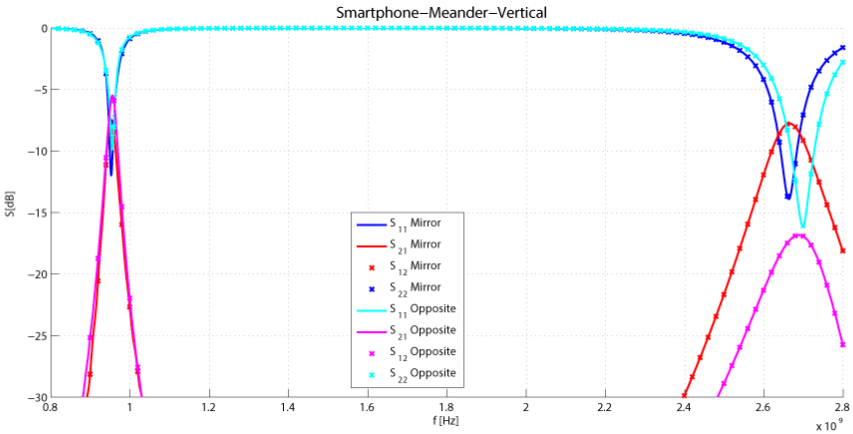

Figure B.8: S-Parameters of the meander model over Smartphone with the PCB oriented in vertical position

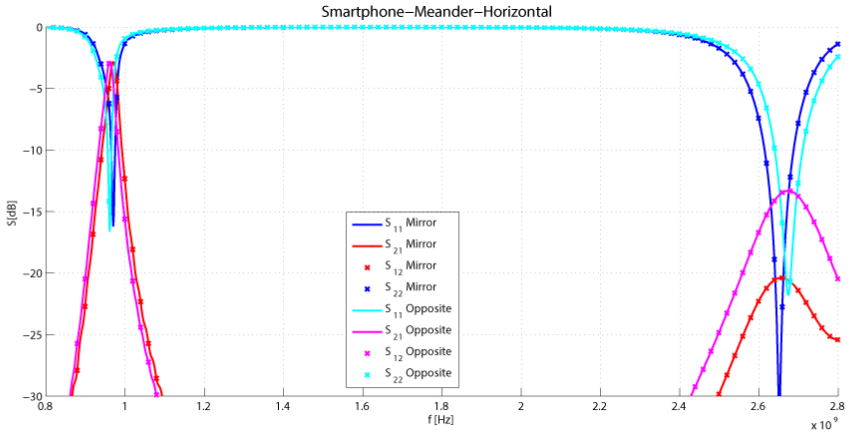

Figure B.9: S-Parameters of the meander model over Smartphone with the PCB oriented in horizontal position

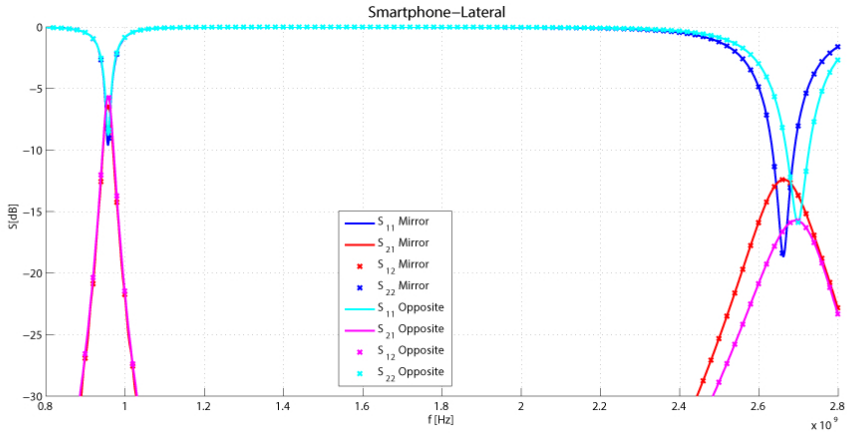

Figure B.10: S-Parameters of the lateral model over Smartphone with the PCB oriented in vertical position

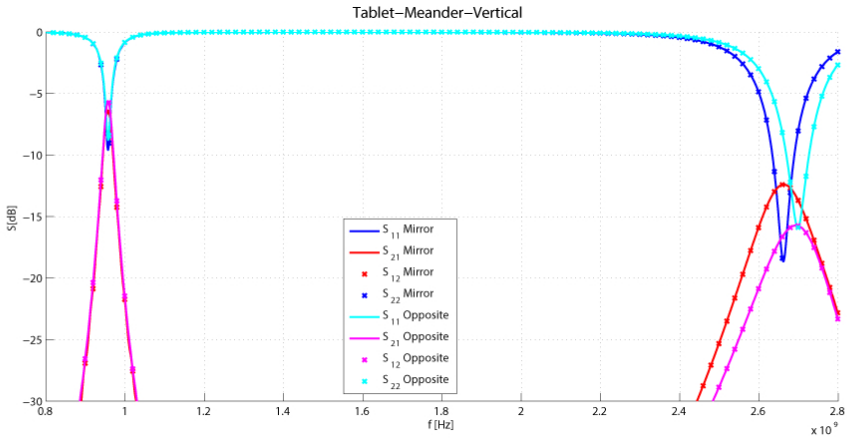

Figure B.11: S-Parameters of the meander model over Tablet with the PCB oriented in vertical position

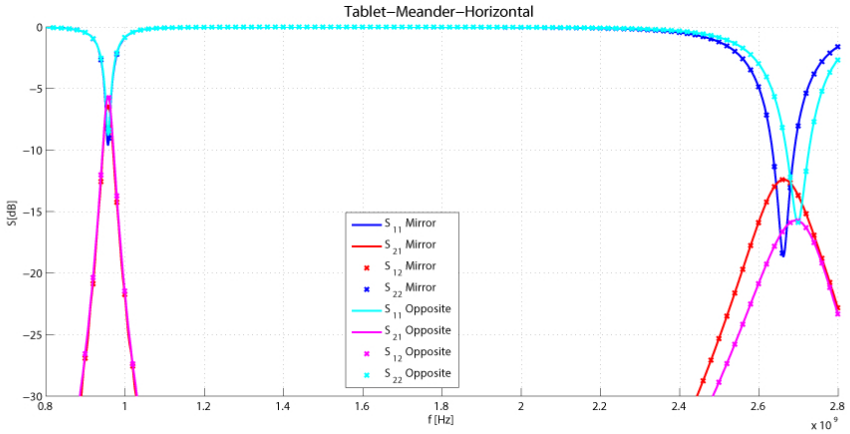

Figure B.12: S-Parameters of the meander model over Tablet with the PCB oriented in horizontal position

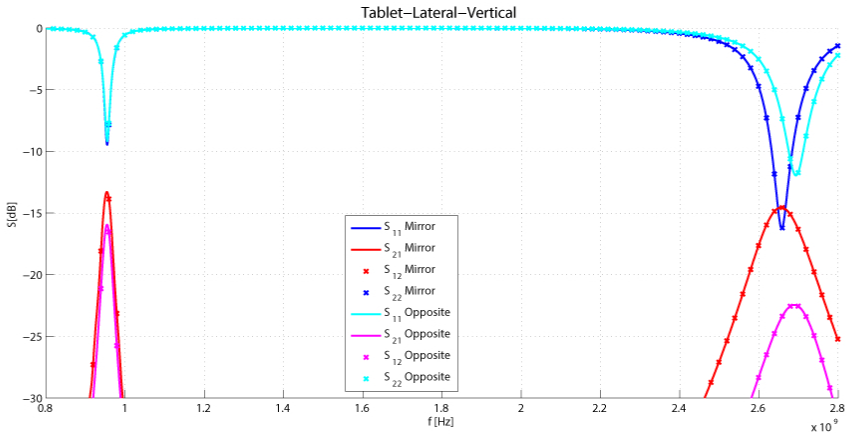

Figure B.13: S-Parameters of the lateral model over Tablet with the PCB oriented in vertical position

B.3 Tuning

Tables B.1, B.2, B.3 and B.4 show all the different bands achieved during the simulations of the tuning techniques when the position of the low-band tuning capacitor C_1 is 12 mm away from the source, and the position of the high-band tuning capacitor C_2 is 2mm away from the short for all the formats.

Low Band		High Band	
Capacitor (pF)	Bandwidth (MHz)	Capacitor (pF)	Bandwidth (GHz)
0	958-978	0	2.587-2.712
		0.375	2.513-2.612
		0.625	2.453-2.535
		0.875	2.389-2.455
		1	2.355-2.414
		1.125	2.321-2.372
		1.25	2.287-2.331
		1.375	2.254-2.291
0.125	929-961	0	2.565-2.694
		0.5	2.475-2.569
		0.75	2.417-2.492
		0.875	2.385-2.492
		1	2.353-2.412
		1.125	2.320-2.371
		1.25	2.286-2.330
		1.375	2.253-2.290
0.25	907-942	0	2.531-2.648
		0.5	2.461-2.558
		0.75	2.409-2.487
		1	2.349-2.409 and 2.648-2.703
		1.125	2.317-2.369
		1.25	2.282-2.329
		1.375	2.251-2.289
		1.5	2.219-2.249
0.375	887-916	0.125	2.477-2.574
		0.75	2.397-2.574
		1	2.343-2.405
		1.125	2.313-2.366 and 2.588-2.615
		1.25	2.282-2.326
		1.375	2.249-2.287
		1.5	2.218-2.287

Table B.1: Frequency bands covered in Candy-bar format (First part)

Low Band		High Band	
Capacitor (pF)	Bandwidth (MHz)	Capacitor (pF)	Bandwidth (GHz)
0.5	870-892	0	2.433-2.506
		0.75	2.377-2.455
		1	2.334-2.396
		1.125	2.307-2.360
		1.25	2.278-2.323
		1.375	2.247-2.287
		1.5	2.216-2.248 and 2.502-2.526
0.625	853-871	0	2.379-2.438 and 2.706-2.743
		0.125	2.675-2.711
		0.25	2.644-2.678
		0.375	2.614-2.644
		1	2.317-2.380
		1.25	2.271-2.317
		1.375	2.243-2.281
		1.5	2.213-2.243
0.75	837-853	0	2.695-2.740
		0.125	2.664-2.708
		0.25	2.631-2.674
		0.375	2.6598-2.638
		1	2.564-2.602
		1.25	2.529-2.565
		1.375	2.500-2.529

Table B.2: Frequency bands covered in Candy-bar format (Second part)

Low Band		High Band	
C_1 (pF)	Bandwidth (MHz)	C_2 (pF)	Bandwidth (GHz)
0	947-962	0.125	2.617-2.721
		0.375	2.561-2.648
		0.625	2.496-2.567
		0.75	2.461-2.525
		0.875	2.425-2.482
		1	2.389-2.439
		1.125	2.352-2.396
		1.25	2.313-2.353
		1.375	2.278-2.313
0.25	934-948	0	2.538-2.607
		0.5	2.477-2.551
		0.75	2.428-2.491
		0.875	2.399-2.455
		1	2.369-2.417
		1.125	2.336-2.417
		1.25	2.301-2.338
		1.375	2.268-2.301
0.5	921-934	-	Nothing
0.625	913-927	-	Nothing
0.75*	905-920	-	Nothing
1**	893-905	0.375	2.656-2.678
		0.5	2.617-2.638
		0.625	2.577-2.597
1.125***	885-896	0	2.764-2.791
		0.125	2.728-2.755
		0.25	2.691-2.717
		0.375	2.653-2.678
		0.5	2.613-2.637
		0.625	2.573-2.596
		0.75	2.492-2.512
1.25***	878-896	0	2.762-2.792
		0.125	2.726-2.754
		0.25	2.688-2.717
		0.375	2.649-2.677
		0.5	2.610-2.637
		0.625	2.569-2.595
		0.75	2.528-2.553
		0.875	2.487-2.511
		1	2.446-2.468

Table B.3: Frequency bands covered in Smartphone format

Band 7 can be covered with criteria * -1 dB, ** -2.5 dB,*** -3 dB

Low Band		High Band	
C_1 (pF)	Bandwidth (MHz)	C_2 (pF)	Bandwidth (GHz)
0	946-961	0	2.650-2.739
		0.125	2.620-2.708
		0.375	2.557-2.635
		0.5	2.518-2.594
		0.625	2.475-2.547
		0.75	2.432-2.498
		0.875	2.388-2.448
		1	2.342-2.395
		1.125	2.298-2.342
0.25	936-949	0	2.600-2.666
		0.375	2.532-2.606
		0.625	2.462-2.532
		0.75	2.422-2.487
		0.875	2.383-2.439
		1	2.337-2.389
		1.125	2.294-2.337
0.25	924-937	0.25	2.511-2.537
		0.5	2.466-2.515
		0.625	2.437-2.515
		0.75	2.437-2.492
		0.875	2.405-2.460
		1	2.368-2.420
0.375	914-925	-	Nothing
0.5*	902-913	-	-
0.625**	891-901	-	-

Table B.4: Frequency bands covered in Tablet format

Band 7 can be covered with criteria * -1 dB, ** -3 dB

B.4 Presentation of other decoupling techniques

In this section will be presented the strengths and weaknesses of the following decoupling techniques to reduce the mutual coupling between MIMO antennas in the lateral model. For some reasons that will be explained in this section, those techniques were not as much effective as the parasitic elements for the lateral design.

B.4.1 Connecting strip

This technique presented in 2.2.1 is very simple and consists in connecting with a strip either the two shorting or feeding points of MIMO antennas. The length of the strips is 26mm with a 1mm thickness and 1mm height from the PCB.

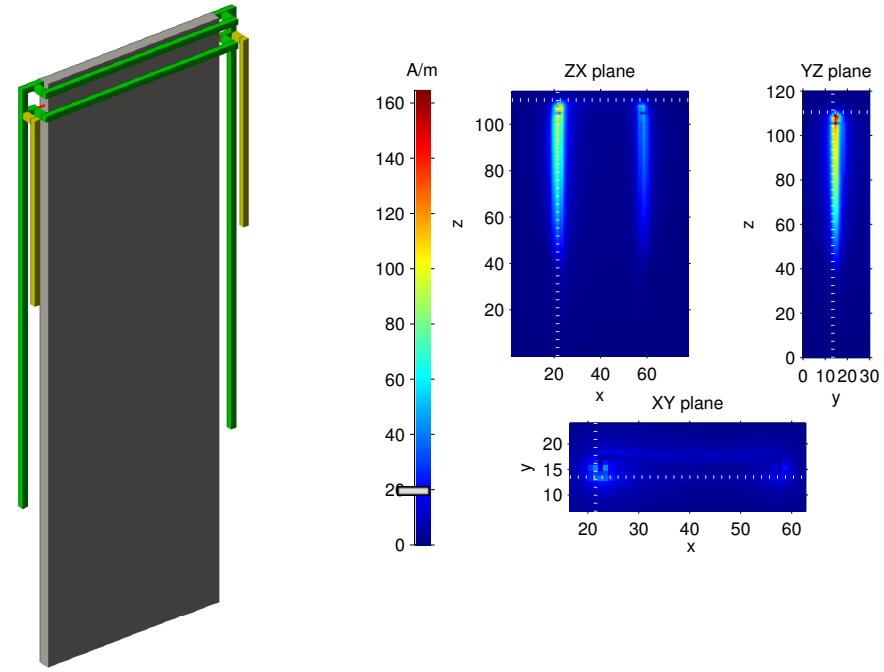

(a) Connecting strips design (b) H fields

Figure B.14: Connecting strip designs (a) and H fields (b)

In the table B.5, the technique connecting together the sources of the antennas decouples correctly only the low band with an $|S_{21}|$ of -10.4dB corresponding to an improvement of -2.5dB and an efficiency of 71,7% instead of 82.7% for the design without any decoupling techniques. The bandwidth also decreases from 3.8% to 1.3% due to the bad matching. The other technique connecting together the feeding points of the antennas decouples correctly only the high band with an $|S_{21}|$ of -15.7dB corresponding to an improvement of -1.2dB and an efficiency of 89,9% instead of 90.4% for the design without any decoupling techniques. The bandwidth decreases slightly only from 9.8% to 9.1% since the matching was not affected. This bad decoupling can be observed in the Figure B.14(b), where only a small amount of current is running through this connecting strip, which is not sufficient for reducing the mutual coupling.

B.4.2 Defected ground plane

This technique presented in 2.2.1 is also very simple to implement and consists in inserting a slot in the middle of the PCB. The thickness of the slot is 2 mm and the length will be approximately $\lambda/4$ of the wavelength for the low band or high band respectively 72mm or 34mm.

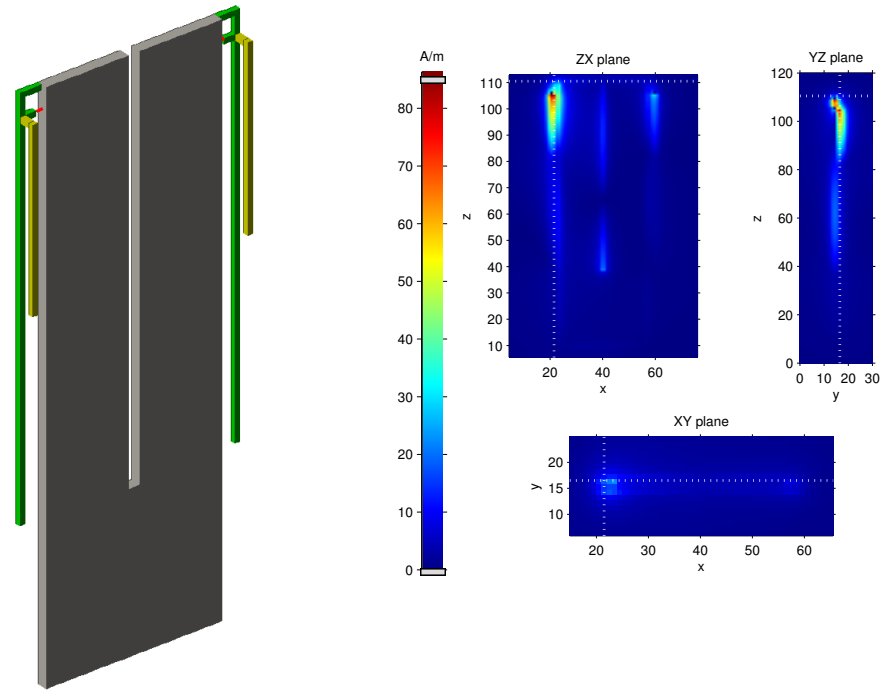

(a) Defected ground plane design (b) H fields

Figure B.15: Defected ground plane design (a) and H fields (b)

In the table B.5, the technique of the defected ground plane decouples correctly both bands when the length of the slot is short. With an $|S_{21}|$ of -10.6dB for the low band corresponding to an improvement of -2.7dB and an efficiency of 90,2% instead of 82.7% for the design without any decoupling techniques. The bandwidth only decreases from 3.8% to 3.4% due to the correct matching and the good decoupling. When the length of the slot is 72mm long, the resonance frequency is shifted since the PCB resonates at the same frequency and the mutual coupling on the low band $|S_{21}|$ of -9dB corresponds to an improvement of -0.6dB and an efficiency of 73.2% instead of 82.7% for the design without any decoupling techniques. The bandwidth decreases from 3.8% to 1.3% since the matching is halved. This slight decoupling can be observed in the Figure B.15(b), where only a small amount of current is running through this connecting strip, which is not sufficient for reducing the mutual coupling since there is some current running through the second antenna.

		Connecting Strips		**Defected ground plane**	
		Source	*Short*	*Long slot*	*Short slot*
Low Band	*Fr (MHz)*	994	974	1071	959
	S11 (dB)	-7,3	-16,78	-8,5	-31,1
	S21 (dB)	-10,44	-7,77	-8,97	-10,56
	Bandwidth (%)	1,3	3,7	1,3	3,44
	Decoupling (dB)	-2,54	+0,13	-0,6	-2,66
	Efficiency (%)	71,7	80,81	73,2	90,17
High Band	*Fr (MHz)*	2611	2650	2594	2683
	S11 (dB)	-18,02	-10,46	-10,38	-45,36
	S21 (dB)	-8,18	-15,72	-12,43	-13,11
	Bandwidth (%)	15,66	9,13	10,14	7,04
	Decoupling (dB)	+6,38	-1,16	+2,13	+1,45
	Efficiency (%)	84,62	89,87	86,57	96,17

Table B.5: Decoupling techniques comparisons

B.5 Matlab codes

In this appendix, a short descirption of all the different scripts implemented is given. The scripts implemented are the following:

- "**aau3_MB.m**": It is the main script used for SISO simulations. Most part of the code is the original code *aau3.m* but with some enhancements in order to get the parameters of interest in this thesis. The modifications done can be found by looking for *'%PAB'* through the code. The modifications are the following:
  - Plotting the $|S_{11}|$ parameter between 0.5 and -15 dB.
  - Drawing a red circumference -6 dB around the center of the Smith Chart in order to know if the bands of interest are under $|S_{11}|$=-6 dB.
  - Showing only10 MHz around the low band resonance frequency and 20 MHz around the high band resonance frequency.
  - Calculating the total efficiency as (1- $|S_{11}|^2$) multiplied by the radiation efficiency calculated by the original script.
  - Every time the results are collected a summary box appears showing the following parameters: resonance frequency and bandwidth for both the low and the high bands, and total efficiency calculated at the frequency input as excitation.
- "**aau3_mauro.m**": It has the same functionality of *aau3_MB.m* but for the two-antennas case. The parameters are simulated over the antenna whose source is defined as the first one in the list of elements.
- "**capacitor_val_MIMO_Mirror.m**" and "**capacitor_val_MIMO_Opp.m**": They are used to create the simulation files used for tuning. Provide as many combinations of capacitors as it is desired for MIMO systems in both mirror and opposite configuration, respectively.
- " **Conclusions.m** ": It is used to plot several S_{11} curves in the same figure, by loading the*s_11.aaf* files returned by the main script *aau3.m*.
- "**Conv_CandySmart_HorMirror.m**": It is used to convert the meander model from the Candybar format to the Smartphone in horizontal position and MIMO mirror configuration.
- "**Conv_CandySmart_HorOpp.m**": It is used to convert the meander model from the Candybar format to the Smartphone in horizontal position and MIMO opposite configuration.
- "**Conv_CandySmart_VertMirror.m** ": It is used to convert the meander model from the Candybar format to the Smartphone in vertical position and MIMO mirror configuration.
- "**Conv_CandySmart_VertOpp.m** ": It is used to convert the meander model from the Candybar format to the Smartphone in vertical position and MIMO mirror configuration.
- "**Conv_CandyTablet_HorMirror.m**": It is used to convert the meander model from the Candybar format to the Tablet in horizontal position and MIMO mirror configuration.
- "**Conv_CandyTablet_HorOpp.m**": It is used to convert the meander model from the Candybar format to the Tablet in horizontal position and MIMO opposite configuration.
- "**Conv_CandyTablet_VertMirror.m** ": It is used to convert the meander model from the Candybar format to the Tablet in vertical position and MIMO mirror configuration.

- "**Conv_CandyTablet_VertOpp.m** ": It is used to convert the meander model from the Candybar format to the Tablet in vertical position and MIMO opposite configuration.
- "**position_ev.m** ": It is used to plot the evolution of four different parameters as function of the position where the antenna is placed. These parameters are: resonant frequency, bandwidth, real part of the input impedance and imaginary part of the input impedance. Each of them is plot in a different figure for all the different models and configurations. In order to get all the data needed, all the *lock.aaf* files of these designs are loaded.
- "**PCB_size.m**": It is used to plot the bandwidth, $|S_{11}|$, $|S_{21}|$ and efficiency of the two models selected over an increasing PCB format from 100x40 mm until 286x146 mm. The *s_11.aaf* and *s_21.aaf* files of all the files are loaded.
- "**Q_MB.m**" and "**Q_MB_lat.m**": They are used to obtain the Q-factor for both resonant frequencies, at low-band and at high-band, and for both meander and lateral models, respectively. The script is based on transmission lines theory. It calculates the values of a combination of lumped components in order to obtain perfect matching. Once the S_{11} graph for the perfect matching configuration is obtained, the Q-factor is calculated as the inverse of the bandwidth under -7 dB weighted by the resonant frequency. In order to get the resonant frequencies and the S_{11} graph of the original design, the lock file is loaded by the script.
- " **s_MIMO.m** ": It is used to plot several S_{11} and S_{21} curves in the same figure, by loading the *s_11.aaf* and*s_21.aaf* files returned by the main script *aau3.m*.
- " $\mathbf{s_{11}}$**_many.m** ": It is used to plot several $S_{11}$the same figure for the tuning simulations. Shift of both capacitors and the range of nominal values they take, are set. The data is obtained by loading the *s*_11.*aaf* files returned by the main script *aau3.m*.
- "**shift_ant_pos.m**" and "**shift_ant_pos_lat.m**": They are used to shift the position of the antenna over the PCB for both meander and lateral model, respectively. The shift is done millimeter by millimeter until a maximum shift set in the script. The shift is towards the rigth side of the PCB in the meander model and towards the bottom of the PCB in the lateral one.